X-RAY RADIOGRAPHY TECHNIQUES FOR MEASURING DIFFUSIVE PROPERTIES OF SEDIMENTARY ROCKS

NWMO TR-2009-03 **February 2009**

L.C. Cavé, T.A. Al and Y. Xiang

University of New Brunswick

nwmo
NUCLEAR WASTE MANAGEMENT ORGANIZATION
SOCIÉTÉ DE GESTION DES DÉCHETS NUCLÉAIRES

Nuclear Waste Management Organization
22 St. Clair Avenue East, 6th Floor
Toronto, Ontario
M4T 2S3
Canada

Tel: 416-934-9814
Web: www.nwmo.ca

X-Ray Radiography Techniques for Measuring Diffusive Properties of Sedimentary Rocks

NWMO TR-2009-03

February 2009

L.C. Cavé, T.A. Al and Y. Xiang
University of New Brunswick

ABSTRACT

Title: **X-RAY RADIOGRAPHY TECHNIQUES FOR MEASURING DIFFUSIVE PROPERTIES OF SEDIMENTARY ROCKS**
Report No.: **NWMO-TR-2009-03**
Author(s): L.C. Cavé, T.A. Al and Y. Xiang
Company: University of New Brunswick
Date: February 2009

Abstract

Characterization of the diffusive properties of low permeability sedimentary rocks is an important component of the safety case for a deep geological repository (DGR) for used nuclear fuel, because diffusion is expected to be the dominant solute transport mechanism in this environment. In low permeability rocks, conventional laboratory tracer techniques for diffusion measurements typically involve experimental times of several weeks or months. Radiography offers the advantages of non-destructive analysis in that several time series measurements can be made on the same sample and with shorter experimental times because a steady-state condition is not required.

This report describes the development and testing of an X-ray radiography technique for characterizing and quantifying the concentration distribution of an iodide tracer solution in rock samples. The pore diffusion coefficient (D_p) for iodide in the rock can be estimated from the iodide concentration distribution by fitting an analytical solution of Fick's Second Law. Diffusion coefficients can be used in predictive models to estimate potential solute transport rates in porous media. The collection of X-ray radiograph images at successive time intervals also gives a valuable visual representation of the movement of tracer inside the rock, which can be used to enhance understanding of the diffusion process. X-ray absorption measurements on samples before and after saturation with iodide can also be used to determine the iodide accessible porosity (ϕ_I).

Initial testing of the radiography method has been conducted using archived drill core samples from the Ordovician-aged Queenston Formation shale and Cobourg Formation limestone, southern Ontario, Canada. Pore diffusion coefficients of $(4.8 \pm 2.5) \times 10^{-11}$ m^2/s (mean ± standard deviation) were measured for six Queenston Formation shale samples and $(2.6 \pm 1.0) \times 10^{-11}$ m^2/s for six samples of Cobourg Formation limestone. The results compare well with D_p data calculated from effective diffusion coefficients measured on adjacent rock samples using a conventional through-diffusion method, which average $(4.6 \pm 2.0) \times 10^{-11}$ m^2/s for shale and $(3.5 \pm 1.8) \times 10^{-11}$ m^2/s for limestone. Low porosity (0.01 to 0.03) and high matrix X-ray absorption are limiting factors that affect the sensitivity of the radiographic technique for the limestone samples because of poor signal to noise ratios. Low porosity and heterogeneous distribution of porosity at the scale of the samples (mm to cm) may also be responsible for the slightly poorer agreement between radiogaphy and through-diffusion results for this rock type.

Mean values of ϕ_I measured by radiography for 2 shale samples (0.060 ± 0.004) and 6 limestone samples (0.028 ± 0.005) were close to mean porosity measurements made on adjacent samples (15 shales and 7 limestones) by the independent water loss technique (0.062 ± 0.007 and 0.020 ± 0.008 for shales and limestones, respectively).

TABLE OF CONTENTS

LIST OF TABLES

Page

LIST OF FIGURES

Page

1. INTRODUCTION

In sedimentary rocks of low permeability, diffusion is expected to be the dominant mechanism for solute transport in groundwater. This has important implications when building a safety case for a deep geological repository (DGR) for used nuclear fuel. Diffusion through the engineered barriers and surrounding rock materials provides a pathway for the migration of radionuclides from the site, but diffusive transport through low permeability rock materials is typically slow. Characterization of the diffusive properties of the rock provides supporting evidence for the expected timeframes for solute transport from the DGR which could be used in predictive models to assess potential risks.

In fractured rock systems, diffusion of solutes into the rock matrix (matrix diffusion) is one of the most important retardation processes for potential contaminants from a deep geologic repository over the time scales of interest for nuclear waste management (Mazurek et al. 1996, Moreno et al. 1997). In unfractured rocks of low permeability, diffusion is the main transport mechanism for the movement of contaminants from the repository through the formation (van Loon et al. 2003a, b). The ability to quantify diffusive properties of rocks is therefore an important requirement for the use of predictive models to support the safety case for a DGR.

Recognizing the importance of diffusion, several nuclear waste management programs have included diffusion measurements in geoscientific investigations supporting the DGR concept in sedimentary rocks. Examples include the investigations of Opalinus clay in Switzerland (van Loon et al. 2003a, b, 2004), Oxfordian limestone and Callovo-Oxfordian argillite in France (Descostes et al. 2004), Boom clay in Belgium (Maes et al. 1999) and Culebra dolomite in New Mexico, USA (Tidwell et al. 2000).

The diffusive properties of sedimentary rocks are most frequently determined in laboratory diffusion cells using a planar or radial configuration (van der Kamp 1996, van Loon et al. 2004), although other configurations have also been used (e.g. Barone et al. 1990). The diffusion of a species such as Cl^- out of the sample, into the sample, or through the sample (out-, in- and through-diffusion experiments, respectively) can be determined using any of these configurations. Analytical chemical techniques are used to quantify solution concentration changes, and hence mass fluxes, over time in solution reservoirs connected to the sample in a diffusion cell. Diffusion coefficients are then derived from the experimental data using Fick's Laws.

Other conventional diffusion experiments often involve destructive measurement techniques, such as slicing and crushing the sample to measure solute concentrations at various distances along the cell at some stage after the initiation of diffusion. These methods only allow bulk diffusion to be measured in 1-D, and tests cannot be repeated on the same material. The advantages of X-ray techniques are that they are non-destructive and allow the rock properties that influence diffusion to be resolved at small spatial scales (μm to cm) in 2-D, or even in 3-D using computed tomography.

In the most recent studies, synthetic pore water with a chemical composition similar to that within the formation is used to minimize potential chemical reactions (e.g. precipitation, dissolution or exchange reactions) which could influence the diffusion parameters and porosity of the samples during measurement (Pearson, 1999).

Although most laboratory diffusion experiments are conducted at laboratory temperatures and pressures, effective diffusion coefficients (D_e) for tritiated water (HTO), anions (^{36}Cl, ^{125}I) and cations (^{22}Na, ^{85}Sr) in the Opalinus Clay have been measured at confining pressures between 1 and 15 MPa (van Loon et al. 2003a, b). Planar through-diffusion experiments conducted at both 1 and 5 MPa demonstrated that pressure had only a small effect on the measured D_e values for HTO, ^{36}Cl and ^{125}I in the Opalinus clay (van Loon et al. 2003a, b). Anisotropy in the diffusion coefficients of HTO, ^{36}Cl and ^{22}Na due to layering in the Opalinus Clay was also investigated by van Loon et al. (2004) using a radial technique to measure the diffusion parallel to the bedding, and a planar configuration to measure diffusion perpendicular to the bedding. Diffusion parallel to the bedding was found to be faster than diffusion perpendicular to the bedding by a factor of 4 to 6 for the radionuclides investigated.

Standard diffusion cell measurements for determining porosity, rock capacity factors, and D_e provide a bulk measurement averaged over the sample thickness. Descostes et al. (2004) used planar through-diffusion experiments to measure D_e and diffusion accessible porosities for HTO in the Oxfordian limestone and Callovo-Oxfordian argillite from the ANDRA Underground Rock Laboratory in Meuse/Marne, France. Different values for D_e and porosity were measured in three replicate experiments with 1 cm-thick discs taken from the same sample. The range of measured D_e values (2.6 to 12.2 x 10^{-12} m^2/s) and porosities (2.4 and 8.6%) demonstrated the potential impact of heterogeneities at the centimetre scale on the measured diffusive properties of these two formations (Descostes et al. 2004).

The effects of spatial heterogeneities in porosity on matrix diffusion in the Culebra dolomite from the Waste Isolation Pilot Plant (WIPP) were investigated in two dimensions by Tidwell et al. (2000) using X-ray absorption imaging. Experiments were conducted in which KI was allowed to diffuse across a single face of 4 cm-thick dolomite slabs while diffusive transport was monitored with time-series measurements of the 2-D relative concentration distribution of I^-. The heterogeneous, 2-D porosity distribution of each rock slab was also determined. Measured D_e values for the Culebra dolomite were observed to depend on both the magnitude and spatial distribution of the porosity (Tidwell et al. 2000).

The objectives of this study were to develop, test and document laboratory protocols for the application of X-ray absorption techniques to determine spatial variations in the sedimentary rock properties that influence diffusion at a scale of μm to cm. In particular, a protocol which uses radiography (an X-ray imaging technique) for the determination and visualization of spatial variations in porosity and the measurement of diffusion coefficients in 1-D will be demonstrated.

In this study, we have developed and tested a non-destructive X-ray absorption technique for characterizing and quantifying diffusion of an iodide tracer in rock samples. The technique has been tested on archived samples of Queenston Formation shale (Niagara) and Cobourg Formation[1] limestone (Darlington), from Southern Ontario, Canada. Tracer solutions and eluant NaCl concentrations matching those used by Vilks and Miller (2007) were used to facilitate a comparison of the bulk rock diffusion properties determined in this experiment to those measured by a classical through-diffusion technique for similar core samples by Vilks and Miller (2007).

[1] The Cobourg Formation is also referred to as the Lindsay Formation in outcrop maps and previous reports.

2. BACKGROUND

2.1 DIFFUSION MEASUREMENTS

In the context of contaminant transport, diffusion is a process whereby solutes are transported through a porous medium (rock matrix, soil or engineered barrier) from a region of high concentration to a region of low concentration. Unlike advection and dispersion, diffusive transport may occur even when the fluid phase is stationary. While there is still some debate as to the driving forces of diffusion, it is generally accepted that diffusion can be described by Fick's laws as reviewed in detail by Crank (1975). The theory of diffusion as applied to contaminant transport through natural porous media is presented by Grathwohl (1997). Diffusion-related terms used in this report are defined in the glossary in Appendix A.

Fick's First Law relates the diffusive mass flux (J) of a solute (mol/s/m^2) in the direction i, to the solute concentration gradient:

$$J_{Di} = -D \frac{\partial C}{\partial x_i} \quad (1)$$

where: D (m^2/s) is the diffusion coefficient, C is the solute concentration (mol/m^3) and x is the spatial dimension in the direction of diffusion (m). By definition $\partial C/\partial x$ is negative in the direction of diffusion. Equation 1 applies to a simple one-dimensional system under steady state conditions at constant temperature and pressure. Diffusion under transient conditions (t = time) is described by Fick's second law:

$$\frac{\partial C}{\partial t} = D \frac{\partial^2 C}{\partial x^2} \quad (2)$$

For diffusion in homogenous solutions, $D = D_0$, the free water diffusion coefficient. Values of D_0 are published for most common inorganic species and range from 1×10^{-9} to 2×10^{-9} m^2/s at 25°C (Robinson and Stokes 1959). The free water diffusion coefficient for iodide at infinite dilution is $D_{0(I)} = 2.045 \times10^{-9}$ m^2/s (Vanýsek 2006).

In a saturated porous medium, diffusion occurs through the pore spaces between the solid matrix particles, which results in a diminished mass flux compared to a comparable cross section in homogenous solution. Diffusive transport is constrained within the pore spaces, and is therefore influenced by the tortuosity (τ) and constrictivity (δ) of the pore network. The effect of the tortuous diffusion pathway in porous media on the diffusive mass flux is commonly accounted for using a pore diffusion coefficient:

$$D_p = D_0 \cdot \delta/\tau \quad (3)$$

where: D_p is the pore diffusion coefficient for a porous medium and D_0 is the free water diffusion coefficient. Diffusion coefficients obtained by the radiographic technique are reported as pore diffusion coefficients.

Pore diffusion coefficients (D_p) are derived by fitting an analytical solution of Fick's Second Law (equation 2) to the concentration versus distance profiles obtained from X-ray radiography diffusion tests. For the appropriate initial and boundary conditions:

$$C_{(x,t)} = 0 \;\Big|\; \begin{matrix} t = 0 \\ x > 0 \end{matrix}$$

$$C_{(x,t)} = C_0 \;\Big|\; \begin{matrix} t \geq 0 \\ x = 0 \end{matrix}$$

$$C_{(x,t)} = 0 \;\Big|\; \begin{matrix} t \geq 0 \\ x = \infty \end{matrix}$$

the analytical solution is (Crank, 1975):

$$C_i(x,t) = C_0 \,\mathrm{erfc}\, \frac{x}{2\sqrt{D_p t}} \qquad (4)$$

where: C_i is the concentration of tracer at a distance x from the diffusion boundary at time t since the start of diffusion; C_0 is the concentration of tracer at the influx boundary and erfc is the complimentary error function.

For through-diffusion experiments, the most commonly-used diffusion coefficient term is an effective diffusion coefficient (D_e) that includes the contribution of porosity (ϕ):

$$D_e = \phi \cdot D_p \qquad (5)$$

Inclusion of a porosity term, ϕ, in equation (5) accounts for the decrease in cross-sectional area for diffusive transport caused by the presence of mineral grains in the porous medium. The porosity term may be obtained in a variety of ways, each resulting in slightly different values and giving slightly different formulations of the effective diffusion coefficient. The various types of porosity used in the description of fluid and solute transport in sedimentary rock are explained by Pearson (1999).

For conservative (non-sorbing) solutes, the diffusion accessible porosity (ϕ_d or ε) is commonly obtained from time-lag analysis of steady-state through-diffusion experiments (for example Choi and Oscarson 1996; Boving and Grathwohl 2001; van Loon et al. 2003a, b and many others). When the conservative solute is not affected by size exclusion in the pore spaces, the solute-specific ϕ_d is typically close in value to the total connected porosity. Total connected porosity, referred to here as the water loss porosity (ϕ_w), is obtained by gravimetric measurement of the water content of a saturated sample (Emerson, 1990). When converting radiography D_p values to D_e values using equation (5) we use iodide-accessible porosity values (ϕ_I) when these are available for the sample in question, or we assume that ϕ_I can be approximated by ϕ_w, which is a good approximation when iodide is not affected by size exclusion in the pore spaces.

If solute transport is retarded by sorption, the porosity term obtained from through-diffusion data is known as the rock capacity factor (α):

$$\alpha = \phi_d + \rho K_d \qquad (6)$$

where: ρ is the bulk dry density of the rock and K_d the distribution coefficient for the solute (van Loon et al. 2003a). The diffusion behaviour of sorbing solutes leads to another formulation of the diffusion coefficient known as the apparent diffusion coefficient (D_a) (Shackelford 1991, Choi and Oscarson 1996, García-Gutiérrez et al. 2004):

$$D_a = D_e/\alpha = D_p/R_f \quad (7)$$

where the retardation of the solute is taken into account by the retardation factor ($R_f = 1+(\rho/\phi)\cdot K_d$). As the behaviour of iodide is considered to be conservative (Tidwell et al. 2000, García-Gutiérrez et al. 2004) i.e. $R_f = 1$, then D_a is equivalent to D_p, and from here onwards we use D_p to describe diffusion coefficients derived from through-diffusion iodide tracer experiments using equation (7).

Although iodide behaves as a geochemically conservative (non-reactive) tracer, its diffusive transport in low permeability clay-rich samples is slower than that of a truly non-sorbing tracer, such as tritiated water, because of effects such as anion exclusion in the small pores (van Loon et al. 2007, Savoye et al. 2001).

A comprehensive review of the conventional techniques for laboratory measurements of diffusion is presented by Shackleford (1991). The review includes steady state and transient methods and the appropriate mathematical expressions for deriving diffusion coefficients from a range of experimental techniques.

2.2 X-RAY TECHNIQUES FOR MEASURING ROCK PROPERTIES

One of the earliest reported uses of X-ray techniques in diffusion studies is the investigation of Rb diffusion profiles in soils by Evans and Barber (1964) who used X-ray autoradiography of an ^{86}Rb tracer. Since then, X-ray radiography techniques have been applied to various problems in the geological sciences using an iodide tracer: to measure spatially distributed (two dimensional) saturation (Tidwell and Glass 1994); to investigate spatial variations in porosity and diffusion in dolomite (Tidwell et al. 2000); and to study heterogeneous diffusion in fractured crystalline rocks (Altman et al. 2004). Three dimensional X-ray computed tomography (CT) techniques have also been employed to characterize phase distributions (minerals and pore fluids); pore geometry (van Geet et al. 2001; Wildenschild et al. 2002; Císlerová and Votrubová 2002) and iodide tracer diffusion (Polak et al. 2003, Zhelezny and Shapiro 2006).

Many methods of determining D require either that the concentration profile of the tracer through the porous medium be known during the experiment or the total mass of tracer within the sample be known at the end of the test (Shackelford, 1991). The most common means of obtaining these measurements is by sectioning the sample and physically or chemically extracting the tracer. X-ray measurements provide a non-destructive alternative for measuring tracer concentrations inside the solid material with the advantage that several time series data sets can be collected on the same sample.

The X-ray techniques for diffusion tests in this study are based on the principle of X-ray attenuation, which increases predictably with increasing concentration of an X-ray attenuating tracer in the rock sample. X-ray attenuation is expressed by the Beer-Lambert law:

$$I = I_0 \exp(-\mu d) \quad (8)$$

where: I_0 is the intensity of an X-ray beam incident on the sample; I is the intensity of the transmitted X-ray beam, which is attenuated during transmission through the sample; d is the thickness (or path length) through the sample and μ is the attenuation coefficient.

The attenuation coefficient depends on the X-ray energy (E), the electron density of the sample (ρ_e) and the chemical composition (effective atomic number, Z_{eff}) of the substance (van Geet et al. 2001):

$$\mu = \rho_e \left(a + b \frac{Z_{eff}^{3.8}}{E^{3.2}} \right) \tag{9}$$

where: a and b are constants. The electron density is a function of bulk density (ρ), atomic number (Z) and atomic weight (A):

$$\rho_e = \rho \frac{Z}{A} NA \tag{10}$$

where: NA is Avagadro's number and the effective atomic number (Z_{eff}) is given by:

$$Z_{eff} = \left(\sum f_i Z_i^{3.8} \right)^{\frac{1}{3.8}} \tag{11}$$

where: f_i is the fraction of the total number of electrons contributed by element i with atomic number Z_i. At constant X-ray source energy, the attenuation coefficient increases with increasing atomic number, which makes high atomic number elements, such as iodide, most suitable for use as tracers in X-ray radiography. Potassium iodide (KI) solutions have been used as tracers throughout this study. Note that although the potassium ions do make some contribution to the X-ray attenuation, their effect is small compared to the attenuation by iodide.

Individual attenuation coefficients are difficult to define for geological samples which are inherently heterogeneous, because the X-ray beam typically passes through several materials of different thickness, density and composition in the sample. For geologic materials containing fluid-filled pores, μ may be defined as:

$$\mu = (1 - \phi) \cdot \mu_m + \phi \cdot \mu_p \tag{12}$$

where: μ_m is the absorption coefficient for the solid material; μ_p is the absorption coefficient for the pores and ϕ is a porosity term. The attenuation coefficient is constant for the rock but changes for the pores due to the changing composition of the fluid as the tracer enters the pores.

To overcome the problem of heterogeneity, we have employed a blank subtraction approach in this work, similar to that used by Tidwell et al. (2000) and Altman et al. (2004). The blank subtraction approach involves using two radiograph images: 1) a reference image without tracer (blank) and 2) a time series image of exactly the same region of the sample during the tracer diffusion. Subtracting the reference image from the time series image allows the effect of the tracer to be visualized in isolation from the X-ray attenuation effects of the rock matrix.

Blank subtraction yields the parameter $\Delta\mu_{i,j}$, which represents the change in the X-ray attenuation coefficient due to the presence of iodide tracer in the pores at each pixel (i,j) in the time series radiograph images.

From equations 8 and 12, for each point in a sample:

$$(\ln I_r - \ln I_0)_{i,j} - (\ln I_t - \ln I_0)_{i,j} = -(\mu_m \cdot (1-\phi) + \mu_{p1} \cdot \phi \cdot d)_{i,j} + (\mu_m \cdot (1-\phi) + \mu_{p2} \cdot \phi \cdot d)_{i,j}$$

$$\ln(I_r)_{i,j} - (\ln I_t)_{i,j} = (\mu_{p2} - \mu_{p1})_{i,j} \cdot \phi_{i,j} \cdot d_{i,j}$$

$$\ln(I_r)_{i,j} - (\ln I_t)_{i,j} = \Delta\mu_{i,j} \qquad (13)$$

where: $(I_r)_{i,j}$ is the transmitted X-ray intensity at pixel (i,j) on the reference radiograph and $(I_t)_{i,j}$ is the transmitted X-ray intensity at the same pixel on the time series radiograph; and μ_{p1} and μ_{p2} are the attenuation coefficients of the pore fluids without and with iodide, respectively. Note that the definition of the term $\Delta\mu_{i,j}$ includes the porosity and thickness terms since $\phi_{i,j}$ and $d_{i,j}$ are constant at each position.

The parameter Δμ is a function of the mass of tracer along the X-ray path and can be calibrated to give quantitative measurements of tracer concentration.

Two techniques can be used to quantify the iodide concentration in the time series radiographs during the diffusion experiments. We have termed these the calibrated technique and relative technique. The calibrated approach uses a multi-point calibration curve for Δμ versus iodide concentration that is derived from standard iodide solutions. The calibration curve is used to relate Δμ values to the iodide mass in pore spaces, and iodide concentration is determined by dividing by the porosity (ϕ_w) (See Sections 4.1.3 and 4.5.1).

The second technique measures relative tracer concentrations by scaling the time series measurements to the results of a final X-ray radiograph collected when all pores in the sample are fully saturated with the tracer solution. This technique is described in detail by Tidwell et al. (2000) and Altman et al. (2004). The difference between the reference (zero tracer) image and the final tracer-saturated image also gives the diffusion-accessible porosity distribution in the sample. The equation for deriving relative concentration values at each point in the 2-D data set is (Tidwell and Glass 1994):

$$\left(\frac{C}{C_0}\right)_{i,j} = \frac{\ln(I_r)_{i,j} - \ln(I_t)_{i,j}}{\ln(I_r)_{i,j} - \ln(I_s)_{i,j}} = \frac{(\Delta\mu_t)_{i,j}}{(\Delta\mu_s)_{i,j}} \qquad (14)$$

where: C is the concentration at pixel i, j; C_0 is the tracer concentration in the influx reservoir; and I is the measured (transmitted) intensity at pixel i, j; with the subscripts t, r and s indicating the time series, reference (zero tracer) and tracer-saturated radiograph images, respectively. In the tracer-saturated and zero-tracer conditions, the density, composition and thickness of the solid rock matrix remain constant for each point on the radiograph. The concentration of the tracer in the pore spaces is also constant in the tracer-saturated sample. Therefore the Δμ values at each pixel are a function of porosity. The value of C/C_0 at each point in the sample is measured by the simple ratio of the change in attenuation coefficient for the time series and the tracer saturated images $\Delta\mu_t/\Delta\mu_s$. This approach could be viewed as a two-point calibration technique using known iodide concentrations (0 and C_0) in the rock matrix.

2.3 OBJECTIVES

The purpose of this work was to develop and test methods for measuring the diffusive properties of sedimentary rocks. The general aims were to:

i) measure D_p for low permeability rocks;
ii) refine methods for measuring spatially-distributed porosity for these materials; and
iii) test new methods for quantifying solute concentrations during diffusion experiments.

The specific objectives were:

1. To develop sample collection and experimental testing protocols for measurement of the diffusive properties of shale and limestone. These protocols would be used to:
   i) examine spatial variations in porosity;
   ii) quantitatively measure the diffusion of a conservative solute (e.g. I^-) into a sample as a function of time; and
   iii) determine values for D_p using the porosity measurements from (i) and the time-series measurements of quantitative solution concentrations from (ii).
2. To develop an experimental testing protocol to determine the magnitude of layering-related anisotropy in porosity and D_p values.

3. SAMPLE CHARACTERIZATION

Two sets of archived drill core samples were received from OPG for the testing of diffusion measurement techniques (Figure 1):

- 4 drill core samples of Queenston Formation shale from hole SI2005-1, drilled in February 2005 at Sir Adam Beck Station in the Niagara region. Samples were collected from depths 78, 88, 93 and 105 metres below surface. The core diameter was 63.3 mm.
- 3 drill core samples of Cobourg Formation limestone from hole DW-46, drilled in 1978 at Darlington reactor site in Ontario. Samples were collected from depths 36, 43 and 56 metres below surface. The core diameter was 54.5 mm. Only the sample from 36 m was investigated.

All cores were dry when received and had been archived in wooden core boxes without temperature or humidity control.

Figure 1: Drill core samples of Queenston Formation shale and Cobourg Formation limestone used for testing diffusion measurements. The location of the diffusion test samples (C036_1 to C036_3) is indicated on the Cobourg Formation core.

3.1 QUEENSTON FORMATION

The core segments that were used to prepare diffusion test samples from the Queenston Formation comprised relatively uniform, red clay/siltstone (commonly referred to as Queenston shale). Nodules of anhydrite are visible in the shale in both hand specimen and thin section. Core from 93 m and 105 m depth also contained irregularly-shaped, pale green, reduced zones over several centimetres of the core.

Petrography, mineralogy and petrophysical properties of Queenston Formation from the S2005-1 drill core samples were examined (Appendix B; Koroleva and Mazurek (2006)). Results from these investigations are summarized in Table 1. Mineralogy was determined by optical microscopy, X-ray diffractometry (Koroleva and Mazurek 2006) and scanning electron microscopy with energy dispersive X-ray spectroscopy (SEM-EDS) (Appendix B). Porosity was estimated from bulk dry density (Hg displacement) and grain density (He pycnometry) measurements by Koroleva and Mazurek (2006), and by a thresholded binary imaging technique using SEM backscattered electron images (Appendix B).

The Queenston shale material is relatively cohesive when dry, but exhibits swelling properties when immersed in dilute aqueous solutions. Samples cracked and pieces spalled off when attempting to saturate the rock with water. Because of the spalling problem all drilling and cutting of Queenston samples was undertaken in kerosene. Samples for gravimetric porosity tests were also saturated with kerosene instead of water. Diffusion test samples were saturated with a 3 M sodium chloride brine solution (see section 4.1.2 for rationale for selection of this solution) before introducing the iodide tracer. The high ionic strength of the solution limits swelling of the expandable clay minerals.

3.2 COBOURG FORMATION

Drill core samples from the Cobourg Formation comprise interbedded limestone and shaley limestone with discontinuous bedding. The limestone samples are relatively heterogeneous at the mm to cm scale, containing varying amounts and sizes of shelly fossil material in a fine-grained matrix of calcite with minor aluminosilicate clay minerals (Figure 2 and Figure 3). Minor phases observed by SEM-EDS include dolomite, quartz, apatite and iron sulfide minerals.

Porosity estimates were attempted using a thresholding technique with SEM backscattered electron images as described for the Queenston Formation samples in Appendix B. The technique is limited for small pore sizes by the spatial resolution of the SEM. Images were collected as non-normalized 16 bit TIFF images and the greyscale histograms used to select a pixel value of 50 for the pore threshold. The porosity estimates for 9 areas on one thin section (each 1.0 mm^2) were highly variable, ranging from 0.4% to 3.6%, with a mean of 1.7%. Heterogeneity in the sedimentary features and porosity distribution make it difficult to select representative areas for measurements. The sample heterogeneity could also be an important factor affecting the diffusion measurements.

The Cobourg limestone core displayed good structural integrity and was easy to cut and drill using water as a coolant. Samples were saturated with distilled water for gravimetric porosity tests and with a mixed cation chloride brine (section 4.1.2), intended to mimic the natural pore water, for diffusion experiments.

Table 1: Mineralogy and petrography of Queenston Formation samples

Sample	Koroleva and Mazurek (2006) Queenston shale 364	Koroleva and Mazurek (2006) Queenston shale 346	Appendix B Queenston shale
Depth (m)	110.82 – 111.25	105.25 – 105.57	78, 88, 93 & 105
Rock type	Shale		Argillaceous clay-silt
Colour	Reddish with reduction haloes around opaque minerals		Red (oxidized) to green (reduced)
Grain size	Very small (clastic quartz grains have diameters < a few tens of μm)		Clay-silt (<62 μm) clastic grains in fine-grained matrix
Clast distribution	Relatively homogeneous at thin section scale		-
Cementation	Not evident at optical microscope scale		Weak cementation by hematite and clays
Dry bulk density (g/cm^3)	2.67	2.67	-
Grain density (g/cm^3)	2.78	2.78	-
Porosity (%)	4.0	4.0	5.3 – 5.6
Mineral content	**(wt %)**	**(wt %)**	**Description**
Hematite	-	-	Pervasive in matrix
Calcite	5	4	Clasts & overgrowths
Dolomite/Ankerite	<1	<1	Diagenetic overprint
Anyhdrite	-	-	Diagenetic concretions
Gypsum	-	-	Fracture coatings
Halite	-	-	Not observed
Siderite	<1	<1	-
Quartz	29	26	Dominant (clasts)
Albite	2	2	Minor (clasts)
K-feldspar	2	2	Minor (clasts)
Pyrite	<0.2	<0.2	-
Illite	42	47	Dominant (matrix)
Illite/smectite	4	3	-
Chlorite	7	7	-
Kaolinite	7	8	-
Sum of sheet silicates	60	65	-
Organic carbon	<0.1	<0.1	In reduced zone
Inorganic carbon	0.7	0.6	-
Total sulfur	<0.1	<0.1	-

- not measured or not reported.

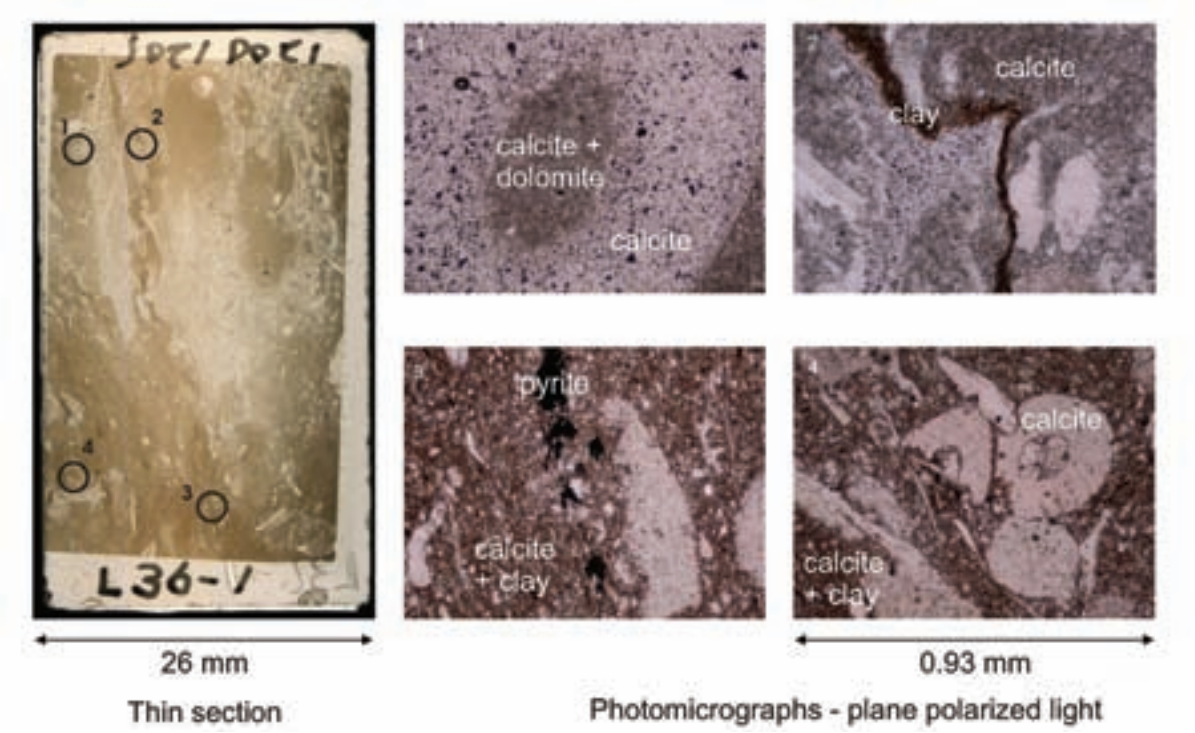

Figure 2: Mineralogy of a thin section from Cobourg Formation limestone sample C036_1. Calcite is dominant in fossil fragments and surrounding matrix with minor dolomite and aluminosilicate clay in the matrix.

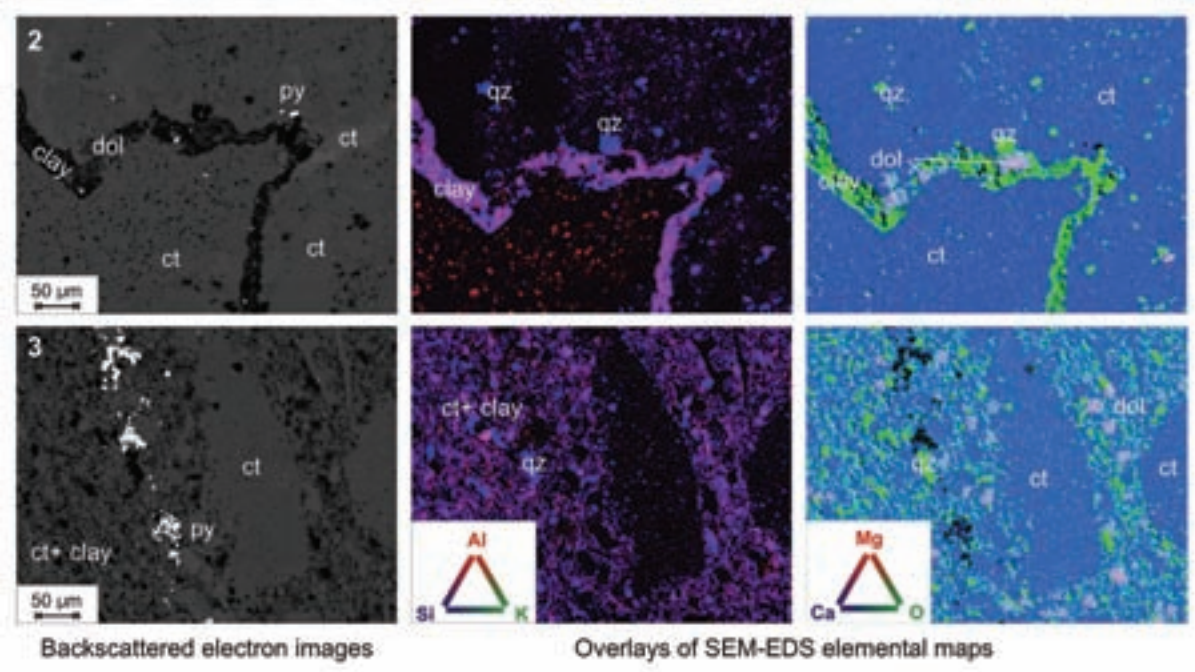

Figure 3: SEM images indicating mineralogy of a thin section from Cobourg Formation limestone sample C036_1. Backscattered electron images display bright areas of iron sulfide (py) and SEM-EDS maps indicate the positions of quartz (qz), dolomite (dol), calcite (ct) and K/Mg/Si/Al-bearing clay mineral phases.

4. RADIOGRAPHY METHOD

Diffusion properties were measured using X-ray radiography to monitor the movement of an iodide tracer through a sample of rock under static (no flow) conditions with a constant tracer concentration at the influx boundary. The radiography technique is in development at the University of New Brunswick and is a modification of the work of Tidwell and Glass (1994), Tidwell et al. (2000) and Altman et al. (2004) using iodide tracers in geological materials. In this section, details of the methodology and related measurements needed to determine diffusion coefficients are described. A step-by-step protocol for the radiography technique is provided in Appendix C.

All radiography data presented in this report were collected on a Skyscan 1072 Desktop X-ray micro computed tomography system (microCT), located in the X-ray laboratory of the Department of Mechanical Engineering at UNB. Both radiographs (two-dimensional X-ray transmission images) and CT scans (for reconstruction of three-dimensional X-ray data sets by computed tomography) can be collected with this instrument.

4.1 PREREQUISITES

For this study we have used a gravimetric method to determine the water loss porosity, ϕ_w, for comparison with iodide accessible porosity (ϕ_I) measurements and as an estimate of bulk porosity for use in calculations where ϕ_I values are not available because samples did not undergo complete iodide tracer saturation.

Knowledge of the composition of the natural pore water in the rock is another prerequisite. Diffusion experiments are conducted on samples saturated with pore solutions of the same ionic strength as the iodide tracer solution. This is done to avoid the influence of osmotic pressure on the measured diffusion rates. A synthetic pore water (SPW) solution with similar composition to the natural pore fluids is preferred to maintain geochemical equilibrium between the fluid and minerals.

The collection of X-ray absorption data for standard solutions is another pre-requisite when using the calibrated technique for determining iodide concentrations. We have used radiographs of aqueous solutions in glass vials to prepare the calibration curves, matching the aqueous matrix to the synthetic pore water for each rock type.

4.1.1 Gravimetric technique for porosity measurements

Gravimetric measurements of water loss porosity (ϕ_w) are based on the technique described by Emerson (1990). The technique estimates the volume of the pores based on the mass difference between a saturated and dry sample, assuming all the pores in the saturated sample are filled with the saturating liquid. The total volume is estimated using Archimedes principle, by submerging the sample in a beaker of the saturating liquid. The porosity is then obtained from the ratio of pore volume to total volume (Figure 4).

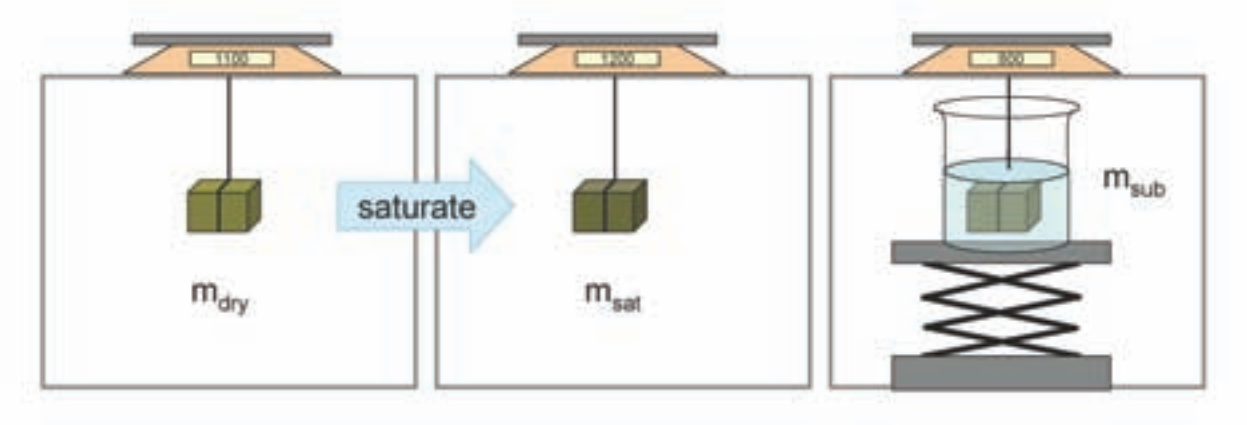

Figure 4: Schematic diagram of the steps involved in the gravimetric measurement of water loss porosity.

Although the samples were received dry, lubricating fluids were used during cutting. The samples were therefore dried again before measuring the dry mass. Rock samples of approximately 30 g were obtained by cutting pieces from the drill segments. Samples were dried in an oven at 105°C for 24 hours, then transferred to a desiccator containing silica gel to prevent the sample from picking up atmospheric moisture while cooling. The sample was suspended from a hook below a balance (Sartorius LP1200S) and the mass measured. All masses used in the calculations were mean values from triplicate measurements. After weighing, the sample was returned to the oven for a further 24 hours. This process was repeated until the change in the mass between readings was less than 0.01%. The final mass measurement was taken as the dry mass, m_{dry}.

Samples were placed in individual beakers of distilled water (Cobourg samples) or kerosene (Queenston samples) and placed in a vacuum chamber. The chamber was evacuated using a vacuum pump and the samples held under vacuum to enhance the rate of saturation. At intervals of 1 to 3 days, the samples were removed from the chamber and their mass measured while suspended in the beaker of the saturating fluid (water or kerosene).

Each sample was also removed from the beaker and the mass measured while suspended in air. Before weighing in air, the outside of the sample was gently dabbed with a paper towel to remove any clinging drops of fluid. Samples were then returned to the beakers of liquid and placed inside the vacuum chamber once more. The final measurements of saturated mass (m_{sat}) and submerged mass (m_{sub}) were obtained when the change between daily readings was less than 0.01%.

Water loss porosity (ϕ_w) was calculated using the equation:

$$\phi_w = \frac{v_1}{v_2} = \frac{m_{sat} - m_{dry}}{m_{sat} - m_{sub}} \qquad (15)$$

where v_1 is the volume of imbibed liquid and v_2 is Archimedes' bulk volume, using the mass terms defined above.

The mass measurements may also be used to calculate grain density (ρ_{gr}), if the density of the saturating fluid (ρ_{fl}) is known:

$$\rho_{gr} = \frac{m_{dry}}{v_2 - v_1} = \frac{m_{dry}}{m_{dry} - m_{sub}/\rho_{fl}} \tag{16}$$

4.1.2 Synthetic pore waters

For the Queenston samples, a simplified SPW was derived from aqueous crush and leach test data that were available for samples from 105 and 111 m depth (Koroleva and Mazurek 2006) and mineralogical observations. The major ions present in the aqueous extract were sodium and chloride. The leach test data (at a solid:liquid ratio of 1:1) were used to estimate pore water concentrations using the expression:

$$C_{pore\,water} = \frac{C_{rock} \cdot \rho_{gr}(1 - \phi_w)}{\phi_w} \tag{17}$$

where $C_{pore\,water}$ is the concentration of an ion in the original pore water, C_{rock} is the concentration of the ion in mol/kg rock from the aqueous leaching data, and ϕ_w is the water loss porosity.

Equilibrium geochemical speciation modelling of the estimated pore water composition using the PHREEQC 2.12.5 software and pitzer.dat thermodynamic database (Parkhurst and Appelo 1999) indicated that the pore water compositions would be supersaturated with respect to halite and highly supersaturated with respect to gypsum and anhydrite using the estimate of 4% porosity given by Koroleva and Mazurek (2006). This could lead to problems if the SPW were to precipitate halite and gypsum in the pores before the diffusion test. Mineralogical studies did not find halite in the pore spaces (Appendix B), but did find anhydrite nodules present in the rock (Appendix B, Koroleva and Mazurek 2006).

As is evident from equation 17, the estimates of pore water composition are strongly dependent on porosity measurements. Pore water compositions were recalculated using our water loss porosity estimate of 6% for the Queenston formation (Section 5.1). These results are given in Table 2.

The pore water composition estimates in Table 2 were used as the basis for choosing a 3.0 M NaCl brine as the SPW. The solution is undersaturated with respect to halite, but still supersaturated with respect to anhydrite and gypsum. Concentrations of sulfate in the pore water may be overestimated because of the possible oxidation of pyrite in the rock. For the SPW, a lower concentration of $CaSO_4$ of 0.05 M was added to bring the solution close to equilibrium, but not supersaturated, with respect to anhydrite (See Table 3).

Pore water data were not available for the Cobourg samples. A crush and leach test was therefore conducted on the sample from 36 m depth to obtain an SPW composition. Small pieces of rock were cut from the core during preparation of the diffusion test samples. These offcuts were crushed with a steel piston crusher and then finely ground with an agate mortar and pestle. The ground material was sieved through a 105 µm mesh size polyethylene mesh

and 50.93 g was weighed out into a 125 mL nalgene plastic bottle. Deionized water (50.93 g) was added to the powdered rock and the sample was capped and shaken horizontally on a wrist-action shaker for 48 hours. After shaking, the leach test sample was left overnight for the fine particles to settle, then decanted and the supernatant liquid filtered through a 0.45 µm nylon filter. Approximately 30 mL were extracted and submitted for analysis of major cations and anions (RPC laboratories, Fredericton). Pore water composition estimates (Table 2) were obtained using equation 17, the aqueous leach test data and gravimetric results of 2.92% porosity and 2.71 g/cm^3 grain density from this study. Modelling with PHREEQC Pitzer data found that the pore water composition estimates were supersaturated with respect to calcium and magnesium carbonate minerals as well as gypsum and anhydrite.

A mixed cation composition containing sodium, calcium, magnesium and potassium, balanced by the chloride anion was used to mimic the pore water for the Cobourg Formation. Sulfate and carbonate salts were not included in the SPW to avoid possible precipitation problems when combining these anions with calcium and magnesium in the solution.

Potassium iodide tracer solutions for the Queenston and Cobourg Formations were prepared using the SPW compositions, but substituting molar quantities of KI for NaCl.

Table 2: Estimated pore water compositions from aqueous crush and leach tests on Queenston and Cobourg Formation samples

	Estimated pore water concentrations (mol/L)	
	Queenston Formation	**Cobourg Formation**
	Sample 346 & 364 mean	**Sample C036_1**
Na	2.57	1.22
Ca	0.36	0.31
Mg	0.08	0.18
K	0.22	0.15
Sr	0.003	Not determined
F	0.15	Not determined
Cl	3.38	2.08
SO_4	0.19	0.10
HCO_3	Not determined	0.13
Br	0.02	Not determined
Ionic strength (PHREEQC)	5.80	3.44

Table 3: Synthetic pore water compositions and KI tracer compositions used in the diffusion experiments

	SPW composition (mol/L)	
	Queenston Formation	**Cobourg Formation**
NaCl	3.00	1.20
$CaCl_2$	-	0.30
$MgCl_2$	-	0.20
KCl	-	0.15
$CaSO_4$	0.05	-
Ionic strength (PHREEQC)	3.91	3.29
	Tracer composition (mol/L)	
	Queenston Formation	**Cobourg Formation**
NaCl	2.40, 2.20 or 2.00	0.20
$CaCl_2$	-	0.30
$MgCl_2$	-	0.20
KCl	-	0.15
$CaSO_4$	0.05	-
KI	0.60, 0.80 or 1.00	1.00

4.1.3 Calibration curve for potassium iodide

Calibration curves were prepared to quantify the relationship between Δμ and iodide concentration. This relationship could then be used to determine spatially distributed iodide tracer concentrations from measured Δμ values in the diffusion samples. Separate curves were generated for the Queenston and Cobourg samples using standard solutions of known KI concentration in a brine matrix that matched the SPW composition for each rock type.

X-ray radiographs were taken of the standard solutions in glass vials using the same instrumental settings as used for diffusion radiographs on rock samples. Data were corrected for possible fluctuations in the X-ray source energy using an internal standard. Blank subtraction was then used to remove the effects of attenuation by the glass vial and other aqueous components (water and SPW brine) so that the measured change in attenuation coefficient, Δμ is a function of the quantity of iodide present in each standard. A quadratic function was fitted through the data points. The calibration procedure used was as follows:

1). Standard solutions of KI ranging in concentration from 0 M (Blank = SPW) to 1 M were prepared by substituting KI for NaCl in SPW solutions (See compositions in Table 3).
2). The standard solutions were transferred to 2 mL glass vials with an Al wire internal standard mounted on one side of the vial.
3). Each vial was mounted on a brass pedestal sample holder, using double-sided tape and positioned in the microCT sample chamber. The sample holder was rotated to align the internal standard along the right hand side of the radiograph.

4). Radiographs of the blank and standard solutions were collected using the same data collection settings as for diffusion test samples.

5). ImageJ v1.36 public domain software (National Institutes of Health, USA) was used to analyze the radiograph images (Figure 5). The mean greyscale intensity of a region of interest (ROI) on the internal standard (Al wire) was measured to obtain a normalization ratio for the greyscale intensity of all images relative to the blank. The normalization ratio for each standard was defined as:

$$N_{Std} = \frac{\ln\left(\overline{gsv}_{Al}\right)_{Blk}}{\ln\left(\overline{gsv}_{Al}\right)_{Std}} \qquad (18)$$

where $\overline{gsv}_{Al}$ is the mean greyscale value for an identically-sized ROI over the Al internal standard attached to the side of the vial of the blank (Blk) and the standard (Std) solutions.

6). The images were cropped to an identical rectangular ROI over the sample vial for each standard solution. The mean greyscale value and standard deviation for each solution was measured and the data exported to a spreadsheet. Mean greyscale values for the solutions were normalized by multiplying by N_{std} after taking the natural logarithm of each value.

7). Normalized values for each standard solution were converted to $\Delta\mu$ by subtracting the natural logarithm of the mean greyscale value for the blank.

8). A plot $\Delta\mu$ vs. KI concentration was prepared and a trend line fitted to determine the calibration function. Calibration functions for the Queenston and Cobourg samples are shown in Figure 6.

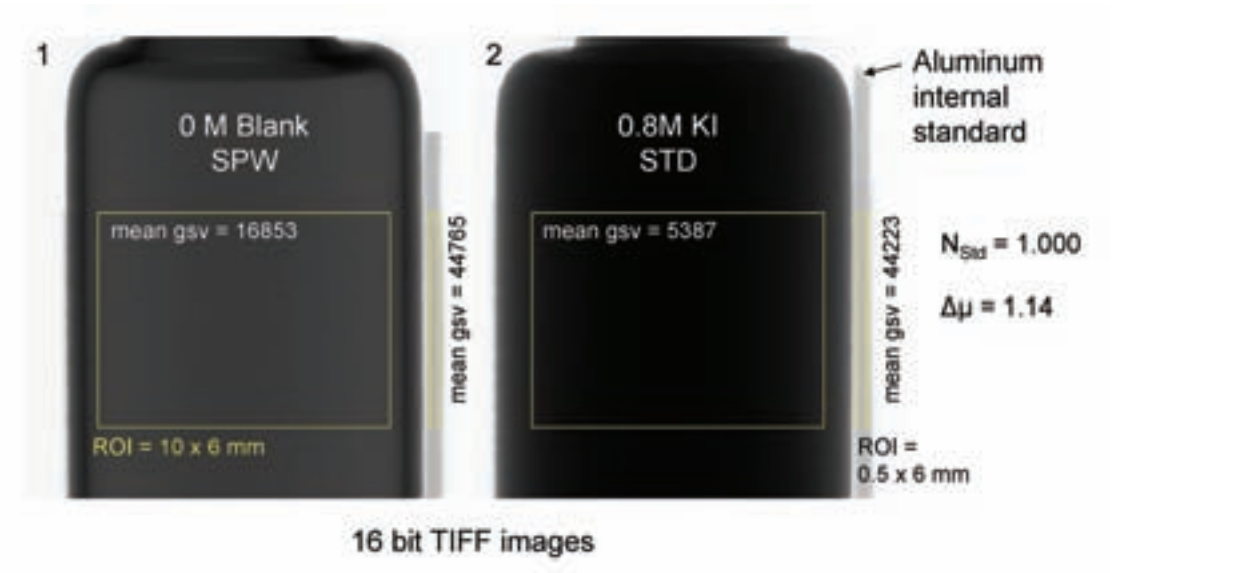

Figure 5: Radiographs of the blank and 0.8 M KI calibration standard for the Queenston Formation in glass vials, indicating examples of regions of interest where greyscale values were measured to calculate the normalization ratio and Δμ.

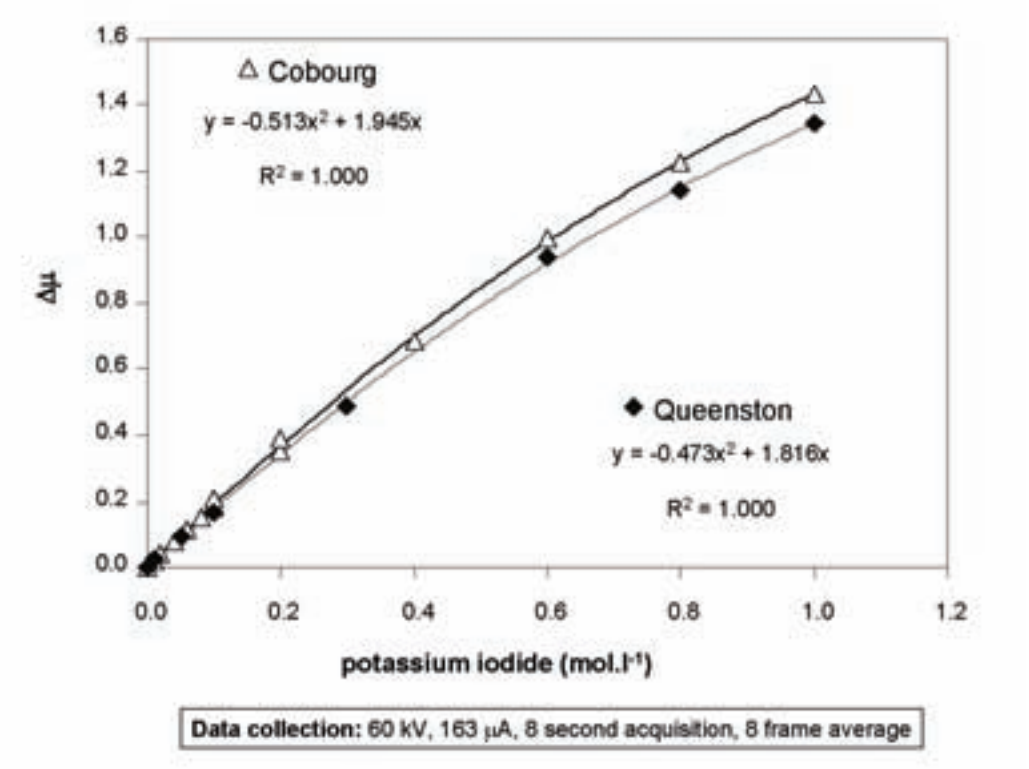

Figure 6: Calibration curves for Δμ versus KI concentrations measured on aqueous solutions in a synthetic pore water matrix for the Queenston and Cobourg Formations.

The glass vials have an internal diameter of approximately 10.5 mm. This means that the X-ray path length through an aqueous solution inside the vial is similar to the path length through the 11 mm diameter rock samples used for the diffusion experiments. Taking the porosity into account, the KI concentrations in the pore space of the rock during the diffusion experiment can be obtained from measurements of mean Δμ for each distance step along the diffusion pathway. Because the measured values of Δμ are low for the low porosity Cobourg Formation samples, additional calibration points were measured in the concentration range <0.1 M KI. The method for the diffusion measurements is explained in detail in Section 4.5.1.

4.2 SAMPLE PREPARATION AND HANDLING

Diffusion experiments were conducted on small cylindrical mini cores mounted in custom-made aluminum diffusion cells designed to be accommodated in the microCT instrument.

The original rock cores were sliced in light oil (Queenston Formation) or water (Cobourg Formation) and cylinders of diameter 11 mm and length 15 to 25 mm were drilled through the slices. These mini core cylinders were drilled using a drill press and diamond-tipped core drill bit (Technodiamant) with cooling fluid (kerosene or water) circulated through the centre of the bit. Cobourg Formation samples were prepared in pairs with two mini cores cut from the same core slice, one parallel and one normal to the bedding planes to investigate effects of anisotropy on diffusion properties (Figure 7). Queenston Formation samples were also

prepared parallel and normal to bedding, but the position of the samples could not be as carefully matched within a core slice as for the Cobourg samples. The tendency of the rock to break commonly necessitated several drilling attempts before an intact Queenston shale sample was obtained.

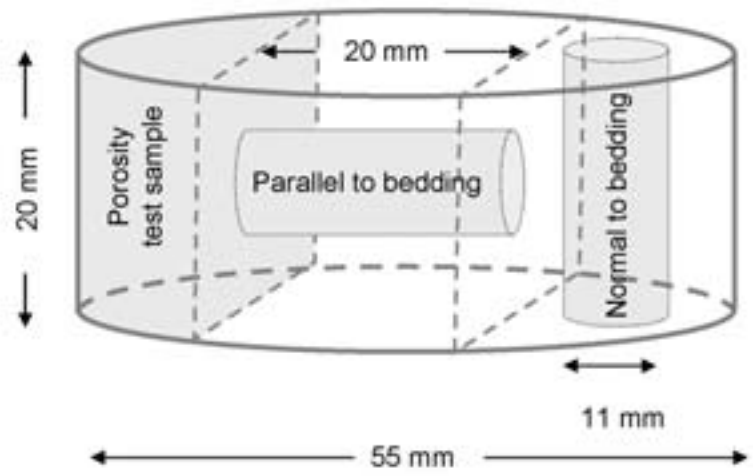

Figure 7: Samples cut from core slices for diffusion experiments and water loss porosity measurements.

The mini core samples were dried with paper towel and left to air dry overnight. Rough edges were smoothed off with 180 grit garnet sandpaper and rinsed off with kerosene or water. The samples were then oven-dried (65°C) for at least 24 hours before coating with epoxy.

The samples were coated by painting with a layer of PRESI Mecaprex MA2 epoxy around the curved side, leaving the flat top and bottom ends uncoated. Several different types of epoxy were tested for possible reaction with the iodide or brine solutions before selecting this brand. The epoxy is sensitive to humidity and samples must be kept in a dry environment for the coating to harden properly. The epoxy seal was hardened by returning the samples to a 65°C oven for 4 hours or by clamping the samples over a hot plate set at a low heat setting overnight.

The top and bottom ends of the mini cores were then fixed in position in aluminum reservoirs and sealed around the joins with epoxy to create the diffusion cells (Figure 8). A piece of aluminum wire (0.635 mm diameter) was mounted with epoxy on the side of each sample to act as an internal standard and alignment guide. The wire was tested on early samples (Queenston), but in later samples (Cobourg) was replaced by a small sheet of aluminum metal (1.5 mm thick). The sheet was preferred for radiographs because it provides a larger area of constant thickness for determining a normalization ratio. The cylindrical geometry of the wire is better suited for three dimensional reconstruction of CT scans.

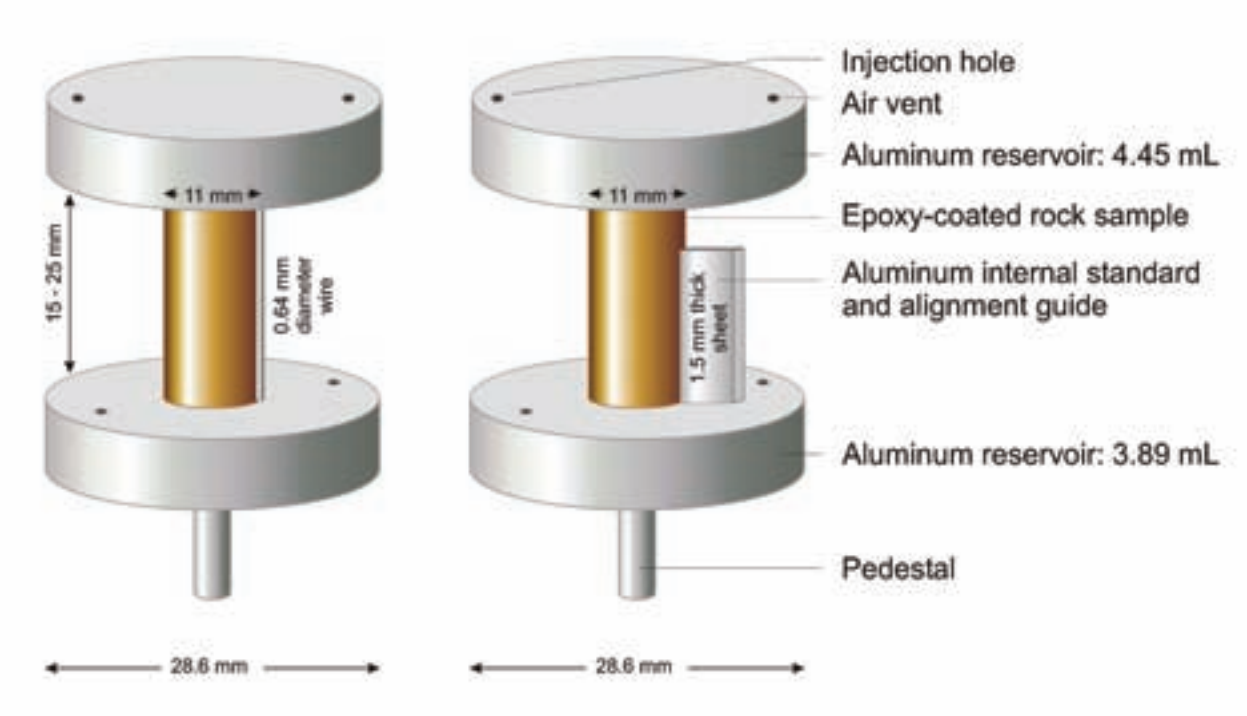

Figure 8: Diffusion cells with mini core rock samples for X-ray imaging experiments using the Skyscan 1072 Desktop MicroCT system.

The rock surface in contact with the solutions in the cells must be uncoated to allow for diffusion into the sample. After curing, any epoxy that seeped onto the top or bottom faces of the cylinder was gently sanded away and the samples rinsed with deionized water. Samples prepared for this study are listed in Table 4.

Table 4: Sample descriptions

Queenston Formation			Cobourg Formation		
Sample	**Core Depth (m)**	**Orientation relative to bedding planes**	**Sample**	**Core Depth (m)**	**Orientation relative to bedding planes**
Q078NB1	78	Normal	C036NB1	36.325	Normal
Q078NB2	78	Normal	C036PB1	36.325	Parallel
Q078NB3	78	Normal	C036NB2	36.300	Normal
Q078NB4	78	Normal	C036PB2	36.300	Parallel
Q105NB	105	Normal	C036NB3	36.275	Normal
Q105PB	105	Parallel	C036PB3	36.275	Parallel

For the initial reference image measurements (blanks), the samples were submerged for several days in a SPW solution. The caps for the diffusion cell reservoirs were removed and the rock sample submerged in a beaker of the appropriate SPW, placed inside a vacuum chamber. A vacuum was applied to accelerate the rate of saturation. Observations from the porosity test were used to estimate how long the samples should take to saturate, but the mass of the samples was also determined periodically to monitor their saturation status. Queenston Formation samples were submerged in synthetic porewater for 11 days and Cobourg samples for 23 to 40 days before collecting the reference image radiographs.

Before X-ray data collection, the diffusion cells were capped and the rim covered with electrical tape to seal the cells. Additional SPW solution was injected through the holes in the reservoir caps to ensure that the reservoirs were full and the injection and vent holes covered with small pieces of electrical tape. The outside of the reservoir was rinsed with deionized water and gently dried with paper towel to remove any salt solution on the outside of the sample and reservoirs. Samples were then ready to be placed in the microCT for radiography.

Between data collection times, the samples were stored upright on a wooden sample holder in a closed plastic container. An open shallow dish of water and sponge were kept in the container to maintain the humidity level and minimize evaporation of the solutions from the diffusion cell reservoirs. The samples were stored in the X-ray laboratory where the temperature is controlled at 22 ± 1 °C.

4.3 DIFFUSION TRACER EXPERIMENTS

The rate of diffusion in rock samples was monitored by conducting tracer tests using KI solutions of known concentration in a SPW matrix. During the tracer tests, periodic measurements of iodide tracer concentrations versus distance along the sample were acquired using the radiography technique.

4.3.1 Reference image

A sample fully-saturated with SPW was placed in the microCT sample chamber for acquisition of the reference image. The sample position was adjusted and rotated to align the guide wire in the centre of the field of view using the internal optical camera. This positions the wire on the side of the sample (no overlap with the rock) in the radiographs, which are collected at 90° to the optical images. The reference radiograph image was collected and the sample was removed from the microCT after a suitable image was saved. In ongoing development of the technique, reference images are collected immediately after injection of the tracer as described in Section 4.3.2. This is done so that X-ray absorption measurements near the influx boundary are not affected by blank subtraction artefacts, arising from the subtraction of a time series image with concentrated iodide solution (tracer) in the reservoir from a reference image with iodide free solution (SPW) in the reservoir.

4.3.2 Tracer injection and time series images

To begin the diffusion experiment, the lower reservoir was filled with a KI tracer solution of known concentration and matching ionic strength to the SPW. The KI tracer solution was injected slowly by syringe (1 to 2 mL/minute) into the bottom of the lower reservoir, using a paper towel to wick away the displaced solution from the air vent hole. At least three times the volume of the reservoir (typically 12 to 20 mL) was flushed through to displace the SPW

solution completely with the tracer solution. The injection and vent holes were sealed with electrical tape and the outside of the reservoir rinsed with deionized water. The time of the injection was marked on the diffusion cell as the start time for the experiment and all time series measurements were benchmarked to this time.

During the diffusion phase of the experiment, the upper reservoir remained filled with iodide-free SPW. The KI tracer solutions were refreshed regularly (every 3 to 7 days) in an attempt to maintain constant concentrations in the reservoir at the diffusion boundary. Solutions were refreshed by injecting a quantity (5 to 10 mL) of fresh tracer solution to displace the solution in the lower reservoir.

Taking a hypothetical sample of 2 cm length, 11 mm diameter and uniform 6% porosity and estimating the tracer flux out of a 4 mL reservoir containing 0.6 mol/L iodide tracer and a relatively fast diffusion rate of 1×10^{-10} m^2/s, we derived a conservative estimate for the maximum loss of tracer from the reservoir between solution changes. The calculation is made by dividing the sample into 0.1 mm increments and accumulating the iodide mass in each incremental volume based on the theoretical C/C_0 curves for a 7 day time step. Using this approach, we estimated that 2.9×10^{-5} mol iodide diffuses out of the reservoir into the rock after 7 days. This represents a change in the iodide mass in the reservoir of 1.2%. This change in iodide mass is small enough that the reservoir concentration may be considered constant.

Time-series radiographs were collected at increasing time intervals as the tracer diffused upwards through the rock. For each time step, the sample was placed in the X-ray chamber and returned to the same position used for the reference image, before collecting and saving a radiograph. Time series images were collected for the Queenston Formation samples after 1, 4, 8, 24, 48, 120, 170, 314, 384, 528 and 840 hours. Radiographs for Cobourg Formation samples were collected after 22, 46, 119, 215 and 383 hours. For two of the Cobourg Formation samples (C036NB3 and C036PB3), complete CT scans were run and radiographs extracted for processing at the time intervals 24, 52, 96, 192, 288 and 456 hours after the start of the experiment. Radiographs were processed following the procedures outlined in Section 4.5.1.

4.3.3 Final iodide-saturated image

Once the radiography processing indicated that iodide had broken through to the upper reservoir, the SPW in the upper reservoir was also replaced by KI tracer solution. Replacing the SPW solution allowed iodide to diffuse in from both ends, to speed up the time until the sample is saturated with iodide. During this phase, the solutions in both reservoirs were refreshed at intervals of approximately one week.

Radiograph images of the sample were collected at one week intervals and processed to monitor the progress of iodide saturation. Once no further changes were observed, and the iodide profile was constant along the entire length of the sample, a final radiograph (I^-_{sat} image) of the iodide-saturated sample was acquired.

4.4 DATA COLLECTION

Data were collected as 2-D radiographs, where the greyscale intensity at each pixel is proportional to the transmitted X-ray intensity (I) along a path between the source and the

detector. All images were collected and saved in digital format, using a 16bit TIFF image file format, which allows up to 65536 distinct greyscale values. The higher greyscale values are represented by light areas (less X-ray absorption) and the lower values by dark areas (more X-ray absorption) in the images.

Consistent sample positioning and instrumental settings (Table 5) were used throughout the experiment to allow for comparison of time series data. After setting the X-ray source parameters and acquisition time, a flat field image (without sample present) was collected and stored in memory to correct the background in later radiographs.

Table 5: Instrumental settings used to collect X-ray radiographs

Parameter	Setting	Parameter	Setting
Source potential	60.6 kV	Flat field correction	On
Source current	163.4 µA	Magnification	14 x
Source filter	1 mm Al	Pixel size	18.68 µm
Acquisition time	7952 ms	Sample height	6 mm
Frame averaging	8 frames	Rotation	Align guide with right side of radiograph
Total acquisition	64 s		

4.5 DATA ANALYSIS

As described in section 4.1.3, radiograph images were processed with ImageJ v 1.36, a Java-based open source image processing application. ImageJ is public domain software developed by the National Institutes of Health, USA and supports a wide range of image processing and analysis functions (Rasband 2006).

4.5.1 Pore diffusion coefficients

The data processing steps are illustrated in Figure 9 using an example.

Step 1: The image scale was set to 18.68 µm per pixel for all radiograph image processing.

Step 2: Each radiograph was rotated approximately 90 degrees to position the diffusion axis horizontally in the images.

Step 3: For each set of radiographs taken of a particular sample, the images were cropped to an identical rectangular region of interest (ROI) over the rock. The position of the ROI was checked by image subtraction of the time series images from the reference image. This allows a visual inspection of the symmetry about the rock cylinder axis and alignment of the pixels for any distinctive features in the images.

Step 4: Once the matching ROIs were selected, profiles of mean greyscale intensity versus distance along the diffusion pathway were plotted. In a manner similar to that described previously for calibration standards, the greyscale intensity of the Al internal standard was used

to normalize the greyscale data for all time series images and iodide-saturated images relative to the reference image for a particular sample.

Step 5: Normalized ln(gsv) profiles were used to calculate profiles of $\Delta\mu$ (change in X-ray absorption coefficient) vs distance for each time step, by subtracting the time series profiles or iodide-saturated profiles from the reference profiles for each sample.

Step 6: Values of $\Delta\mu$ were used to calculate values of C/C_0 for iodide that were plotted versus distance along the direction of diffusion. There are two different techniques which were used for calculating C/C_0 in this study (see also section 2.2):

a) *Relative technique:* The $\Delta\mu$ values for the time series profiles were divided by the $\Delta\mu$ values for the iodide-saturated profiles to obtain C/C_0 profiles using equation 14. This is the method illustrated in Step 6 of Figure 9 and is effectively a two point iodide calibration using the $\Delta\mu$ values for zero iodide and tracer iodide concentration. If iodide-saturated data were not available for a sample, the value of $\Delta\mu$ near the influx boundary for a late time series profile was used to scale the profiles, assuming $C/C_0 \approx 1$ at this position at late time. This was done for samples Q078NB1 to Q078NB4 which were not run to iodide-saturation.

b) *Calibrated technique:* The value of C was determined directly from $\Delta\mu$ using the multipoint calibration curve prepared from iodide standard solutions (see Section 4.1.3). The concentration data were scaled up to the concentrations in the pores by dividing by ϕ_w. The relative concentration at each point in the profile was then obtained by dividing by C_0, the original concentration of iodide in the tracer reservoir.

The profiles of C/C_0 versus distance were used to fit an analytical solution of Fick's Second Law (equation 2) to find the D_p value. Plots of C/C_0 versus x were prepared using the t values for the time steps at which radiographs were collected. The value of D_p was then estimated and adjusted to obtain a good fit with the observed C/C_0 profiles by visual inspection. The curve-fitting required a shifting of the analytical profiles in the –x direction to account for the first few mm of the sample near the influx boundary, which are inside the diffusion cell and do not appear in the radiographs. The D_p values were multiplied by ϕ_l (or ϕ_w) to give the effective diffusion coefficients, D_e.

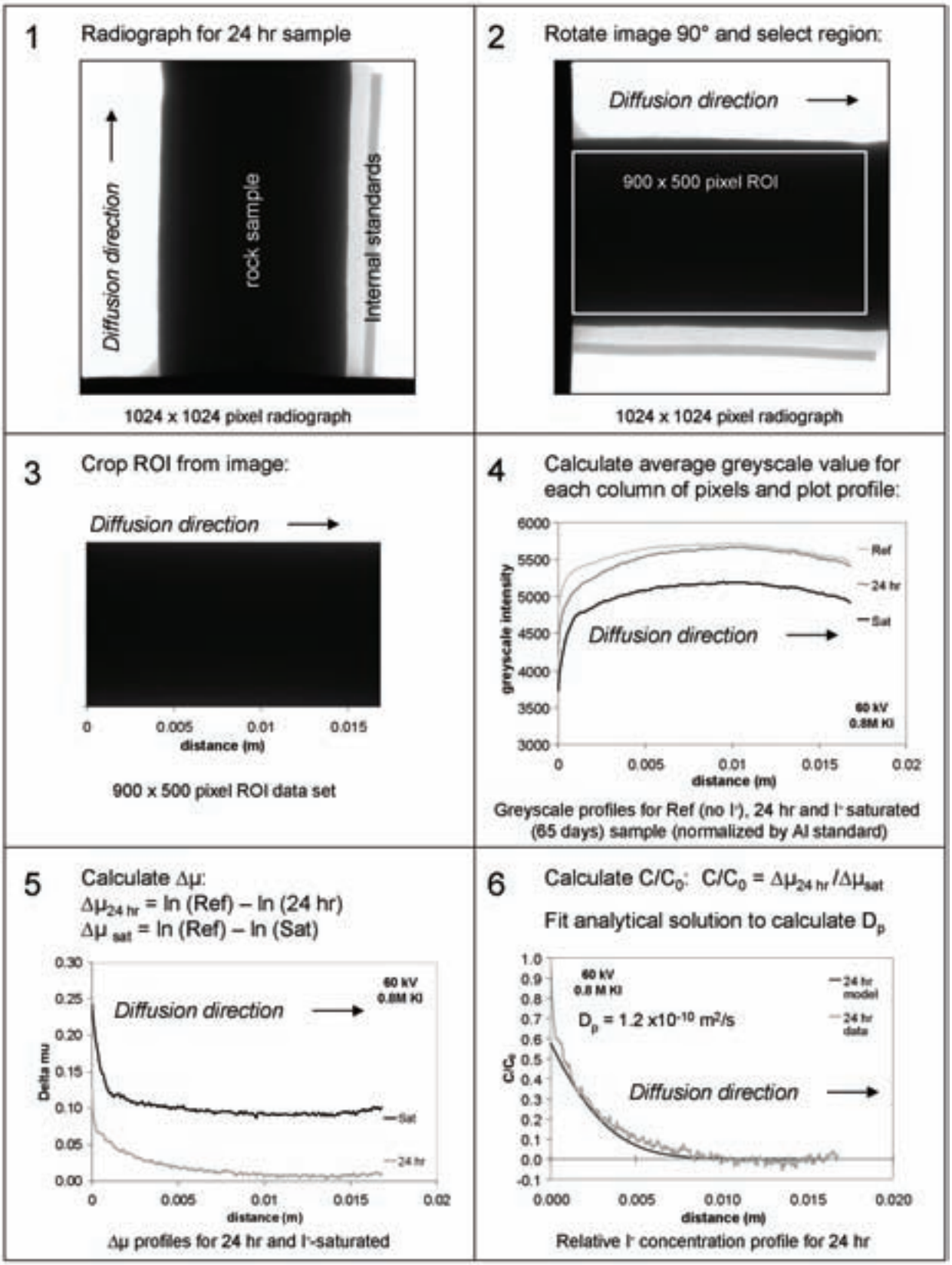

Figure 9: Data processing to determine diffusion coefficients from radiographs.

4.5.2 1-D Porosity distribution

Using blank subtraction, the radiograph image of a sample that is fully saturated with iodide tracer provides an X-ray attenuation map of the iodide distribution in the rock, and hence the distribution of rock porosity. With a cylindrical sample, these cannot be interpreted directly as two dimensional porosity maps, because of the changes in sample thickness across the field of view, but the iodide-saturated images can be processed to give a one-dimensional profile of the changes in porosity with distance along the axis of the cylinder.

Profiles of $\Delta\mu_{sat}$ were determined from the greyscale profiles of the reference and iodide-saturated radiographs as described in Steps 1 to 5 in the previous section. The $\Delta\mu_{sat}$ values were then used to calculate 1-D iodide-accessible porosity versus distance profiles. At each point (i) in the $\Delta\mu_{sat}$ profile, the value of $\Delta\mu$ gives a measure of the mass of iodide tracer in the rock pores at that point in the profile, which can be calculated from the calibration curve (Section 4.1.3, Figure 6). Taking the ratio of the mass of iodide in the pores (assuming full saturation) to the known mass of iodide in the tracer solution (at 100% porosity), gives an estimate of the path length occupied by saturated pores at each point in the profile, i.e. the iodide-accessible porosity:

$$\phi_i = \frac{m_{i\ sat}}{m_0} \qquad (19)$$

Where ϕ_i is the iodide accessible porosity value at point i in the profile, $m_{i\ sat}$ is the calculated mass of iodide at the same point from the quadratic calibration function and m_0 is the mass (or concentration) of iodide in the aqueous tracer solution. The 1-D porosity distribution profiles provide an independent measure of porosity in the sample.

5. RESULTS

5.1 WATER LOSS POROSITY

Gravimetric water loss porosity (ϕ_w) measurements were made on eight samples of Queenston shale and three samples of Cobourg limestone using the method described in Section 4.1.1. Results for the porosity measurements are reported in Table 6 and Table 7. For comparison, the tables also include data for samples from the same drill cores determined by a modified water immersion method (Vilks and Miller 2007), which is very similar to the gravimetric method used in this study. The comparison samples used water, not kerosene, for immersion of Queenston shales.

Table 6: Water loss porosity measurements for Queenston shale samples

Core depth	**78 m**	**88 m**	**93 m**	**105 m**
Porosity (%)				
Sample 1	6.34	6.03	4.96	5.82
Sample 2	5.99	6.01	4.80	5.94
Mean porosity	6.16	6.02	4.88	5.88
Grain density (g/cm^3)[1]	2.83	2.82	2.79	2.83
Comparison samples (Vilks and Miller 2007)				
Core depth	**84.0 m**	**93.4 m**	**101.7 m**	**104.8 m**
Porosity (%)				
Sample 1	6.14	7.08	6.77	6.25
Sample 2	7.05	-	7.05	6.08
Mean porosity	6.59	7.08	6.91	6.16
Grain density (g/cm^3)	2.81	2.80	2.82	2.77

[1] calculated using a density of 0.810 g/cm^3 for kerosene.

Table 7: Water loss porosity measurements for Cobourg limestone samples

Sample ID **Core depth**	**C036_3** **36.275 m**	**C036_2** **36.300 m**	**C036_1** **36.325 m**
Porosity (%)	2.96	1.04	3.03
Grain density (g/cm^3)	2.71	2.70	2.67
Comparison samples (Vilks and Miller 2007)			
Sample ID **Core depth**	**Core #4** **36 m**	**Core #9** **36 m**	**Core #10** **36 m**	**Rectangle*** **36 m**
Porosity (%)	1.48	1.49	2.00	1.87
Grain density (g/cm^3)	2.72	2.72	2.72	2.72

*Sample ID as given in Vilks and Miller, 2007

Both laboratories found that the archived Queenston shale has higher ϕ_w than the Cobourg limestone. The Cobourg limestone samples are very heterogeneous so the comparison between UNB and AECL data may be misleading. The porosity may vary both within and between samples containing varying amounts of fossiliferous and argillaceous material. Mean and standard deviation values for each rock type from all the gravimetric measurements are 6.15 ± 0.67% for Queenston shales and 1.98 ± 0.76 % for Cobourg limestones.

5.2 DIFFUSION COEFFICIENTS

A summary of the estimated pore water and effective diffusion coefficients is presented in this section. Table 8 presents the iodide diffusion parameters for the Queenston shale samples and Table 9 presents the iodide diffusion parameters for the Cobourg limestone samples (as D_p and D_e). The tables compare radiography measurements made in this study with conventional through-diffusion measurements made by Vilks and Miller (2007) on adjacent rock samples from the same archived cores.

The diffusion coefficients obtained by radiography were found to vary at different time steps in the experiment.(See Section 6.3.2 below for an explanation of this phenomenon). Diffusion coefficient data in Tables 8 and 9 summarize the D_p estimates for the latest time step before the iodide tracer breaks through to the upper reservoir, which we consider the most accurate data. Concentration profiles, fitted analytical solutions and diffusion coefficients for all time steps for the radiography samples are included in Appendix D.

Mean values of ϕ_I from radiographic profiles (or ϕ_w when ϕ_I was not available) were used to calculate D_e from the D_p values measured using radiography and ϕ_d values were used to calculate D_p from D_e values measured by AECL using through-diffusion (equation 5). It should be noted that only four of the through-diffusion experiments, Q089NB1, Q089NB2, C056NB1 and C056NB2, were conducted using the same tracer composition in SPW as the radiography samples (1.0 M KI in Queenston or Cobourg SPW). A comparison of the two data sets (radiography and through-diffusion) for D_p values is also made in Figure 10.

Table 8: Iodide diffusion parameters for Queenston shale samples

Radiography					
Sample	**Iodide D_p m^2/s**	**Iodide D_e m^2/s**	**Mean ϕ_w %**	**Mean ϕ_I %**	**Tracer**
Q078NB1	9.0×10^{-11}	5.5×10^{-12}	78 m: 6.16	-	0.6 M KI
Q078NB2	4.0×10^{-11}	2.5×10^{-12}		-	0.6 M KI
Q078NB3	6.0×10^{-11}	3.7×10^{-12}		-	1.0 M KI
Q078NB4	5.0×10^{-11}	3.1×10^{-12}		-	1.0 M KI
Q105NB	2.0×10^{-11}	1.1×10^{-12}	105 m: 5.88	5.7	0.8 M KI
Q105PB	3.0×10^{-11}	1.9×10^{-12}		6.2	0.8 M KI
Shale (mean ± s.d.)	$(4.8 \pm 2.5) \times 10^{-11}$	$(3.0 \pm 1.5) \times 10^{-12}$	5.73 ± 0.54[a]	6.0 ± 0.4	

Through-diffusion (Vilks and Miller 2007)					
Sample	**Iodide D_p m^2/s**	**Iodide D_e m^2/s**	**Mean ϕ_w %**	**ϕ_d %**	**Tracer**
Q078NB1	3.1×10^{-11}	1.3×10^{-12}	-	4.1	0.06 M NaI
Q078NB2	3.7×10^{-11}	1.7×10^{-12}	-	4.5	0.06 M NaI
Q084NB	2.1×10^{-11}	1.0×10^{-12}	-	4.9	0.06 M NaI
Q089NB1	6.8×10^{-11}	2.4×10^{-12}	-	3.6	1.0 M KI
Q089NB2	8.2×10^{-11}	2.6×10^{-12}	-	3.1	1.0 M KI
Q105NB1	3.0×10^{-11}	8.7×10^{-13}	-	2.9	0.06 M NaI
Q105NB2	3.3×10^{-11}	1.1×10^{-12}	-	3.4	0.06 M NaI
Q087PB	7.0×10^{-11}	1.6×10^{-12}	-	2.4	0.06 M NaI
Q096PB	3.9×10^{-11}	9.4×10^{-13}	-	2.4	0.06 M NaI
Shale (mean ± s.d.)	$(4.6 \pm 2.0) \times 10^{-11}$	$(1.5 \pm 0.6) \times 10^{-12}$	6.63 ± 0.48[b]	3.5 ± 0.9	

Notes: Sample identifiers indicate rock type, depth and orientation: Q = Queenston; 078 = 78 m below surface; NB = normal to bedding, PB = parallel to bedding. Final digit denotes replicate samples.

ϕ_w = water loss porosity; ϕ_d = diffusion accessible porosity for iodide; s.d. = standard deviation.

[a] Mean of 8 adjacent shale samples from 78 to 105 m from kerosene immersion method (UNB).

[b] Mean of 7 adjacent shale samples from 84 to 104 m from water immersion method (AECL).

- indicates where no measurements were available.

Table 9: Iodide diffusion parameters for Cobourg limestone samples

Radiography					
Sample	**Iodide D_p m^2/s**	**Iodide D_e m^2/s**	**Mean ϕ_w %**	**Mean ϕ_I %**	**Tracer**
C036NB1	4.5×10^{-11}	1.4×10^{-12}	3.03	3.0	1.0 M KI
C036PB1	2.0×10^{-11}	6.2×10^{-13}		3.1	1.0 M KI
C036NB2	2.5×10^{-11}	4.8×10^{-13}	1.04	1.9	1.0 M KI
C036PB2	2.5×10^{-11}	7.5×10^{-13}		3.0	1.0 M KI
C036NB3	2.5×10^{-11}	8.3×10^{-13}	2.96	3.3	1.0 M KI
C036PB3	1.5×10^{-11}	3.5×10^{-13}		2.3	1.0 M KI
Limestone (mean ± s.d.)	$(2.6 \pm 1.0) \times 10^{-11}$	$(7.3 \pm 3.5) \times 10^{-13}$	2.34 ± 1.13	2.8 ± 0.5	

Through-diffusion (Vilks and Miller 2007)					
Sample	**Iodide D_p m^2/s**	**Iodide D_e m^2/s**	**Mean ϕ_w %**	**ϕ_d %**	**Tracer**
C036NB1	1.7×10^{-11}	2.0×10^{-13}	-	1.2	0.06 M NaI
C036NB2	2.2×10^{-11}	9.5×10^{-14}	-	0.4	0.06 M NaI
C036NB3	3.0×10^{-11}	1.6×10^{-13}	-	0.5	0.06 M NaI
C044NB	3.0×10^{-11}	4.2×10^{-13}	-	1.4	0.06 M NaI
C056NB	3.4×10^{-11}	3.8×10^{-13}	-	1.1	0.06 M NaI
C056NB2	4.6×10^{-11}	1.4×10^{-12}	-	3.0	1.0 M KI
C056NB3	4.7×10^{-11}	6.2×10^{-13}	-	1.3	1.0 M KI
C036PB	1.8×10^{-11}	2.8×10^{-13}	-	1.5	0.06 M NaI
C044PB	7.2×10^{-10}	7.0×10^{-12}	-	9.7	0.06 M NaI
Limestone (mean ± s.d.)	$(3.5 \pm 1.8) \times 10^{-11}$	$(1.2 \pm 2.2) \times 10^{-13}$	1.71 ± 0.27[a]	3.4 ± 6.4	
Excluding C044PB	$(3.1 \pm 1.2) \times 10^{-11}$	$(4.4 \pm 4.1) \times 10^{-13}$		1.3 ± 0.8	

Notes: Sample identifiers indicate rock type, depth and orientation: C = Cobourg; 036 = 36 m below surface; NB = normal to bedding, PB = parallel to bedding. Final digit denotes replicate samples.

ϕ_w = water loss porosity; ϕ_d = diffusion accessible porosity for iodide; s.d. = standard deviation.

[a] Mean of 4 samples from 36 m depth by water immersion method (AECL).

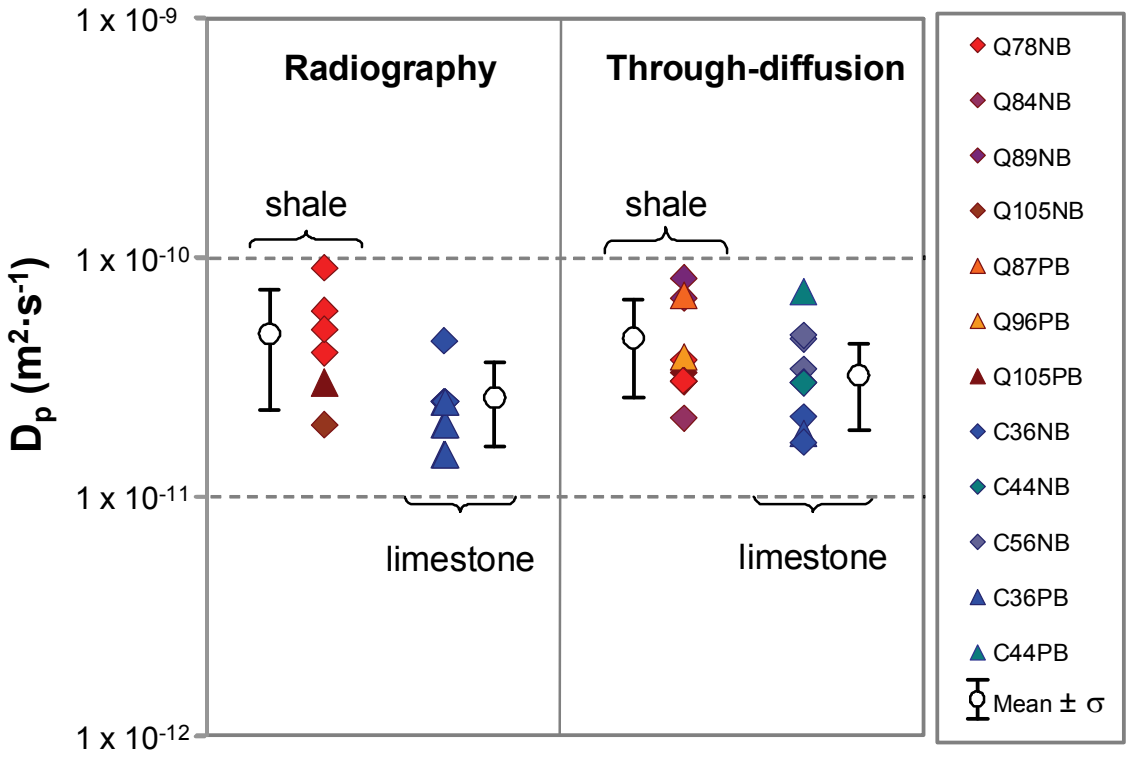

Figure 10: Comparison of pore diffusion coefficients measured by radiography (this study) and through-diffusion (Vilks and Miller, 2007).

In general, Cobourg Formation limestone samples have slightly lower diffusion coefficients for iodide than the Queenston Formation shale samples, although the D_p values for all samples were of the same order of magnitude (10^{-11} $m^2.s^{-1}$).

Comparison of results from the radiography and through-diffusion methods shows similar D_p and D_e values obtained by both techniques. Values of D_e calculated for Queenston shales are slightly higher (1.1×10^{-12} to 5.5×10^{-12} m^2/s) than those measured by through-diffusion (8.7×10^{-13} to 2.6×10^{-12} m^2/s). The samples measured with 1.0 M KI tracer give a better comparison, having D_e values at the upper end of the range. Radiography estimates from Cobourg limestones give D_e values (3.5×10^{-13} to 1.4×10^{-12} m^2/s) that fall within the range of values measured by through-diffusion experiments (9.5×10^{-14} to 7.0×10^{-12} m^2/s). Sample heterogeneity may be responsible for the large range of D_p and D_e values obtained for the limestone samples by the through-diffusion technique, particularly for the two samples with diffusion direction parallel to bedding (Vilks and Miller 2007).

Comparing samples prepared for diffusion normal to the bedding planes and those prepared parallel to bedding, it appears that there is no significant effect of anisotropy on the diffusion coefficients obtained by radiography in this limited sample set. The Queenston shale, in

particular has no visible bedding features. The bedding features in the Cobourg limestone are poorly defined and samples prepared “parallel to bedding” do not necessarily contain bedding planes that run parallel to the diffusion direction.

Diffusion coefficients appear to be insensitive to tracer concentration when using iodide concentrations between 0.6 and 1.0 M for radiography. There is greater variation between duplicate samples measured using the same tracer concentration (e.g. Q078NB1 and Q078NB2) than between samples measured with different concentrations of iodide (e.g. Q078NB1 and Q078NB3) (Table 8). All Cobourg limestone radiography samples were measured with a concentrated 1.0 M KI solution in an attempt to improve analytical sensitivity.

Two different solution compositions and tracer concentrations were used for through-diffusion experiments: NaI tracer (9.1 g/L NaI with 6.9 g/L $LiNO_3$, 1.0 g/L uranine and 1.3 x 10^8 Bq/L tritium) and KI tracer in SPW (166 g/L KI with SPW solutions for shale and limestone as given in Table 3). In this case the solution composition does appear to affect the results, with D_e values a factor of 2 to 4 higher obtained with the KI tracer in SPW than with the lower salinity NaI tracer (Table 8; Table 9; Vilks and Miller, 2007). Diffusion accessible porosity did not appear to change significantly with the change in solution composition and Vilks and Miller (2007) suggest that the higher D_e values using synthetic pore water might be an experimental artefact due to a difference in TDS values between the tracer and eluent solutions, since the tracer solution TDS was a factor of 1.7 higher.

Some of the limestone samples present challenges to the analytical sensitivity of the radiography measurements, because of:

- strong X-ray absorbing properties of the Ca-rich rock. Under these circumstances of high background X-ray absorption, the calibrated C/C_0 approach has proven to be more reliable than the relative C/C_0 approach;
- very low porosity (1 to 3 %). Below about 3% water-loss porosity, the detection sensitivity of the iodide tracer in the rock is poor and the height of the C/C_0 versus distance curve, which is sensitive to the porosity value, may not be distinguished from the background signal; and
- heterogeneous distribution of porosity. The calibrated technique requires knowledge of the material porosity, but the mean ϕ_w from measurements made on adjacent core segments may not represent the porosity of the diffusion test sample.

For the low porosity sample C036NB2, diffusion profiles could not be obtained from $\Delta\mu$ profiles using the measured ϕ_w or mean ϕ_I because of the high background X-ray absorption. Instead, we have used a porosity of 3.0 % to ensure that the relative concentration profiles project back to the correct C/C_0 value of 1.0 at the influx boundary. The magnitude of the porosity adjustment is small and the fitted value is within the range of ϕ_w and ϕ_I measurements for the Cobourg limestone samples.

5.3 POROSITY PROFILES

Following completion of the diffusion tests, two samples of Queenston shale and all six samples of Cobourg limestone were allowed to saturate with iodide by filling the upper and lower

diffusion cell reservoirs with KI tracer solution. Four of the Queenston samples (Q078NB1 to Q078NB4) were not included because the condition of the epoxy coating had deteriorated.

The porosity profiles calculated from $\Delta\mu_{sat}$ profiles for iodide-saturated samples using equation (19) are presented in Figure 11 and Figure 12. Because $\Delta\mu$ values are low for the iodide-saturated samples, the $\Delta\mu_{sat}$ profiles for porosity measurements have first been corrected to remove a curved distortion in the profiles arising from the cone-beam geometry of the X-ray system (See Section 6.3.2) before calculating iodide mass in the pores. The times indicated on the figures are the number of days after the KI tracer was introduced to the upper reservoir.

These data provide independent porosity measurements for comparison with the water loss porosity measurements in Table 6 and Table 7. Mean values of ϕ_I measured by radiography for 2 shale samples (0.057 and 0.062) compare well with the mean ϕ_w value for the 105 m samples (0.059) and the mean ϕ_w of all shale samples measured by UNB and AECL (0.062 ± 0.007) (Figure 11, Table 8). The mean ϕ_I for 6 limestone samples (0.028 ± 0.005) overlaps with the range of porosity measurements made on 7 adjacent samples from 36 m depth by the independent water loss technique (0.020 ± 0.008) (Figure 12, Section 5.1).

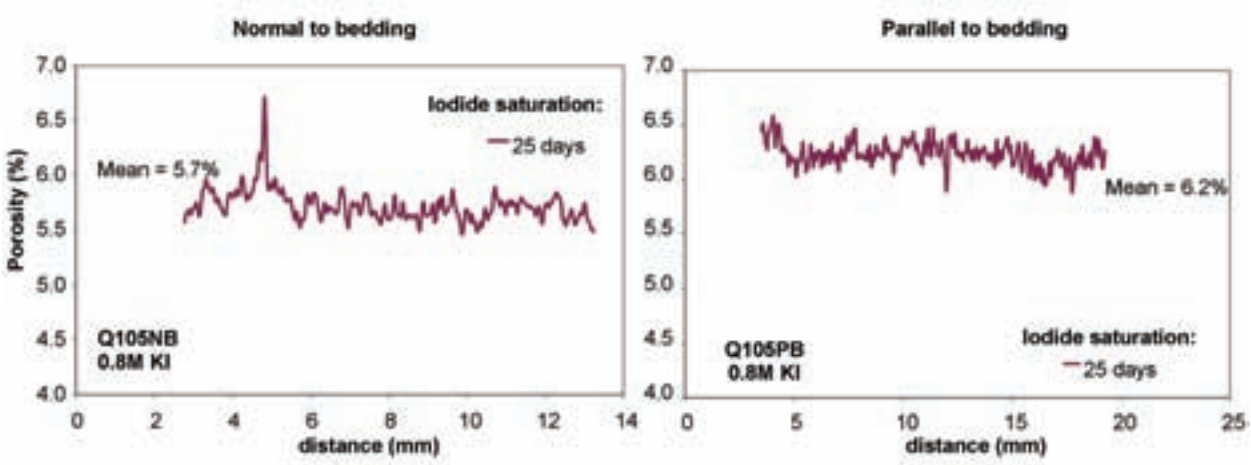

Figure 11: One dimensional porosity profiles along the direction of diffusion for the Queenston shale samples from 105 m depth.

The porosity profiles for the Queenston samples display uniform porosity both normal and parallel to the presumed bedding direction. The sample Q105NB (normal to bedding) displays a slight increase in porosity at the position of a small horizontal fracture near 5 mm from the influx boundary that opened up in the later stages of the experiment. As anticipated from the heterogeneity of the hand specimens, the porosity profiles for the Cobourg limestone samples have slightly greater spatial variability than the Queenston shale. Porosity shows greater variability normal to bedding than parallel to bedding, as would be anticipated from layering-related changes in pore distribution.

The limestone samples are, however, approaching the lower limit of our sensitivity for measuring $\Delta\mu$ above background and the errors in the measurements are likely to be larger than for the Queenston Formation samples. The regular variation in the profile for the lowest

porosity sample, C036NB2, for example, may be related to a second-order distortion in the $\Delta\mu_{sat}$ profile which is not removed by our curve correction.

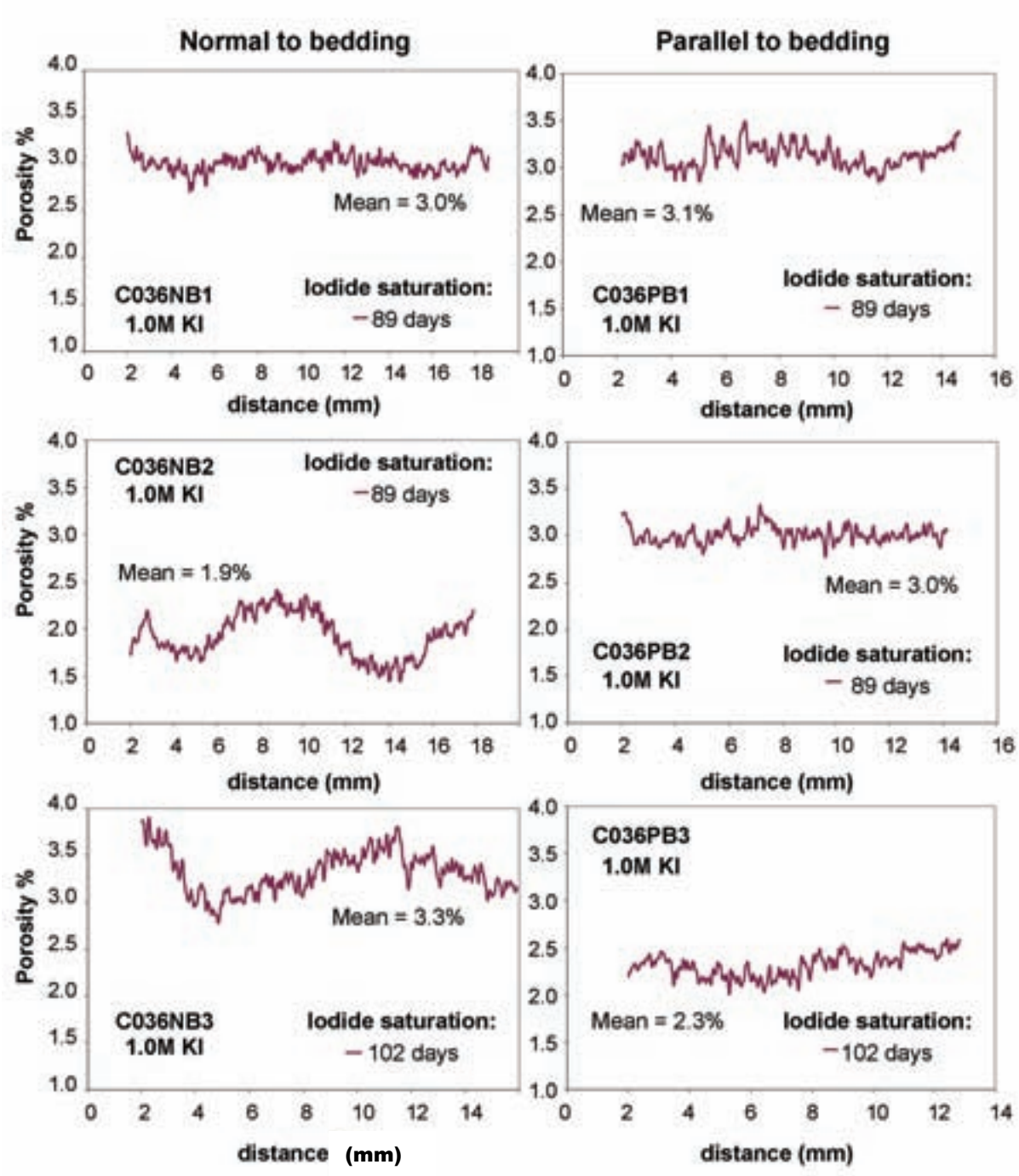

Figure 12: One dimensional porosity profiles along the direction of diffusion for the Cobourg limestone samples from 36 m depth.

6. DISCUSSION

The radiography technique for making diffusion measurements on sedimentary rock materials is still under development and modifications have been, and will continue to be made to the experimental design and data processing to improve the results. Some of the problems faced and solutions found are presented in this section.

6.1 ADVANTAGES OF RADIOGRAPHY

The use of radiography offers several advantages for diffusion measurements. Measurements using X-rays are non-destructive meaning that repeat time series measurements can be made on the same sample. In contrast, conventional diffusion measurements based on concentration profiles have typically required cutting of the sample into sections and extracting the solute for quantitative analysis (Shackelford 1991), and in order to obtain data for more than one time step, several similar, but not identical, samples would be run in parallel. The non-destructive nature of the measurements also means that the same sample could be used for several successive diffusion tests using, for example, different solute concentrations. The spatial resolution capabilities of the microCT system permit these measurements at a spatial resolution of about 20 μm, allowing diffusion profiles to be measured on small sample sizes. The nature of radiography allows for visualization of the tracer distribution in the sample during diffusion, which can be used to detect preferential pathways for diffusion or to assess the influence of heterogeneity using three dimensional scans.

Radiography methods offer another advantage when working with low permeability materials, where diffusion is typically slow. Diffusion coefficients can be obtained more rapidly than for through-diffusion techniques on the same materials, because the concentration profiles are collected before the tracer breaks through. In contrast, through-diffusion measurements require the flux of solute through the rock to reach steady state and this process could take several weeks or months for low permeability materials, depending on the sample thickness.

Because of its high atomic number, iodide is strongly X-ray attenuating which, together with its conservative behaviour, makes it an excellent tracer for this type of study. The iodide tracer solution also provides an analogue for ^{129}I, which is a radionuclide of interest for the safety case for a deep geologic repository because of its long half life (1.6×10^7 years).

6.2 COMPARISON WITH THROUGH-DIFFUSION MEASUREMENTS

Conventional through-diffusion experiments have been conducted on adjacent samples of rock from the same drill cores, allowing for comparison of the diffusion coefficients and porosity measurements. While the through-diffusion measurements provide a good benchmark for testing the results of the radiography experiments, there are a number of reasons, which we summarize in Table 10, why the two techniques should not be considered directly comparable.

Table 10: Comparison between through-diffusion and radiography techniques for measuring diffusion coefficients

Feature	Through-diffusion technique	Radiography technique
Sample size	54.5 or 63.3 mm in diameter 5 to 60 mm in length	11 mm in diameter 15 to 25 mm length
Type of data collected	solute mass flux at steady state	solute concentration profiles before steady-state
Tracer	Any solute that can be quantified in the outflux reservoir solution	Only high atomic number solutes that have sufficient contrast in radiographs after blank subtraction
Type of porosity contributing to the measurements	measures only the connected pores that contribute to diffusion	measures all pores filled with tracer, which in some cases may be "dead-end" pores that do not contribute to the total mass flux through the rock
Methods of data analysis	linear regression to fit a line through the flux versus time data	trial and error iteration to match an analytical solution to a measured concentration-distance profile
Diffusion properties measured directly in diffusion experiments	Effective diffusion coefficient (D_e) Rock capacity factor (α) = diffusion accessible porosity (ϕ_d) for non-sorbing tracer	Pore diffusion coefficient (D_p)

6.3 ERRORS AND UNCERTAINTIES

At present, there are several known sources of uncertainty or error in the radiographic diffusion measurements, including analytical errors and errors in the fitting of diffusion models to experimental data. The analytical errors may contribute to imprecision and the fitting errors lead to inaccuracy of the measurements. These errors and some of the efforts made to minimize them are described in the following sections.

6.3.1 Analytical errors

Instrument noise

The stability of the microCT system was tested by replicate measurements on homogeneous materials, including a quartz rod and aluminum internal standards attached to the diffusion cells. The variability in the CT instrument signal may be quantified as signal-to-noise ratio (SNR), defined as the ratio of the mean greyscale value to the standard deviation of the greyscale values over an ROI in the image containing only the homogeneous material. Table 11 reports various SNR measurements made under the operating conditions used for radiography.

Table 11: Signal-to-noise ratios for homogeneous materials measured by microCT

Material	Number of measurements	Frame averaging	ROI (pixels)	Mean SNR
Quartz rod	3 consecutive	2	750x750	580
(12 mm diameter)	1	8	750x750	644
	1	16	750x750	626
Aluminum wire	76 over 35 days	8	15x600	139
(~0. 7 mm diameter)		8	15x600	160
Aluminum sheet (1.5 mm thick)	35 over 35 days	8	20x500	164
Aluminum disc (11 mm diameter)	13 over 3 days	8	10x500	520

The X-ray source fluctuates slightly over time and the SNR for consecutive measurements on the quartz rod over a short period of about 10 minutes are higher than the long term SNR for the aluminum standards, where sampling intervals varied from a few hours to more than 10 days over a 35 day period. The larger ROI for the quartz and homogeneity of the material compared with the smaller aluminum standards may also influence these SNR measurements. Greyscale values for diffusion samples are normalized by the intensity of the Al internal standards to correct for variations in the X-ray source over time.

Instrument noise is reduced by longer counting times and increasing the number of image frames collected (frame averaging). The quartz rod was used to test some of the instrument settings and to optimize the transmitted X-ray signal. During these trials, it was discovered that the SNR for the quartz rod was improved by averaging 4 or 8 frames for each radiograph. The improvement in SNR flattens out at 8 to 16 frames and the 8-frame average was chosen for the diffusion experiments because of the shorter total collection time.

Background variation

Despite the use of the Al wire internal standard, inconsistency in the X-ray source between the reference and time series data collection commonly led to variations in the background for the difference profiles ($\Delta\mu$). This background was corrected based on the assumption that there should be zero iodide at the outflux boundary in the early time series data. The background correction was made by subtraction (effectively shifting the concentration profiles up or down the y-axis) to bring the far end of the sample to $C/C_0 = 0$. However, determination of the magnitude of the background shift correction becomes problematic when the iodide tracer is close to breakthrough, because the assumption of zero iodide at the outflux boundary is no longer valid. A modification to the diffusion cell now uses an 11 mm diameter, 2 mm thick removable Al disc instead of the upper reservoir. Data normalized using the Al disc greyscale values at the end of the sample do not require the additional background correction. The Al disc design was, however, not used for any of the samples reported in this study.

Sample alignment

Image artefacts may occur from misalignment of physical features (epoxy sealant, mineral grains of contrasting density, poor matching of sample rotation) in the ROI of time series images, especially along the lower influx boundary. Even when the diffusion cell is repositioned in the sample holder and the mechanical stage moved to the same position, the radiograph images may display horizontal and vertical shifts up to approximately 0.5 mm and 0.25 mm, respectively. Anomalous values of Δμ due to misalignment could easily be misinterpreted as increases or decreases in iodide concentration, so great care is taken in choosing the same ROI for all time series images. Samples are also rinsed and dried before making measurements to ensure that no salts on the outside of the epoxy seal are incorrectly interpreted as being present in the pores.

During data processing, the greyscale averaging across the sample width compensates for a small amount of horizontal or rotational misalignment of the sample in the CT sample holder, but vertical alignment (i.e. along the direction of diffusion) between the reference and time series images is critical for the success of the blank subtraction approach. Features of contrasting greyscale intensity, such as the rock/reservoir boundaries and sample heterogeneities are used to assist in the vertical alignment of the greyscale profiles relative to the reference profile.

Iodide calibration and porosity scaling assumptions

There are additional uncertainties in converting calibration measurements made on aqueous iodide standard solutions in a brine matrix to measured iodide concentrations in a solid rock matrix, using water loss porosity measurements to scale the values. The generally good agreement (see Appendix D) between the concentration profiles obtained by calibration and those obtained by the relative measurement, however, gives confidence that the calibration approach can produce reasonable results.

Measurement precision

The effect of instrumental and sample alignment variations was measured by collecting repeat radiographs of the Cobourg limestone samples saturated with synthetic pore water before the start of the diffusion test. The sample was removed from the chamber and replaced between radiographs, to simulate sample handing during a diffusion test. By treating the first radiograph as a reference and the duplicate as a time series sample, Δμ profiles were obtained which give a measure of the repeatability of the measurements. These measurements have been used to derive the errors in C/C_0, indicated as error bars on the concentration profile plots in Appendix D. The average instrumental and alignment errors in measurements for iodide using the radiography technique are estimated to be around $C/C_0 = 0.05$.

6.3.2 Data fitting errors

Fitting the analytical solution

In applying the analytical solution, it is assumed that diffusion occurs through a homogeneous porous medium and errors may arise if the sample is actually heterogeneous. Consideration of this source of error is particularly relevant to some of the Cobourg limestone samples. The fit

could probably be improved using numerical modeling, which would allow the diffusion profiles to be derived using variable diffusion coefficients across the sample.

Experimental data are fitted to the theoretical curve using an iterative curve-matching process that relies on visual inspection and trial-and-error estimates of D_p. Curve matching by eye may introduce some error, especially where the uncertainties in the C/C_0 values are large and a relatively wide range of D_p values could produce curves that appear to fit the concentration profile. Radiographic measurements of D_p produce results with a smaller number of significant figures (lower precision) than through-diffusion D_e measurements.

Early vs. late time data

Some concentration profiles do not display the typical curve of a diffusion profile and finding a best fit curve is difficult. This was found to be the case with many of the profiles measured on the first day of the diffusion test for the Queenston shale samples (1, 4 and 8 hour data). It is possible that diffusion is not the dominant solute transport process in the samples at the early times and there may be an osmotic contribution to the solute transport. Mechanical damage of the sample by cutting and grinding could also produce a damaged zone which allows faster movement of solute near the influx boundary. For the Cobourg samples time series data collection began at 24 hours. Table 8 and Table 9 report the values for the diffusion coefficients obtained in the time step immediately before breakthrough, because this value is considered to be the most representative for any particular sample. By this time, the tracer has encountered all of the heterogeneity in the sample.

Zhelezny and Shapiro (2006) also found that measured diffusion coefficients decreased over time during iodide tracer experiments using X-ray CT measurements on samples of sandstone and chalk. In all but the most heterogeneous sample, the diffusion coefficients “stabilized” after the first few days of measurement after the tracer had passed through around 10 mm of sample.

We have recently discovered that the presence of iodide tracer inside the reservoir makes a small, but significant contribution to the X-ray absorption near the influx boundary at early times due to the X-ray beam geometry. At 1, 4 and 8 hrs for the Queenston shale samples, the increase in $\Delta\mu$ near the influx boundary is not a true reflection of the mass of iodide in the rock sample, but rather an artefact of the blank subtraction approach because we are using an iodide-filled reservoir for the time-series image and an iodide-free, SPW-filled reservoir for the reference image. Because of the cone-beam geometry of the source, a small contribution to the X-ray absorption that appears near the base of the rock in the images is actually made when the beam passes through the reservoir. After time periods of 50 to 100 hours, the tracer has encountered all of the heterogeneity in the sample and the magnitude of the reservoir effect is negligible.

Influx boundary position

One of the problems with the radiography method is that the position of the influx boundary is outside the field of view for the X-ray camera. Yet knowing the position of the boundary is a requirement for accurate fitting of the analytical solution to the concentration profiles. At present, the boundary has been estimated, knowing the depth of the sample inside the lower reservoir (about 1 mm) and the lower edge of the region of interest on the radiographs (about 0.5 to 1 mm above the reservoir). The analytical solution is fitted by applying a shift of 1.5 to 2

mm to the zero position on the x (distance) axis. The shift is then adjusted to find a good fit for the diffusion profile curves from the analytical solution that can be applied to all time series profiles. This method is not entirely satisfactory, since there are two unknowns (x-position and diffusion coefficient, D_p) that must be resolved to fit the curves and an incorrect choice of x may influence the derived value of D_p.

The magnitude of this error was examined using the diffusion profiles for the time step immediately before breakthrough. The position of the boundary was shifted by ±0.5 mm (considered to be a reasonable estimate of the error in choosing the boundary position) and the diffusion curves re-fitted to test the influence on D_p. For example, for sample Q105PB at 170 hours, a boundary position offset of 2 mm allows the data to be fitted with $D_p = 2.5 \times 10^{-11}$ m^2/s and an offset of 3 mm, with $D_p = 3.5 \times 10^{-11}$ m^2/s. The value of 3.0×10^{-11} m^2/s reported in Table 8 is for a shift of 2.5 mm. In general, it was estimated that a ±0.5 mm error in the boundary position would give rise to an error of around $\pm 5 \times 10^{-12}$ m^2/s in the value of D_p.

Source-detector geometry

There is a potential source of error associated with the geometry of the X-ray source and detector system. The microCT system uses an X-ray cone beam and flat CCD detector. Radiographs of uniform materials (glass rod and aqueous solutions) display a slight decrease in the greyscale intensity towards the top and bottom of the radiograph. This arises from slightly longer path length through the sample away from the centre of the cone (Figure 13).

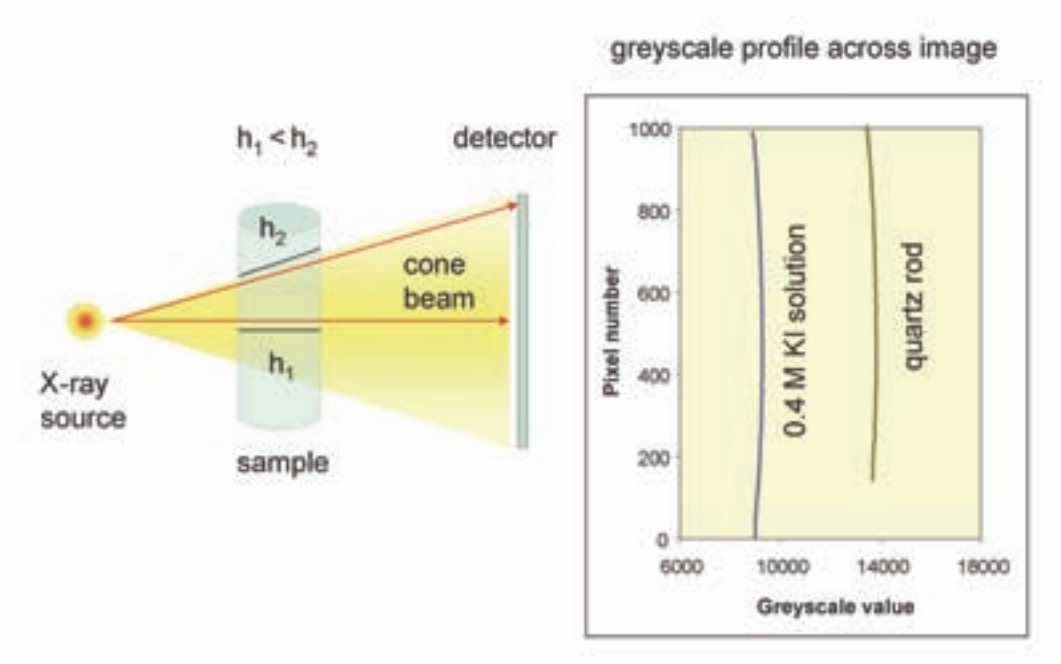

Figure 13: Slight distortions at the edges of the greyscale profile arise from the cone geometry of the X-ray beam in the microCT.

The blank subtraction process removes most of this distortion from the data, because the effect is present in both the reference and time series images. However, observations of Δμ profiles for uniform standard materials indicate that the effect is not completely corrected and some

slight curvature remains. There was a concern that this error in the Δμ profiles may lead to overestimation of the diffusion coefficients, since the Δμ value, and hence the iodide concentration, may be slightly overestimated near the influx boundary. However, radiographs of standard solutions showed that the measured difference in iodide concentration between the centre and the ends of the profile (systematic error) was less than 5%. This is slightly smaller than the random analytical error in the individual measurements and is likely to be less significant than the errors introduced by the porosity correction to calculate iodide concentrations in the rock matrix. The error in the diffusion profiles due to image distortion was therefore disregarded.

For the porosity profiles, however, the $\Delta\mu_{sat}$ profiles used to calculate iodide mass (Equation 19) are near the limits of sensitivity for the technique and the magnitude of the curvature at the ends of the profiles was of the extent that correction was necessary. For example, for the homogeneous Queenston shale sample, Q105NB, the curvature in the Δμ profile for the iodide-saturated sample produced an apparent 20% increase in porosity (6.8 % instead of 5.7%) at the right hand edge of the porosity profile. The data in Figure 11 and Figure 12 have been corrected with a quadratic function derived from the profiles to remove this effect.

6.4 FUTURE RESEARCH DIRECTIONS

The radiography method for measuring pore diffusion coefficients is under continuous development and several changes to the sample preparation technique, data collection and processing of results will be tested and implemented to improve the quality of results.

The design for the diffusion cell is undergoing several improvements such as:

- replacing the aluminum reservoir and pedestal with a machinable plastic (Delrin®) that has a lower X-ray absorption coefficient and is not susceptible to corrosion after extended contact with high salinity solutions.
- replacing the upper reservoir with a thin layer of porous fabric saturated with synthetic pore water solution.
- fitting an 11 mm diameter aluminum cap of 2- to 3-mm thickness to the top of the sample over the porous fabric. The cap provides a larger internal standard that has the same variations in thickness across the field of view for normalizing radiograph data
- coating the outside of the rock sample with a silicone seal inside clear plastic heat shrink tubing. This eliminates the epoxy coating which is prone to cracking after extended exposure to high salinities and the 60°C curing is no longer necessary.

The calibrated approach is being modified by collecting improved radigraphy data for standard solutions. The solutions are now placed in new glass vessels with internal diameter matching the external diameter of the rock sample and the brass pedestal replaced with a plastic reservoir base to mimic the rock diffusion cells.

An artefact relating to the interaction of the X-ray beam with the concentrated iodide tracer solution in the influx reservoir was noted in the early time diffusion data (See Section 6.3.2). Future reference images will be collected immediately after the injection of the tracer to eliminate the possibility of this measurement artefact.

The solutions used in the diffusion experiments are also being modified. Sodium iodide will be used instead of potassium iodide as a tracer to avoid the high concentrations of potassium and

their potential for changing the interlayer structure of clay minerals, particularly in the shales. The use of a sodium-based tracer is also closer to the natural pore waters which have a sodium-dominated cation composition.

Tracer solutions are limited to high atomic number solutes that have strong X-ray attenuation properties, but iodide is not the only ion that can be used. Future investigations of diffusion and sorption of a non-conservative ion in sedimentary rock samples are planned using the cesium cation.

The characterization of pore water composition is challenging under these high salinity conditions and in low porosity rocks. In particular, there are uncertainties that arise from the use of porosity measurements to calculate solute concentrations from leach test data and the possibility that soluble minerals, such as halite or anhydrite may contribute to the concentrations of leached salts. Future research efforts to improve pore water characterization may involve extraction of pore water by physical means, modified techniques for leaching of pore water, or diffusive equilibration techniques.

Sample preservation is another area that is receiving more attention for future work. The radiography technique was tested on old archived samples that had been stored without any attempt to preserve the pore water in the core. New measurements are being made on freshly-drilled core that has been flushed with an inert gas to limit oxidation and vacuum-sealed to prevent drying out before sample preparation. The preserved core will retain some of the original pore water, decreasing the time necessary for saturation at the start of the diffusion test. It is inevitable, however, that some of the pore solution will be lost during cutting and coating of the samples and saturation with synthetic pore water will still be necessary. The use of preserved core also does not avoid changes in porosity due to depressuring of the core once it is removed from the ground. Although the radiography technique is not easily adaptable to experiments under confining pressure, through-diffusion tests are planned using cells that can pressurize the rock core to determine the magnitude of this effect.

Radiography has been tested on the limestone samples using a high source energy of 90kV and current of 110 μA in an attempt to improve the signal to noise for the $\Delta\mu$ profiles of these low porosity samples, but there has been little improvement in the quality of the data. It is possible that decreasing the sample radius will decrease the matrix absorption, but there will also be a loss of iodide tracer mass. The investigation of more powerful X-ray systems may be necessary as a step towards more reliable diffusion coefficient measurements on the limestone samples.

The power of the MicroCT system is in the ability to collect and reconstruct three-dimensional data sets and the applications of 3-D tomography to porosity and diffusion measurements is under development at the University of New Brunswick.

7. CONCLUSIONS

An X-ray radiography method has been developed for determining iodide pore diffusion coefficients and 1-D iodide-accessible porosity profiles in porous geological materials. The method is based on the quantification of spatially-resolved iodide concentrations inside the rock pores by X-ray absorption measurements during tracer tests.

The radiography technique is simple, non-destructive and requires only a small amount of intact sample (about 1 cm diameter x 2 cm length). Radiography can be used to make several time series measurements on the same sample. The diffusion measurements are made under transient conditions, so experimental times are shorter than classical steady-state through-diffusion measurements. This is an advantage for low porosity, low diffusion coefficient samples of comparable size, which might take a month or more for the required steady-state condition to be achieved. Radiographic D_p measurements were possible from about 48 hours onwards with some of the samples tested. Another advantage of X-ray radiography is the visual nature of the data collected. Processed radiograph data provide images of an iodide tracer solution at each time step as it moves through the rock.

A microCT X-ray system provides a means of quantifying iodide tracer concentration profiles inside rock samples during diffusion tracer experiments. A blank subtraction approach, involving a reference radiograph (sample blank before tracer injection) is used to quantify the parameter $\Delta\mu$, which provides a measure of the change in X-ray attenuation due to the presence of iodide tracer solution in the rock pores during diffusion. Future measurements will collect the reference radiograph immediately after tracer injection so that artefacts related to the absence of iodide in the reservoir of the reference image are avoided. Profiles of $\Delta\mu$ versus distance along the diffusion direction are generated from the measurements of changes in X-ray intensity. These $\Delta\mu$ profiles can then be related to profiles of relative iodide concentration (C/C_0) using either a calibration curve, or a relative technique which normalizes the data to a $\Delta\mu$ profile obtained from the iodide-saturated rock sample. Fitting an analytical solution of Fick's Second Law to the C/C_0 profiles provides a means of measuring the pore diffusion coefficient, D_p, for each time step in a diffusion experiment.

The radiography method has been tested on low permeability rock samples, including six samples of Queenston Formation shale and six of Cobourg Formation limestone prepared from archived drill core. The unpreserved samples were intended for method development and any possible changes in porosity and diffusion properties as a result of their long-term storage were not considered in this project. Future studies will use freshly-drilled and preserved core.

Diffusion coefficients obtained by radiography were compared with results from through-diffusion measurements made on adjacent samples in a companion study (Vilks and Miller, 2007). Diffusion-accessible porosity values (ϕ_d) for iodide, measured during the through-diffusion tests, were used to calculate pore diffusion coefficients (D_p) from the measured effective diffusion coefficients (D_e). Both radiography and through-diffusion methods gave similar diffusion coefficient values. Pore diffusion coefficients (D_p) measured for Queenston shale samples by radiography ranged from 2.0×10^{-11} to 9.0×10^{-11} m^2/s using potassium iodide tracers of 0.6 to 1.0 M in a synthetic pore water solution. The through-diffusion measurements made on shale using a matching 1.0 M KI tracer in synthetic pore water gave a mean D_p of 7.5×10^{-11} m^2/s. Using a much more dilute tracer (0.06M NaI) in a low TDS solution (17 g/L) the range of D_p values measured for the shales by through-diffusion was slightly lower at 2.1×10^{-11} to 7.0×10^{-11} m^2/s.

Measured D_p for the Cobourg limestone were typically lower than for the shales, ranging from 1.5×10^{-11} to 4.5×10^{-11} m^2/s by radiography. The upper end of the range compares well with of the limestone samples (C056NB2 and C056NB3) used in through-diffusion experiments with a matching 1.0 M KI tracer solution, which gave D_p values of 4.6×10^{-11} and 4.7×10^{-11} m^2/s. The through-diffusion measurements on limestones with the 0.06 M NaI tracer were also slightly lower ($D_p = 1.7 \times 10^{-11}$ to 3.4×10^{-11} m^2/s) than the measurements with 1 M KI in the higher TDS synthetic pore water, with the exception of a single sample with a high diffusion coefficient ($D_p = 7.2 \times 10^{-10}$ m^2/s) parallel to the bedding. The limestone samples are considerably more heterogeneous than the shales, which may be responsible for the large range of D_p and D_e values obtained for the limestone samples by through-diffusion and the differences between through-diffusion and radiography results.

One of the objectives of the study was to develop a protocol for determining the magnitude of layering-related anisotropy in porosity and D_p values. This was achieved by subcoring adjacent samples with the diffusion axis parallel and perpendicular to the original drill core axis. Comparing samples prepared normal and parallel to the bedding planes, no effects of sample orientation on the diffusion coefficients measured by radiography were observed for this limited set of samples. It appears that the diffusive properties of the shale samples are isotropic at the scale of the measurements under atmospheric pressure conditions. The D_p values for the limestone through-diffusion samples measured parallel to bedding display greater variability than those measured normal to bedding or those measured by radiography. However, the investigations of anisotropy by both techniques were based on only a small number of samples prepared parallel to bedding (3 shale and 5 limestone) and more data are required to establish effects of sample orientation with confidence.

Radiography also allows for characterization of the porosity in a sample by comparing data collected for the samples with and without iodide tracer. After diffusion experiments, eight of the samples (2 shale and 6 limestone) were fully saturated with iodide tracer solution. Blank subtraction of reference images from iodide saturated images was used to generate 1-D profiles of $\Delta\mu_{sat}$ versus distance along the long axis of the samples. The $\Delta\mu_{sat}$ profiles are a reflection of the distribution of porosity along the sample axis and the calibration curves relating $\Delta\mu$ to iodide concentrations can be used to calculate a porosity profile. Mean values from the X-ray porosity profiles were found to compare well with independent measurements of water loss porosity for the bulk rock. Mean values from porosity profiles for 2 samples of Queenston shale (5.7% and 6.2%) are close to the water-loss porosity value (5.9%) for an adjacent sample. Mean X-ray derived porosity values for 6 Cobourg limestones range from 1.9% to 3.3% while the water-loss porosity range for 3 adjacent limestone samples is 1.0 to 3.0%.

In on-going development of the radiography technique, sample preparation and data collection methods are being modified and tested to overcome some of the uncertainties and reduce errors. Internal X-ray standards are included with each sample and various materials and configurations of the standard are being tested so that intensity data can be normalized to remove the effects of small variations in the X-ray source between measurements. Misalignment of the sample or changes to the cell materials (e.g. drops of solution, tape, etc.) in reference and time series images is a potential source of error that can lead to overestimation of iodide concentrations. Rinsing of salts from the outside of the sample, exact vertical positioning of the rock sample, a rotational alignment guide, sample features used as markers and very careful image registration are used to minimize these image artefacts. The $\Delta\mu$ calibration technique has also been improved by using vials of matching diameter to the rock samples and collecting several calibration points in the low concentration range, to refine the

slope of the curve in the area where most measurement points are found for low porosity rock samples. The good comparison between our calibrated approach and an independent relative approach using iodide-saturated samples gives confidence in the results obtained from the calibration curves are reasonable for the samples with porosity of around 3% or higher.

Data fitting errors may also affect the precision of the measured D_p values. The use of an analytical solution assumes a homogeneous sample with constant boundary conditions. Refreshing the tracer solution maintains close to constant influx concentrations, but there will be small deviations from the theoretical conditions for which the analytical solution is valid. Curve fitting is achieved by visual inspection, but the errors introduced are likely to be smaller than the errors due to the noise in the C/C_0 signal. For heterogenous samples, numerical modelling may improve the data analysis in future.

From our comparison with through-diffusion results, the radiography technique works well for relatively homogeneous samples of low porosity, particularly the Queenston Formation shales. The technique is limited, however, by the low $\Delta\mu$ values and high noise in the profiles for Cobourg Formation limestone samples when the porosity falls below 3%. The high X-ray absorption of the calcium-rich rock matrix contributes to the poor signal and the MicroCT instrument is limited by the maximum source energy available. Further development is required before the radiography method can be used to determine diffusion coefficients for samples with 3% or lower porosity with the Skyscan microCT system.

ACKNOWLEDGEMENTS

Radiography was assisted by John Bowles, Siva Thangavelu and Paul Arsenault of the LTMD X-ray laboratory, Department of Mechanical Engineering, University of New Brunswick. Supplementary X-ray techniques for rock materials are under development by PhD students Mosi Agbogun and Ranjit Subudhi, who have willingly shared their experience and advice in the laboratory. We would like to acknowledge Dr. Esam Hussein for helpful comments on the workings of X-ray systems and diffusion processes and Dr. Monique Hobbs for her enthusiastic support for this work.

REFERENCES

Altman, S.J., M. Uchida, V.C. Tidwell, C.M. Boney and B.P. Chambers. 2004. Use of X-ray absorption imaging to examine heterogeneous diffusion in fractured crystalline rocks. Journal of Contaminant Hydrology: 69, 1-26.

Barone,F.S., R.K. Rowe and R.M. Quigley. 1990. Laboratory determination of chloride diffusion coefficient in an intact shale. Canadian Geotechnical Journal: 27, 177-184.

Boving, T.B. and P. Grathwohl. 2001. Tracer diffusion coefficients in sedimentary rocks: correlation to porosity and hydraulic conductivity. Journal of Contaminant Hydrology: 53, 85-100.

Choi, J.-W. and D.W. Oscarson. 1996. Diffusive transport through compacted Na- and Ca-bentonite. Journal of Contaminant Hydrology: 22, 189-202.

Císlerová, M. and J. Votrubová. 2002. CT derived porosity distribution and flow domains. Journal of Hydrology: 267, 186-200.

Crank, J. 1975. The mathematics of diffusion. Clarendon Press, Oxford, 2nd edition, 414 pp.

Descostes, M., V. Blin, B. Grenut, P. Meier and E. Tevissen. 2004. HTO diffusion in Oxfordian limestone and Collovo-Oxfordian argillite formations. Materials Research Society Symposium Proceedings: 824.

Emerson, D.W. 1990. Notes on mass properties of rocks – density, porosity, permeability. Exploration Geophysics: 21, 209-216.

Evans, S.D. and S.A. Barber. 1964. The effect of cation-exchange capacity, clay content and fixation of rubidium-86 diffusion in soil and kaolinite systems. Proceedings of the Soil Science Society of America: 28(1), 53-56.

García-Gutiérrez, M., J.L. Cormenzana, T. Missana and M. Mingarro. 2004. Diffusion coefficients and accessible porosity for HTO and ^{36}Cl in compacted FEBEX bentonite. Applied Clay Science: 26, 65-73.

Grathwohl, P. 1997. Diffusion in porous media: Contaminant transport, sorption/desorption and dissolution kinetics. Kluwer Academic Publishers, Boston, 207 pp.

Koroleva, M. and M. Mazurek. 2006. Characterisation of pore-water composition in the Queenston shale (Niagara, Ontario): First steps based on a mineralogical and leaching study. RWI Technical Report 2006-03, 15 May 2006, Rock-Water Interaction, Institute of Geological Sciences, University of Bern, Bern, Switzerland.

Maes, N., H. Moors, A. Dierckx, P. De Cannière and M. Put. 1999. The assessment of electromigration as a new technique to study diffusion of radionuclides in clayey soils. Journal of Contaminant Hydrology: 36, 231-247.

Mazurek, M., W. R. Alexander and A. B. MacKenzie. 1996. Contaminant retardation in fractured shales: matrix diffusion and redox front entrapment. Journal of Contaminant Hydrology: 21, 71-84.

Moreno, L., B. Gylling and I. Neretnieks. 1997. Solute transport in fractured media – the important mechanisms for performance assessment. Journal of Contaminant Hydrology: 25, 283-298.

Parkhurst, D.L. and C.A.J. Appelo. 1999. User's guide to PHREEQC (Version 2) - A computer program for speciation, batch-reaction, one-dimensional transport, and inverse geochemical calculations: U.S. Geological Survey Water-Resources Investigations Report 99-4259, 310 p.

Pearson, F.J., 1999. What is the porosity of a mudrock. In: Aplin, A. C; Fleet, A.J., Macquaker, J.H.S. (eds). Muds and mudstones: Physical and fluid flow properties. Geological Society London Special Publication: 158, 9-21.

Polak, A., A.S. Grader, R. Wallach and R. Nativ. 2003. Chemical diffusion between a fracture and the surrounding matrix: Measurement by computed tomography and modeling. Water Resources Research: 39(4), 1106, SBH10-1 - SBH10-14.

Rasband, W. 2006. ImageJ Version 1.36, 13 March 2006. Complete release notes. National Institutes of Health, USA. Available online at http://rsb.info.nih.gov/ij/

Robinson, R.A. and R.H. Stokes. 1959. Electrolyte solutions. The measurement and interpretation of conductance, chemical potential and diffusion in solutions of simple electrolytes. 2nd edition, Butterworths, London, 559 pp.

Savoye, S., L. DeWindt, C. Beaucaire, G. Bruno and N. Guitard. 2001. Are artificial tracers conservative in argillaceous media? The Tournemire claystone case. In: Cidu, R. (e.d.) Water-Rock Interaction 2001. Vol 2. Proceedings 10th International Symposium on Water-Rock Interaction, Villasimius, Italy, 10 -15 July 2001. A.A. Balkema, Lisse, 1383 - 1385.

Shackelford, C.D. 1991. Laboratory diffusion testing for waste disposal – A review. Journal of Contaminant Hydrology: 7, 177-217.

Tidwell, V.C. and R.J. Glass. 1994. X ray and visible light transmission for laboratory measurement of two-dimensional saturation fields in thin-slab systems. Water Resources Research: 30(11), 2873-2882.

Tidwell, V.C., L.C. Meigs, T. Christian-Frear and C.M. Boney. 2000. Effects of spatially heterogeneous porosity on matrix diffusion as investigated by X-ray absorption imaging. Journal of Contaminant Hydrology: 42, 285-302.

van der Kamp, G., D.R. van Stempvoort and L.I. Wassenaar. 1996. The radial diffusion method 1. Using intact cores to determine isotopic composition, chemistry and effective porosities for groundwaters in aquitards. Water Resources Research: 32, 1815-1822.

van Geet, M., R. Swennen, and M. Wevers. 2001. Towards 3-D petrography: application of microfocus computer tomography in geological science. Computers and Geoscience: 27, 1091-1099.

van Loon, L.R, J.M. Soler and M.H Bradbury. 2003a. Diffusion of HTO, $^{36}Cl^-$ and $^{125}I^-$ in Opalinus Clay samples from Mont Terri. Effect of confining pressure. Journal of Contaminant Hydrology: 61, 73-83.

van Loon, L.R., J.M. Soler, A. Jakob and M.H. Bradbury. 2003b. Effect of confining pressure on the diffusion of HTO, $^{36}Cl^-$ and $^{125}I^-$ in a layered argillaceous rock (Opalinus Clay): diffusion perpendicular to the fabric. Applied Geochemistry: 18, 1653-1662.

van Loon, L.R., J.M. Soler, W. Müller and M.H. Bradbury. 2004. Anisotropic diffusion in layered argillaceous rocks: A case study with Opalinus Clay. Environmental Science and Technology: 38, 5721-5728.

van Loon, L.R., M.A. Glaus and W. Müller. 2007. Anion exclusion effects in compated bentonites: Towards a better understanding of anion diffusion. Applied Geochemistry: 22, 2536-2552.

Vanýsek, P. 2006. Ionic conductivity and diffusion at infinite dilution. In Lide, D.R. (ed). CRC Handbook of Chemistry and Physics. 87th edition, CRC Press: 5-76 – 5-78.

Vilks, P. and N.H. Miller. 2007. Evaluation of experimental protocols for characterizing diffusion in sedimentary rocks. Nuclear Waste Management Organization Technical Report TR-2007-11, Toronto, Canada.

Wildenschild, D., J.W. Hopmans, C.M.P. Vaz, M.L. Rivers, D. Rikard and B.S.B. Christensen. 2002. Using X-ray computed tomography in hydrology: systems, resolutions and limitations. Journal of Hydrology: 267, 285-297.

Zhelezny, P.V. and A.A. Shapiro. 2006. Experimental investigation of the diffusion coefficients in porous media by application of X-ray computer tomography. Journal of Porous Media: 9(4), 275-288.

APPENDIX A: GLOSSARY OF DIFFUSION-RELATED TERMINOLOGY

Constrictivity (δ) - A geometric factor of the porous medium that is intended to account for the effects of constricted pathways or channels along the diffusive path within the porous medium. It is a dimensionless factor (≤ 1) that is relevant to diffusive transport calculations when the pore throat diameter is of similar or smaller size than the solute diameter. Note that ***constrictivity*** cannot be measured directly and is typically combined with ***tortuosity*** to yield the ***tortuosity factor*.** Also note that the ***constrictivity*** term is solute specific because of the relationship between solute diameter and pore-throat diameter.

Diffusion - The process by which both ionic and molecular species dissolved in water move from areas of higher concentration to areas of lower concentration. Movement is random and is proportional to the gradient of concentration. The process tends to distribute the particles more uniformly.

Diffusion Coefficient - Based on the premise that diffusive solute transport can be described mathematically by Fick's Laws, the diffusion coefficient is a constant of proportionality [$L^2 T^{-1}$] relating the solute flux to the solute concentration gradient.

e.g. Fick's First Law: $$J_{Di} = -D\frac{\partial C}{\partial x_i}$$

where: J_{Di} = the diffusive flux in direction i
D = the ***diffusion coefficient***
C = the solute concentration
x = distance
i = coordinate directions x, y and z

Free-Water Diffusion Coefficient (D_0) - The ***diffusion coefficient*** for a solute in bulk solution (no porous media) at 25 °C. The ***free-water diffusion coefficient*** is solute specific.

Effective Diffusion Coefficient (D_e) - The ***diffusion coefficient*** for a porous medium that accounts for the 3-dimensional geometry of the pore space, including its ***tortuosity,*** ***constrictivity*** and ***diffusion accessible porosity***. It is the product of the ***diffusion accessible porosity,*** the ***tortuosity factor***, and the ***free-water diffusion coefficient*** as follows:

$$D_e = \phi_d \cdot \tau_f \cdot D_0$$

where: D_e = the ***effective diffusion coefficient***
D_0 = the ***free-water diffusion coefficient***
ϕ_d = the ***diffusion accessible porosity (solute-specific)***
τ_f = the ***tortuosity factor***

In the current study, the value of ϕ_d is sometimes approximated by the water loss porosity (ϕ_w). This assumption should be a reasonable approximation for a conservative solute which is not affected by size exclusion in the pore spaces.

Note that the ***effective diffusion coefficient*** is solute specific through the inclusion of the ***constrictivity*** term in τ_f.

Apparent Diffusion Coefficient (D_a) - The ***diffusion coefficient*** for a porous medium that accounts for the 3-dimensional geometry of the pore space, including its ***tortuosity*** and ***constrictivity***, as well as the sorption behaviour of the solute. It is related to the ***effective diffusion coefficient*** as follows:

$$D_a = \frac{D_e}{\alpha}$$

where: D_a = the ***apparent diffusion coefficient***
D_e = the ***effective diffusion coefficient***
α = the ***rock capacity factor*** (in the case of a conservative solute, α = the ***diffusion accessible porosity***)

Note that the ***apparent diffusion coefficient*** is solute specific through the inclusion of the ***constrictivity*** term in D_e. Also note that the ***apparent diffusion coefficient*** is equal to the ***pore diffusion coefficient*** (described below) when the solute is conservative and the ***diffusion accessible porosity*** is equal to the ***water loss porosity***.

Pore Diffusion Coefficient (D_p) - The ***diffusion coefficient*** for a porous medium that accounts for the 3-dimensional geometry of the pore space, including its ***tortuosity*** and ***constrictivity***. It is the product of the ***free-water diffusion coefficient*** and the ***tortuosity factor*** as follows:

$$D_p = \tau_f \cdot D_0$$

For the case of a conservative solute that is not affected by size exclusion in the pore spaces, the value of ϕ_w should approach ϕ_d. The ***pore diffusion coefficient*** can then be formulated as follows:

$$D_p = \frac{D_e}{\phi_d} \approx \frac{D_e}{\phi_w}$$

where: D_p = the ***pore diffusion coefficient***
D_e = the ***effective diffusion coefficient***
ϕ_d = the ***diffusion accessible porsoity***
ϕ_w = the ***water loss porosity***

Note that the ***pore diffusion coefficient*** is solute specific through the inclusion of the ***constrictivity*** term in τ_f. Also note that the ***pore diffusion coefficient*** is equal to the

apparent diffusion coefficient when the solute is conservative and the ***diffusion accessible porosity*** is assumed to be equal to the ***water loss porosity***.

Rock Capacity Factor (α) - A dimensionless factor accounting for retention of solute mass in a unit volume of the porous medium, which results from changes in solution concentration and sorption of the solute to the solid surfaces. The ***rock capacity factor*** is measured using time lag analysis of steady-state through-diffusion experiments. Mathematically, the ***rock capacity factor*** is defined as:

$$\alpha = \phi_d + \rho K_d$$

where: ϕ_d = ***diffusion accessible porosity***,
ρ = dry bulk density
K_d = sorption coefficient

Note that the ***rock capacity factor*** is equal to the ***diffusion accessible porosity*** when the diffusing tracer is conservative (non-sorbing).

Tortuosity (τ) - A geometric factor of the porous medium accounting for the difference between the effective transport path length (L_e) compared to the shortest straight-line transport path length (L) between two points. It is defined mathematically as:

$$\tau = \left(\frac{L_e}{L} \right)^2$$

where: L = the straight-line path length between two points
L_e = the (longer) effective transport path length between the same two points

Note that in this definition $\tau > 1$, but it is also common for the reciprocal to be used in which case $\tau < 1$. Also note that in some cases ***tortuosity*** has been defined simply as the ratio of L_e to L rather than the square of the ratio.

Tortuosity Factor (τ_f) - An empirical factor that combines the ***tortuosity*** and the ***constrictivity*** to describe the geometric properties of the porous medium that influence diffusive transport. It is defined as:

$$\tau_f = \frac{\delta}{\tau}$$

where: τ_f = the tortuosity factor
τ = the tortuosity and
δ = the constrictivity

Porosity – The ratio of the volume of void spaces in a porous medium to the total volume of the porous medium.

Diffusion Accessible Porosity (ϕ_d) - The volume of pores, per total volume, accessible for a given solute. The **d*iffusion accessible porosity*** is solute specific and is typically determined from diffusion experiments.

Porous medium – A medium that has numerous interstices (voids or pores), whether connected or isolated, in a solid matrix.

Physical Porosity – The volume of pores per total volume of sample. Pores are defined as everything which is not solid. Interlayer water of clays is considered as part of the pore space.

Water Loss Porosity (ϕ_w) – The volume of pores per total volume of sample, derived from water extraction at 105°C (additional specification if extracted e.g. under vacuum). In argillaceous rocks, ***water loss porosity*** at 105°C is usually somewhat smaller than the ***physical porosity***, because the bound water is only partially released at this temperature.

APPENDIX B: MICRO COMPUTED TOMOGRAPHY FOR CHARACTERIZATING ROCK PROPERTIES

CONTENTS

LIST OF TABLES

LIST OF FIGURES

B.1 SPATIAL RESOLUTION

B.1.1 Scanning Electron Microscopy (Thresholded Imaging Technique for Porosity)

Scanning electron microscopy (SEM) studies are conducted on polished sections of rock materials, therefore requiring irreparable cutting and polishing of the sample. The pore spaces in sediments and sedimentary rocks are impregnated with epoxy to maintain sample integrity and spatial relationships during sample preparation. Although 2-D images are collected, in the case of back-scattered-electron imaging (BSEI) and energy-dispersive X-ray spectroscopy (EDS) imaging, the fundamental resolution of the images is a function of the three dimensional interaction volume for the electron beam in the sample material. In these cases, resolution is generally limited by the z-dimension because, although the beam diameter can be much less than 1 μm, the depth of beam penetration into the sample may be much greater than the beam diameter at common operating accelerating voltages and currents. Consequently, spatial resolution for the BSE- and EDS-imaging methods is on the order of 1 to 3 μm. A decrease in pixel size below this limit does not provide an improvement.

When porosity is determined using BSEI and image analysis, the spatial resolution of the images has a direct influence on the resulting porosity determinations as illustrated in Figure B1. The standard method of quantifying porosity with digital BSE images involves thresholding, whereby, a threshold pixel value (grey-scale) is determined below which the dark shades represent epoxy-filled voids and above which the brighter shades represent mineral grains. The total porosity (n) is then calculated as:

$$n = \frac{\sum_{pixels} pv \leq threshold}{total\ \ pixels} \qquad [B1]$$

where: $pv \leq threshold$ represents pixel values that are less than or equal to the threshold.

When the voids are large with respect to the pixel size, this method is very effective. However, the effects of pixel size (x-y resolution) can be understood when considering the effect of thresholding at boundaries between mineral grains and voids. In digital images, the pixel values (0 to 255 for 8-bit grey-scale images) represent an average for the material within the area of the pixel. In the case where an interface between a void (epoxy) and a mineral grain cross cuts a pixel, the assigned pixel value represents a weighted average of the material properties for the void area and the mineral area. This causes a numerical blurring of the interface and leads to corresponding error in the porosity measurement.

The effect of electron-beam penetration (z resolution) can be understood when the interface between epoxy-filled voids and underlying mineral grains is inclined at a shallow angle to the plane of the thin section. In this case, the electron beam penetrates easily through the low-atomic number (Z) epoxy and a BSE signal from the underlying mineral is detected giving rise to pixel values above the threshold. The combination of these effects is evident in Figure B1b where the dashed red line represents the boundary between the mineral grain and the epoxy-filled voids. The large perimeter region with pixel values intermediate between the bright shades of the mineral grain and the dark shades of the voids arises primarily from electron beam penetration through a thin overlying layer of epoxy. Using the image histogram (Figure B1c) a choice of threshold value must be made, and then a thresholded binary image is created (Figure B1d) and used to determine total porosity (Equation B1). Note that the representation

of the mineral-void interface in the binary image is poor in region 1 (Figure B1b) where the mineral grain lies just below the surface of the epoxy, while the representation of the interface in region 2 is much better. These issues of resolution are particularly problematic when the pore size is small and approaches the dimensions of the volume of the electron beam interaction in the sample material.

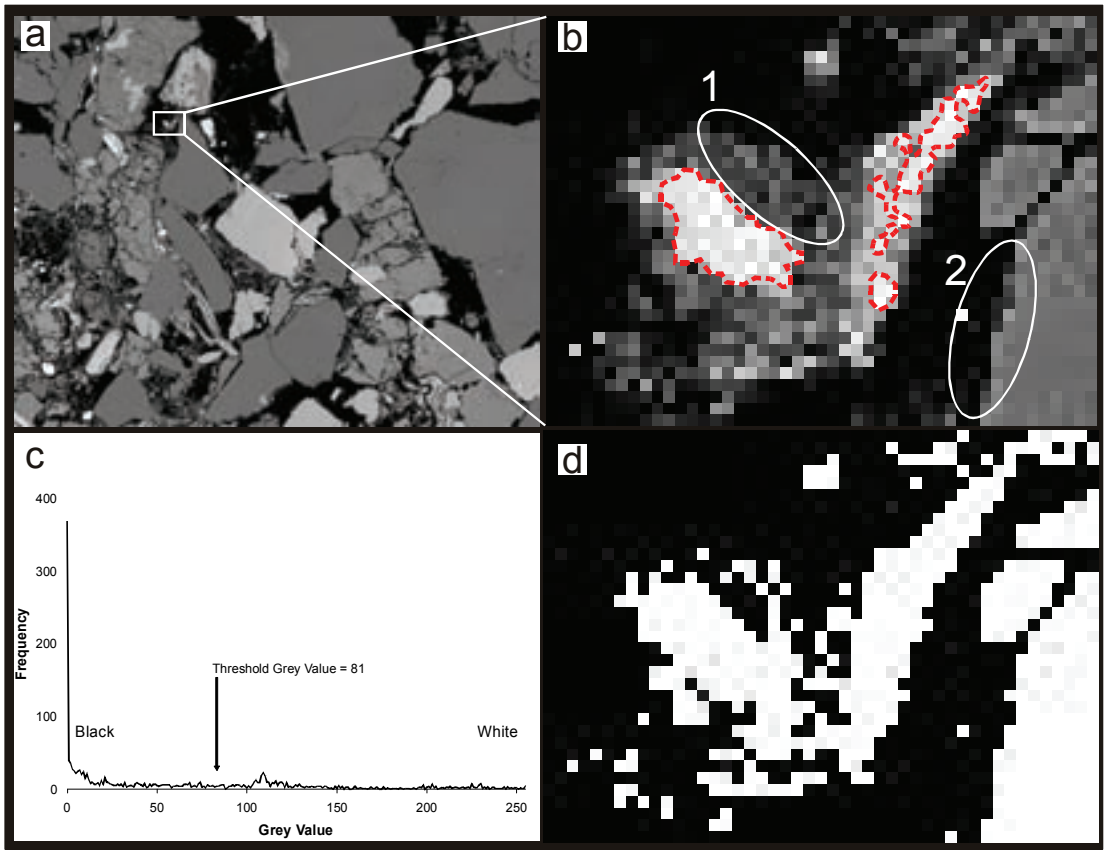

Figure B.1. Description of the effects of spatial resolution on porosity measurements using the thresholding technique. A) digital BSE image of sandstone with dark void space and bright mineral grains, b) selected region of interest showing the approximate area of intersection between the mineral grain and the upper plane of the thin section (red dashed line), c) histogram of pixel values for the image shown in (b), and d) thresholded binary image derived from (b). See the text for additional details.

B.2 METHODS

B.2.1 Conventional Mineralogy

Conventional determinative mineralogical methods were used in the course of this project in an effort to identify halite in samples of Queenston Formation shale. Thin sections were examined with optical microscopy and SEM/EDS, and white powder precipitates, observed coating the surface of several fractures, were identified using X-ray diffraction (XRD).

B.2.2 Optical and Scanning Electron Microscopy

Five polished petrographic thin sections were prepared in the Department of Geology at the University of New Brunswick. The sections were prepared using cutting and polishing methods that utilize kerosene rather than water to prevent dissolution of soluble salt precipitates such as halite. These methods are well established, as the technical staff responsible for sample preparation routinely prepare sections from halite- and sylvite-rich samples for potash mining companies that operate in New Brunswick.

Optical microscopy was conducted using a Lietz Laborlux Pol petrographic microscope equipped with a Nikon Coolpix 4500 digital camera. SEM imaging and analyses were conducted with a JEOL JSM-6400 instrument equipped with an EDAX Genesis EDS system. Images were acquired using both BSE and EDS imaging techniques.

B.2.3 Powder X-Ray Diffraction

Samples were prepared for XRD analysis by scraping the precipitate powders from the fracture surfaces using a dissecting needle, then pulverizing to a fine powder using an agate mortar and pestle. Analyses were conducted using a Bruker D-8 Advance diffractometer equipped with a solid-state energy-dispersive detector.

B.2.4 SEM-BSEI: Porosity Determination

In order to provide some constraint on porosity calculations from the microCT technique, a total of 15 BSE images were acquired from polished thin sections and analyzed with grey-scale thresholding (see Section B1.1) to determine total porosity. Image analysis was conducted using the US National Institute of Health public-domain software ImageJ v. 1.33 (http://rsb.info.nih.gov/ij/).

B.3 RESULTS AND DISCUSSION

B.3.1 Conventional Mineralogy

B.3.1.1 Optical and Scanning Electron Microscopy

Based on examination of five thin sections, these samples of Queenston Formation shale consist of clay-silt size (< 62 μm) clastic grains supported by a fine-grained matrix. The shale varies from red (oxidized) to green (reduced) facies, the red colour resulting from pervasive fine-grained hematite in the matrix (Figure B2a,c). The hematite probably contributes to the cementing of the clastic particles; however, the shale samples that were studied are poorly cemented and have been observed to break apart when saturated with water.

The mineralogy has been characterized on the basis of chemical composition as determined by EDS imaging (Figure B3). The results suggest that the clastic particles are mostly quartz, with lesser amounts of K- and Na-rich feldspar, while the matrix is dominantly composed of K-Al-silicates, probably illite or muscovite. The hematite that occurs in the matrix with the K-Al silicates is evident in the EDS Fe image (Figure B3c). Calcite occurs as angular to subrounded particles suggestive of a clastic origin, but also occurs as secondary overgrowths on primary mineral grains (Figure B3b). Dolomite is common as subhedral to euhedral crystals (ten to several hundred μm across) that overprint the primary shale matrix (Figure B2c; Figure B3a,b). Brogly et al. (1998) describe gypsum nodules in various facies within the Queenston Formation and these were observed in several samples, however, the two nodules that were studied in detail are comprised primarily of anhydrite, with a rim of calcite and a thin discontinuous layer of gypsum between the calcite and anhydrite (Figure B2b).

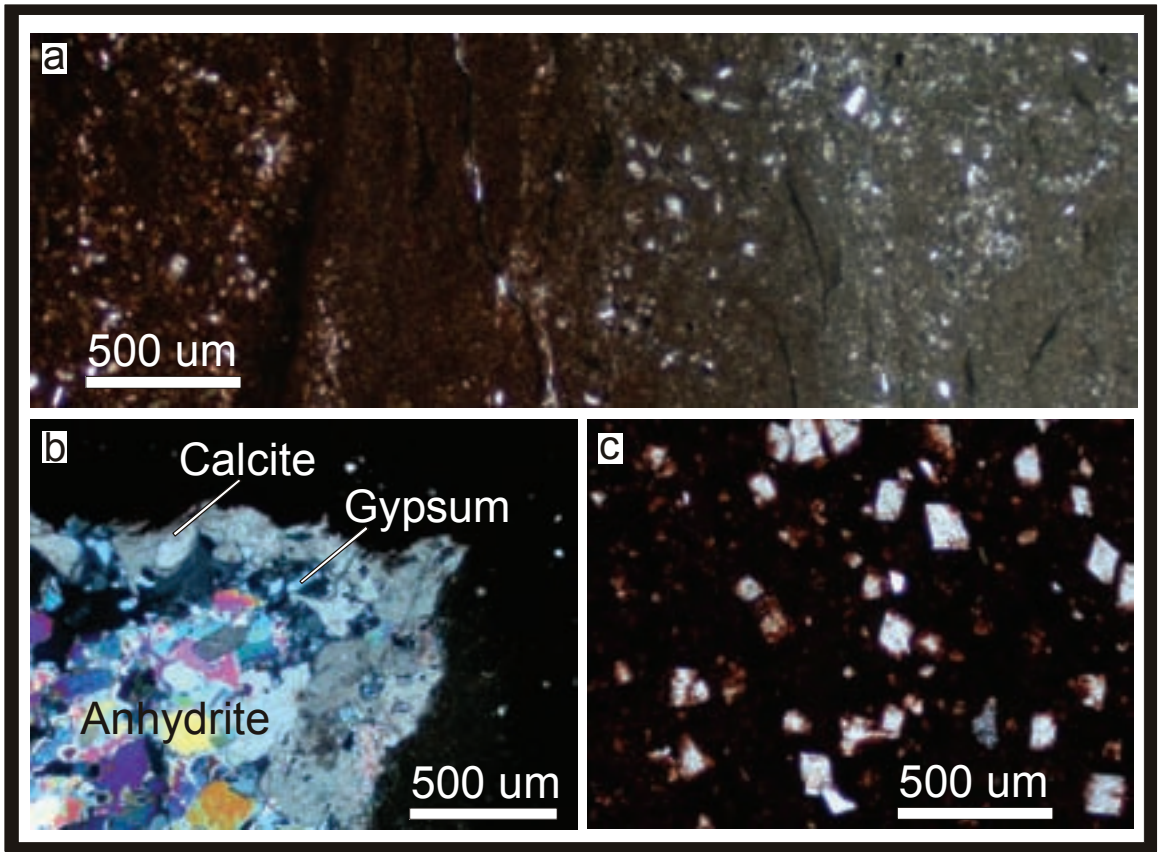

Figure B.2. Photomicrographs of shale demonstrating the occurrence of: a) redox boundaries between oxidized (left) and reduced (right) zones with dark grey-black wispy fragments of organic carbon evident in the reduced zone – plane polarized light; b) the margin of a "gypsum" nodule showing the anhydrite core surrounded by calcite and intervening discontinuous layer of gypsum – cross-polarized light; c) typical shale matrix with overprinting dolomite crystals – plane polarized light.

An effort was made to identify halite in the samples using optical microscopy and SEM-EDS methods. Halite is in the isometric crystal class and therefore, optically, it is isotropic and would appear to be black under cross-polarized light. There was no indication of the presence of halite using optical microscopy, so the next level of investigation involved the collection of analytical images for Na and Cl using SEM-EDS (similar to the Fe image in Figure B3c). Images of the Na and Cl distribution in the shale were obtained at 1000x magnification in order to achieve a resolution capable of identifying small amounts of halite in the pore spaces of the shale. These analytical images were collected at a resolution of 256 x 200 pixels, with each pixel having dimensions of 0.435 x 0.435 μm. Five analytical images of this type were collected from random locations in each thin section, and no indications of coincident Na and Cl concentrations were noted.

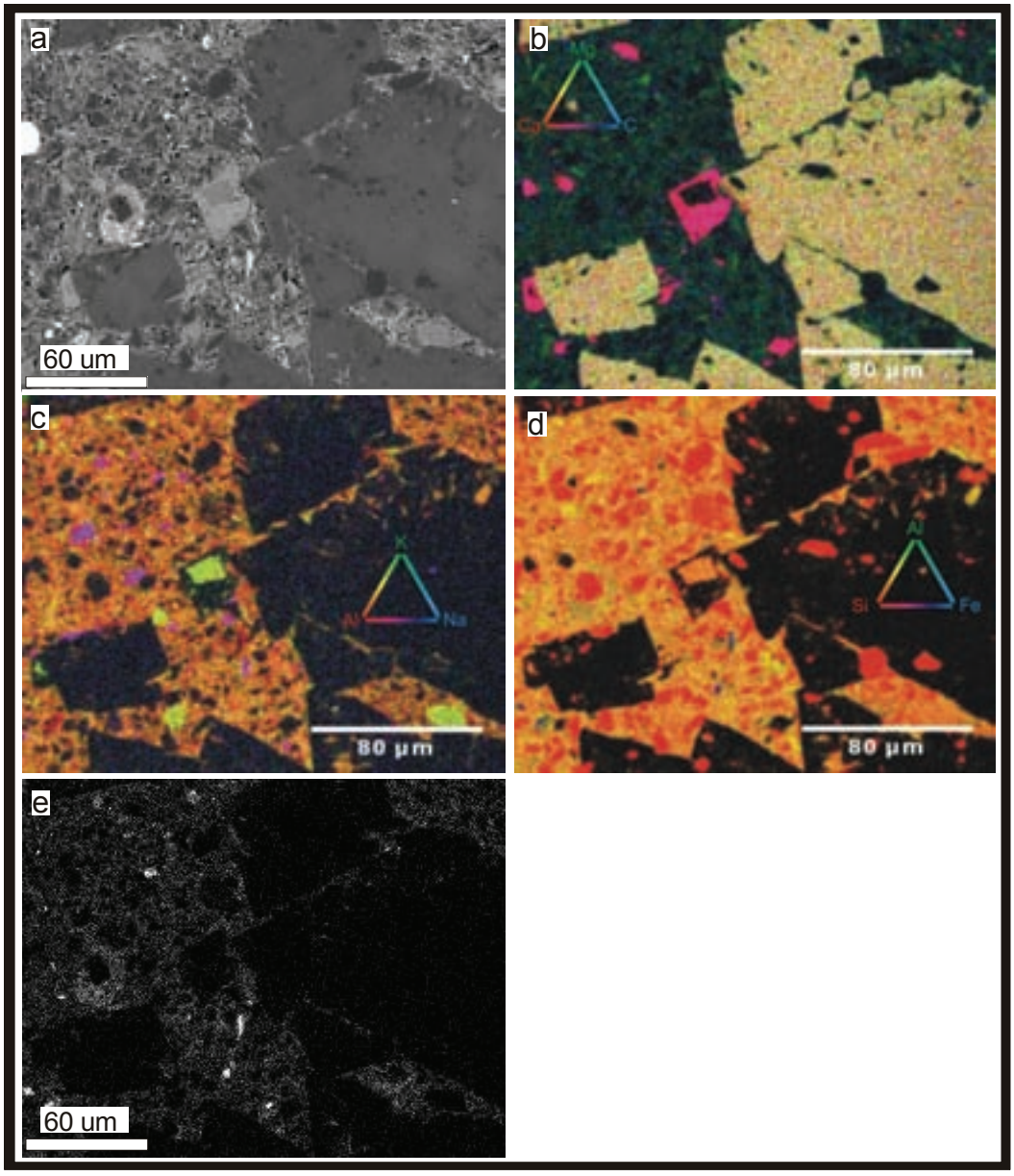

Figure B.3. SEM-BSE and SEM-EDS images indicating the principal mineralogy of the shale. a) SEM-BSE reference image showing large dolomite and calcite crystals overprinting the shale matrix. b) Red-green-blue (RGB) image formed by merging individual analytical EDS images, red for Ca, green for Mg and blue for C, with the resulting colour mixtures reflecting the 3-component chemical composition of the minerals. Note that the Ca-Mg-C components of dolomite result in a pale cream colour and the Ca-C components of calcite result in a red-purple colour. c) RGB image, red for Al, green for K and blue for Na. This image illustrates the distribution of K feldspars (yellow-green) and Na feldspars (purple). d) RGB image, red for Si, green for Al, and blue for Fe, illustrating the distribution of quartz (red) and the dominance of Al-silicate clay minerals (yellow-orange) in the matrix. e) SEM-EDS image illustrating the distribution of Fe in the matrix (the grey-scale intensity has been increased by a factor of 10 to enhance visibility).

B.3.1.2Powder X-ray Diffraction

White mineral fracture coatings were investigated from two samples with powder X-ray diffraction. In each case the mineral coating was determined to be gypsum (Figure B4).

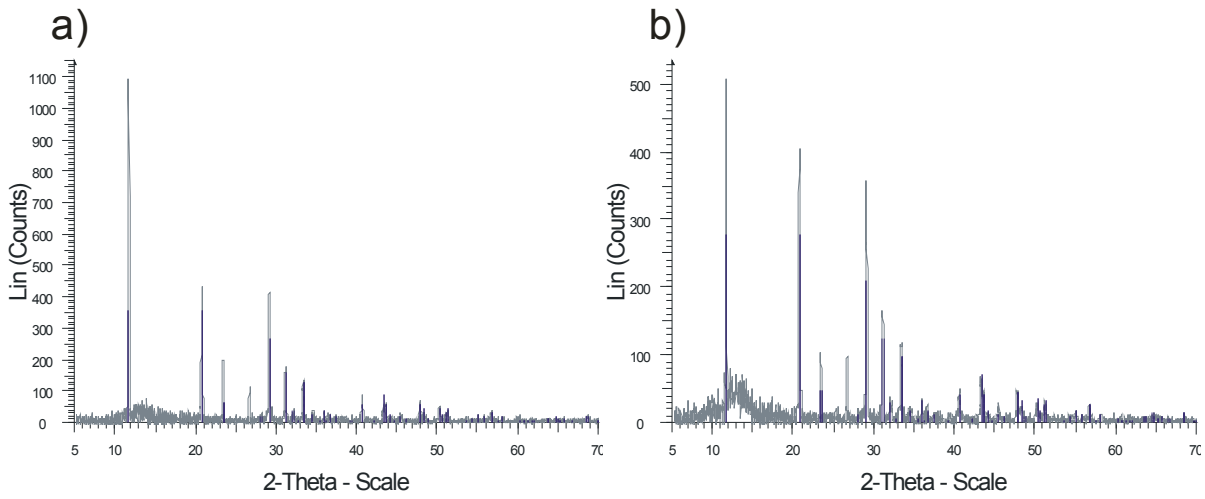

Figure B.4. Powder X-ray diffraction patterns collected from white fracture-coating precipitates on core sample a) S2005-1-88 and b) S2005-1-78. Note that the sample diffraction patterns match well with the known locations for gypsum diffraction lines (blue index lines). There is one unidentified peak at 26° 2-theta which corresponds to the principal diffraction line for quartz.

B.3.1.3SEM-BSEI: Porosity Determination

The porosity of the shale was determined in five areas that were selected at random on each of three thin sections (a total of 15 measurements; Figure B5; Table B1). Based on the thresholded binary image presented in Figure B5b, the pore sizes range from 0.06 to 130 μm^2, with a mean of 0.55 μm^2. There is a systematic bias in these measurements as a consequence of the resolution-related errors that were discussed above (see Section B1.1), and the actual porosity will be higher. However, independent measurements are required in order to state the magnitude of the bias.

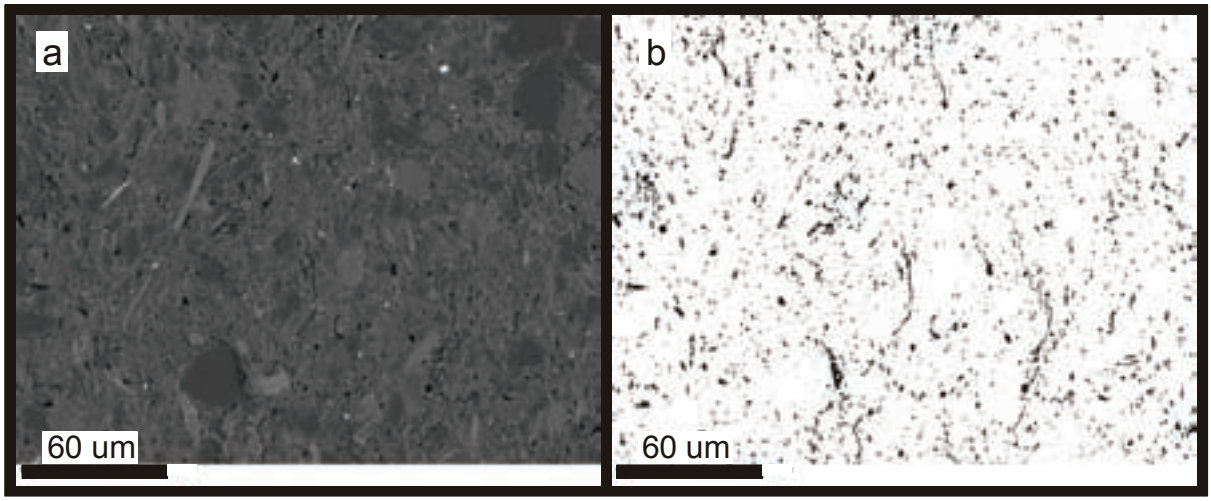

Figure B.5. Example of a) SEM-BSE image (sample 78-1-5) illustrating porosity (dark grey-black) and b) thresholded binary image created from (a) where the black regions represent pore spaces.

Table B.1. Porosity as determined from BSE images and image analysis

	Porosity (%)		
Sample	**78-1**	**88-1**	**93-1**
1	4.5	6.0	5.2
2	6.3	6.6	4.5
3	6.9	3.9	5.7
4	5.1	6.0	6.4
5	4.3	5.5	4.7
Average	5.4	5.6	5.3

REFERENCE

Brogly, P.J., I.P. Martini, and G.V. Middleton. 1998. The Queenston Formation: shale-dominated, mixed terrigenous carbonate deposits of Upper Ordovician, semiarid, muddy shores in Ontario, Canada. Canadian Journal of Earth Science 35, 702-719.

APPENDIX C: PROTOCOL FOR MEASUREMENT OF DIFFUSION PROPERTIES BY X-RAY RADIOGRAPHY

CONTENTS

C.1: PROTOCOL FOR MEASUREMENT OF DIFFUSION PROPERTIES BY X-RAY RADIOGRAPHY

The steps for X-ray radiography measurements of 1-D diffusion coefficients are:

1) Cut a cylindrical rock sample (11 mm diameter, 1 to 2 cm length) from the drill core. Orient the cylinder axis along the desired direction of measurement (e.g. parallel or perpendicular to bedding).

2) Dry the outside of the sample in an oven set at 60°C overnight, coat around its perimeters with epoxy or similar non-permeable coating and allow to cure for at least 12 hours.

3) Mount the sample ends in aluminium diffusion cells, consisting of two solution reservoirs. Seal around all joints with epoxy and allow to cure.

4) Immerse the open diffusion cell with the rock sample in a container of synthetic pore water solution (no I^-). Place under vacuum for at least 1 week to allow the sample to saturate.

5) Fill the upper and lower reservoirs with synthetic pore water solution and seal the reservoir caps and injection holes (e.g. with electrical tape). Mount an internal X-ray standard material (e.g. aluminum bar or wire) and alignment guide alongside the sample.

6) Rinse the outside of the sample with distilled water to remove any salt precipitated from overflow during filling and gently pat dry. Place the sample in the microCT sample chamber, adjust magnification, height and rotation so that the sample is completely in field of view and the internal standard is perpendicular to the X-ray beam. Collect Time = 0 X-ray radiograph image. Save the image as a 16 bit TIFF data file (65536 greyscale values).

7) To start the diffusion test, slowly inject KI tracer solution into the bottom of the lower reservoir, using paper towel to wick away the displaced solution from the air vent hole. Inject at least three times the reservoir volume to displace synthetic pore water solution completely with the tracer solution. Store the diffusion cells in a temperature-controlled environment and maintain 100% humidity to prevent evaporation of solutions, for example, an airtight container with a shallow, water-filled, evaporation dish in a temperature-controlled laboratory may be used for this purpose.

8) After 24 hours, return the sample to the X-ray chamber, align exactly as for Time = 0 image and collect the Time = 24 hr radiograph.

9) Repeat radiograph data collection daily for the first 3 days and then at increasing time intervals during the diffusion test, adjusting the time interval to the measured rate of diffusion as the experiment progresses.

10) At 1-week intervals, replace the tracer solution in the lower reservoir by injecting at least 5 ml of fresh tracer solution of the same concentration as the initial solution and wicking away the displaced solution. Rinse the outside of the epoxy-coated sample with distilled water to remove salt.

11) Once the X-ray data processing shows that I^- has broken through to the upper reservoir, replace the synthetic pore water in the upper reservoir with KI tracer solution. Inject at least three times the reservoir volume to displace the synthetic pore water solution. Allow I^- to diffuse in from both ends until the sample is saturated with I^- solution. Collect an X-ray radiograph image of sample saturated with KI tracer solution. Continue to diffuse iodide from both sides of the sample and collect radiographs weekly to check on the progress of I^- through the rock. Once no further change is observed, and the I^- profile is constant along the entire length of the sample, collect a final image of the I^--saturated sample.

12) Use image processing software to analyze the radiograph data. The following description relates to the freeware image analysis package *ImageJ*.

13) Determine the average greyscale intensity of the internal standard (e.g. Al) and use this result to correct the image intensity of all other time steps relative to Time = 0.

14) Crop the images to an identical rectangular region of interest (ROI) over the rock sample for each time step. Set the image scale, rotate images by 90 degrees and plot profiles of greyscale intensity (integrated across the width of the sample) vs. length along the diffusion pathway. Export the data to a spreadsheet.

15) Convert the greyscale profiles to plots of $\Delta\mu$ (X-ray absorption coefficient) vs distance by taking the natural logarithm of the greyscale values and subtracting: ln (Time = 0) – ln (Time = n) for each time step. Use the calibration standard data and measured bulk gravimetric porosity values (for homogeneous samples) or, alternatively, the final I^--saturated image data, to convert $\Delta\mu$ profiles to plots of normalized I^- concentration (C/C_0) vs. distance for each time step.

16) Fit solutions of Fick's law to the C/C_0 vs distance plots, correcting for distance discrepancies between the solution boundary inside the reservoir and the ROI in the images. The 1-D pore diffusion coefficient (D_P) is found by iterating until the analytical solution best matches the measured profiles for all time steps before I^- breakthrough.

17) Align an ROI over radiographs for initial (brine-saturated) and final (I^--saturated) images and crop the images to the ROI. Create images of the natural logarithm of

the greyscale values for each image and subtract the ln (final) image from the ln (Time = 0) image. Rotate the resultant image by 90 degrees and plot a profile. Export the data to a spreadsheet and process as for diffusion time series. Fit a quadratic function through the $\Delta\mu_{sat}$ profile and correct profile to remove curvature from cone beam effect. Use calibration function to calculate the mass of pore water iodide (m_{Ix}) at each distance x from and divide by m_0, the mass (or concentration) of iodide in the tracer. This gives the 1-D iodide-accessible porosity profile (ϕ_I) versus distance. The ϕ_I profile can be used in conjunction with the data collected in Step 14) for determining I^- concentrations in heterogeneous samples. For homogeneous samples, a mean ϕ_I value can be used to calculate D_e using the equation: $D_e = \phi_I \cdot D_p$.

APPENDIX D: DIFFUSION TEST DATA

CONTENTS

Page

D.1 QUEENSTON SHALE SAMPLES

D.1.1 Q078NB1

Table D.1: Iodide diffusion coefficients for Queenston shale sample Q078NB1

Sample: Q078NB1		**ϕ_w: 0.0616**	
Time step (hours)	**D_p (m^2/s)**	**D_e (m^2/s)**	**Curve fit**
1	1.5×10^{-9}	9.2×10^{-11}	poor
4	5.0×10^{-10}	3.1×10^{-11}	poor
8	2.0×10^{-10}	1.2×10^{-11}	poor
24	**7.8×10^{-11}**	**4.8×10^{-12}**	**good**
48	**6.3×10^{-11}**	**3.9×10^{-12}**	**good**
120	**7.5×10^{-11}**	**4.6×10^{-12}**	**good**
170	9.0×10^{-11}	5.5×10^{-12}	poor
314	-	-	epoxy cracked
384	-	-	epoxy cracked
528	-	-	epoxy cracked
Mean (24 - 120 hr)	**7.2×10^{-11}**	**4.4×10^{-12}**	**good**

Experimental conditions:

- Sample axis normal to bedding.
- 0.6 M KI tracer in 3M brine (NaCl).
- Tracer diffusion for 22 days.
- Did not fully saturate sample with iodide. Epoxy coating started cracking after 170 hr.
- No 1-D porosity profile available.
- All concentration data corrected for ϕ_w.
- Relative concentration profiles calculated from mean $\Delta\mu$ near influx boundary from 314 hours onwards.
- x-axis boundary shift: 2.3 mm

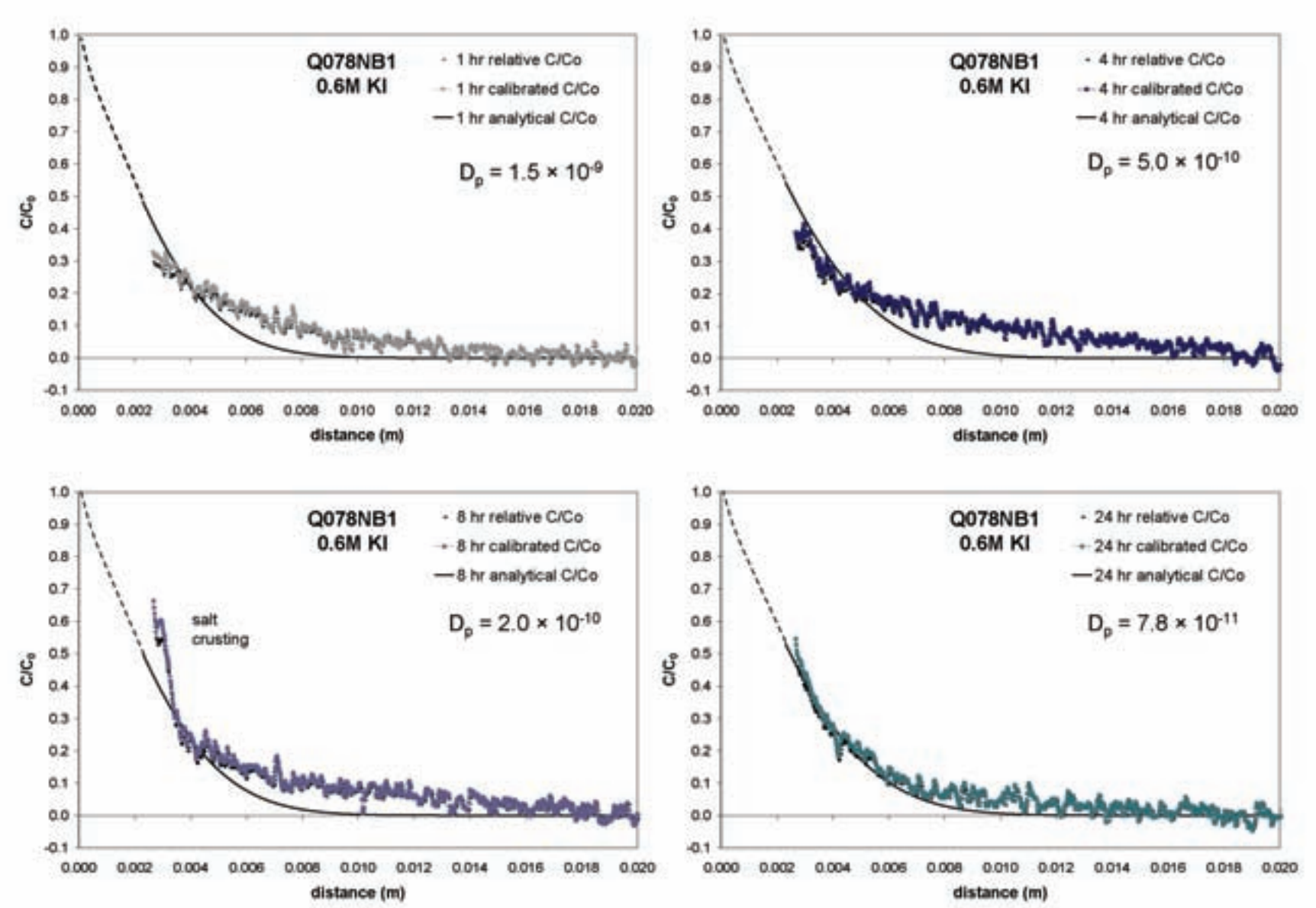

Figure D.1: Iodide concentration profiles and analytical diffusion profiles for Q078NB1

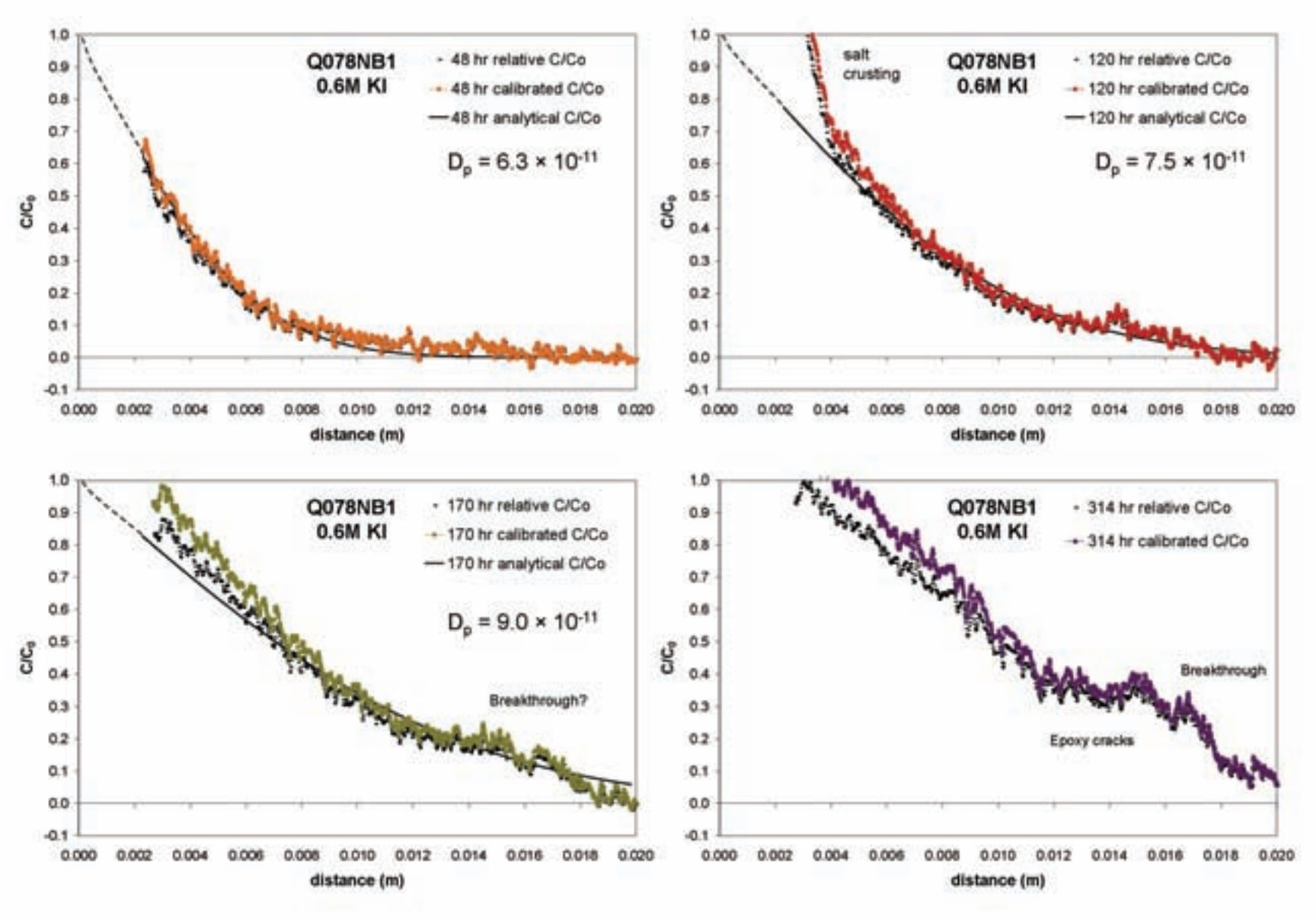

Figure D.1 (continued): Iodide concentration profiles and analytical diffusion profiles for Q078NB1.

D.1.2 Q078NB2

Table D.2: Iodide diffusion coefficients for Queenston shale sample Q078NB2

Sample: Q78NB2		**ϕ_w: 0.0616**	
Time step (hours)	**D_p (m^2/s)**	**D_e (m^2/s)**	**Curve fit**
1	3.0×10^{-9}	1.9×10^{-10}	poor
4	5.0×10^{-10}	3.1×10^{-11}	poor
8	3.0×10^{-10}	1.9×10^{-11}	poor
24	**6.2×10^{-11}**	**3.8×10^{-12}**	**good**
48	**5.5×10^{-11}**	**3.4×10^{-12}**	**good**
120	**4.5×10^{-11}**	**2.8×10^{-12}**	**good**
170	**4.0×10^{-11}**	**2.5×10^{-12}**	**good**
314	-	-	breakthrough
384	-	-	breakthrough
528	-	-	breakthrough
840	-	-	breakthrough
Mean (24 - 170 hr)	**5.1×10^{-11}**	**3.1×10^{-12}**	**good**

Experimental conditions:

- Sample axis normal to bedding.
- 0.6 M KI tracer in 3M brine (NaCl).
- Tracer diffusion for 22 days.
- Did not fully saturate sample with iodide.
- No 1-D porosity profile available.
- All concentration data corrected for ϕ_w.
- Relative concentration profiles calculated from mean $\Delta\mu$ near influx boundary at 384 hr.
- x-axis boundary shift: 2.3 mm

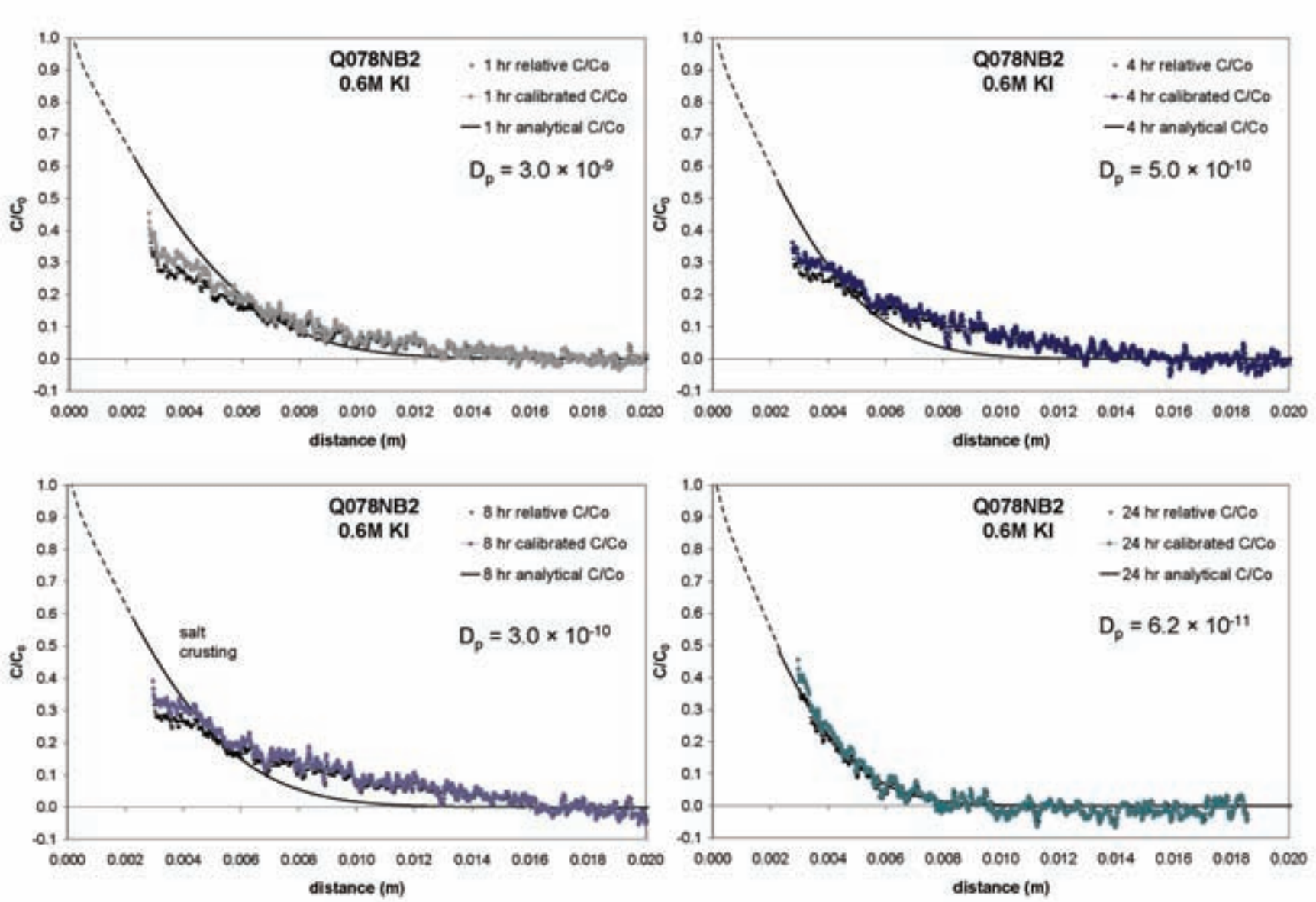

Figure D.2: Iodide concentration profiles and analytical diffusion profiles for Q078NB2.

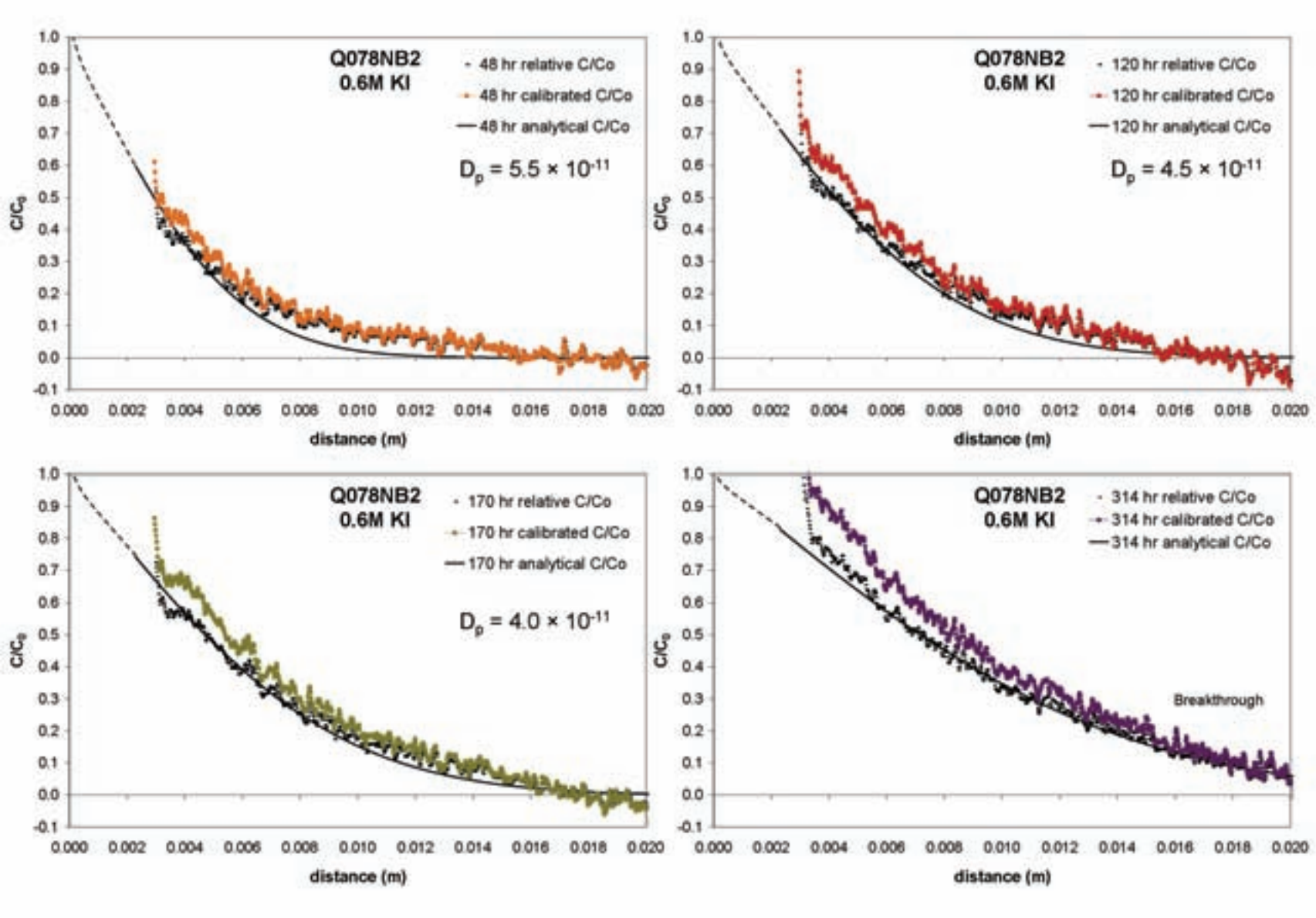

Figure D.2 (continued): Iodide concentration profiles and analytical diffusion profiles for Q078NB2.

D.1.3 Q078NB3

Table D.3: Iodide diffusion coefficients for Queenston shale sample Q078NB3

Sample: Q078NB3		**ϕ_w: 0.0616**	
Time step (hours)	**D_p (m^2/s)**	**D_e (m^2/s)**	**Curve fit**
1	1.0×10^{-9}	6.2×10^{-11}	poor
4	4.0×10^{-10}	2.5×10^{-11}	poor
8	2.0×10^{-10}	1.2×10^{-11}	poor
24	**9.5×10^{-11}**	**5.9×10^{-12}**	**good**
48	**1.0×10^{-10}**	**6.2×10^{-12}**	**good**
120	**6.0×10^{-11}**	**3.7×10^{-12}**	**good**
170	**8.0×10^{-11}**	**4.9×10^{-12}**	**good**
314	-	-	breakthrough
384	-	-	breakthrough
528	-	-	breakthrough
840	-	-	breakthrough
Mean (24 - 170 hr)	**8.4×10^{-11}**	**5.2×10^{-12}**	**good**

Experimental conditions:

- Sample axis normal to bedding.
- 1.0 M KI tracer in 3M brine (NaCl).
- Tracer diffusion for 22 days.
- Did not fully saturate sample with iodide.
- No 1-D porosity profile available.
- All concentration data corrected for ϕw.
- Relative concentration profiles calculated from mean $\Delta\mu$ near influx boundary at 384 and 840 hr.
- x-axis boundary shift: 2.4 mm

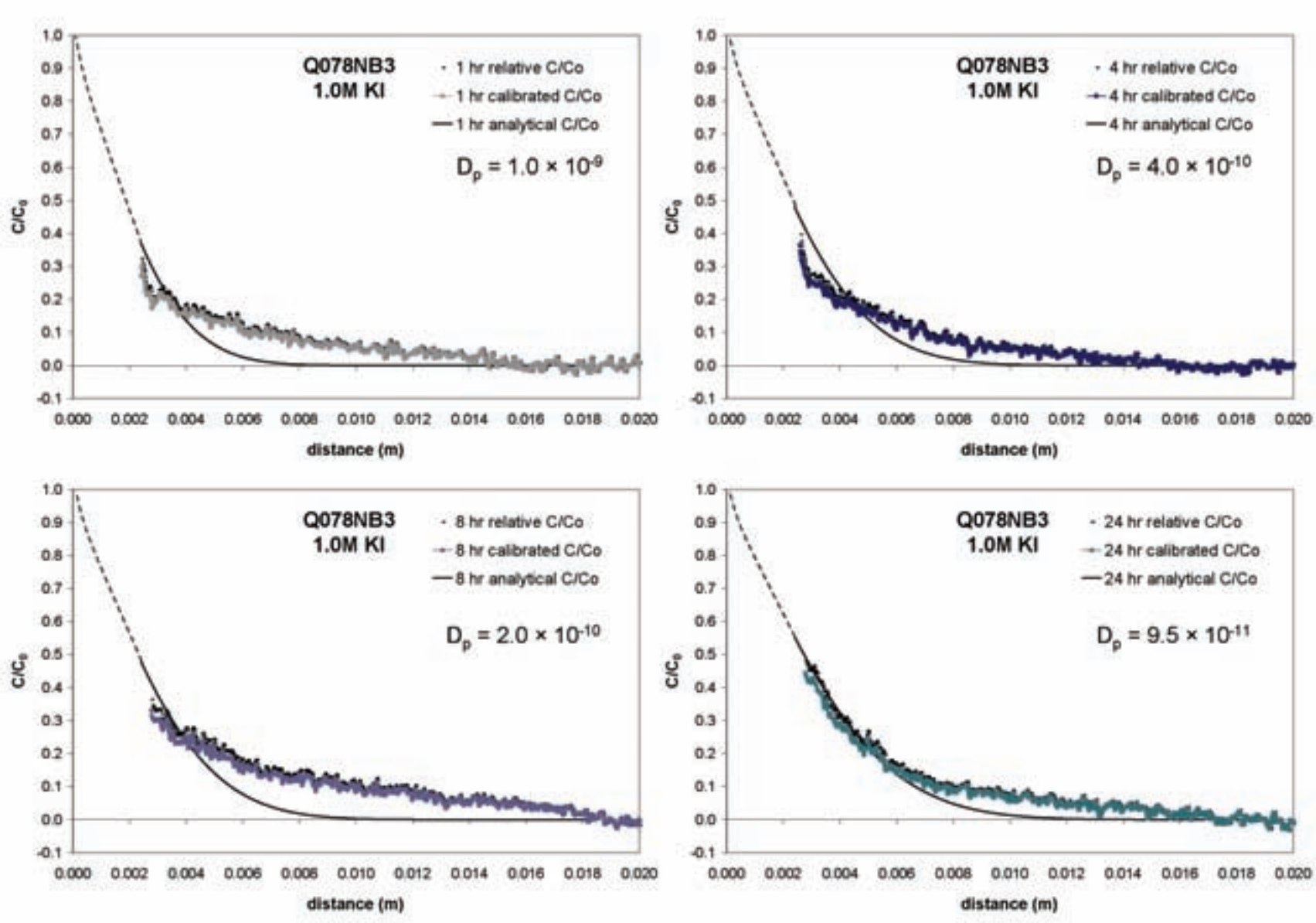

Figure D.3: Iodide concentration profiles and analytical diffusion profiles for Q078NB3.

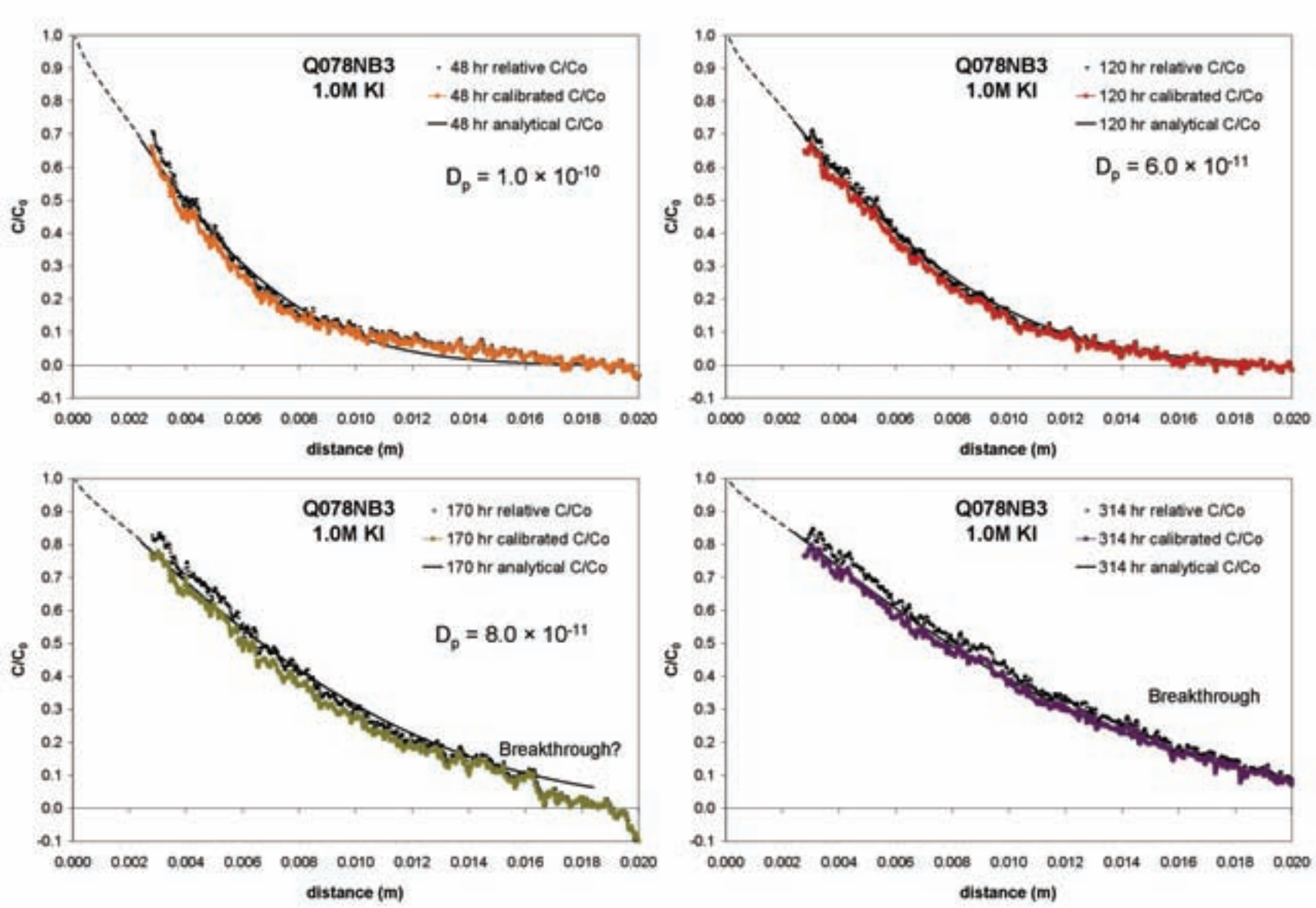

Figure D.3 (continued): Iodide concentration profiles and analytical diffusion profiles for Q078NB3.

D.1.4 Q078NB4

Table D.4: Iodide diffusion coefficients for Queenston shale sample Q078NB4

Sample: Q078NB4		**ϕ_w: 0.0616**	
Time step (hours)	**D_p (m^2/s)**	**D_e (m^2/s)**	**Curve fit**
1	1.0×10^{-9}	6.2×10^{-11}	poor
4	2.0×10^{-10}	1.2×10^{-11}	poor
8	2.0×10^{-10}	1.2×10^{-11}	poor
24	**8.0×10^{-11}**	**4.9×10^{-12}**	**fair**
48	**8.0×10^{-11}**	**4.9×10^{-12}**	**good**
120	**5.5×10^{-11}**	**3.4×10^{-12}**	**good**
170	**5.0×10^{-11}**	**3.1×10^{-12}**	**fair**
314	-	-	breakthrough
384	-	-	breakthrough
528	-	-	breakthrough
Mean (24 - 170 hr)	**6.7×10^{-11}**	**4.1×10^{-12}**	**good**

Experimental conditions:

- Sample axis normal to bedding.
- 1.0 M KI tracer in 3 M brine (NaCl).
- Tracer diffusion for 22 days.
- Did not fully saturate sample with iodide.
- No 1-D porosity profile available.
- All concentration data corrected for ϕ_w.
- Relative concentration profiles calculated from mean $\Delta\mu$ near influx boundary at 528 hr.
- x-axis boundary shift: 2.3 mm

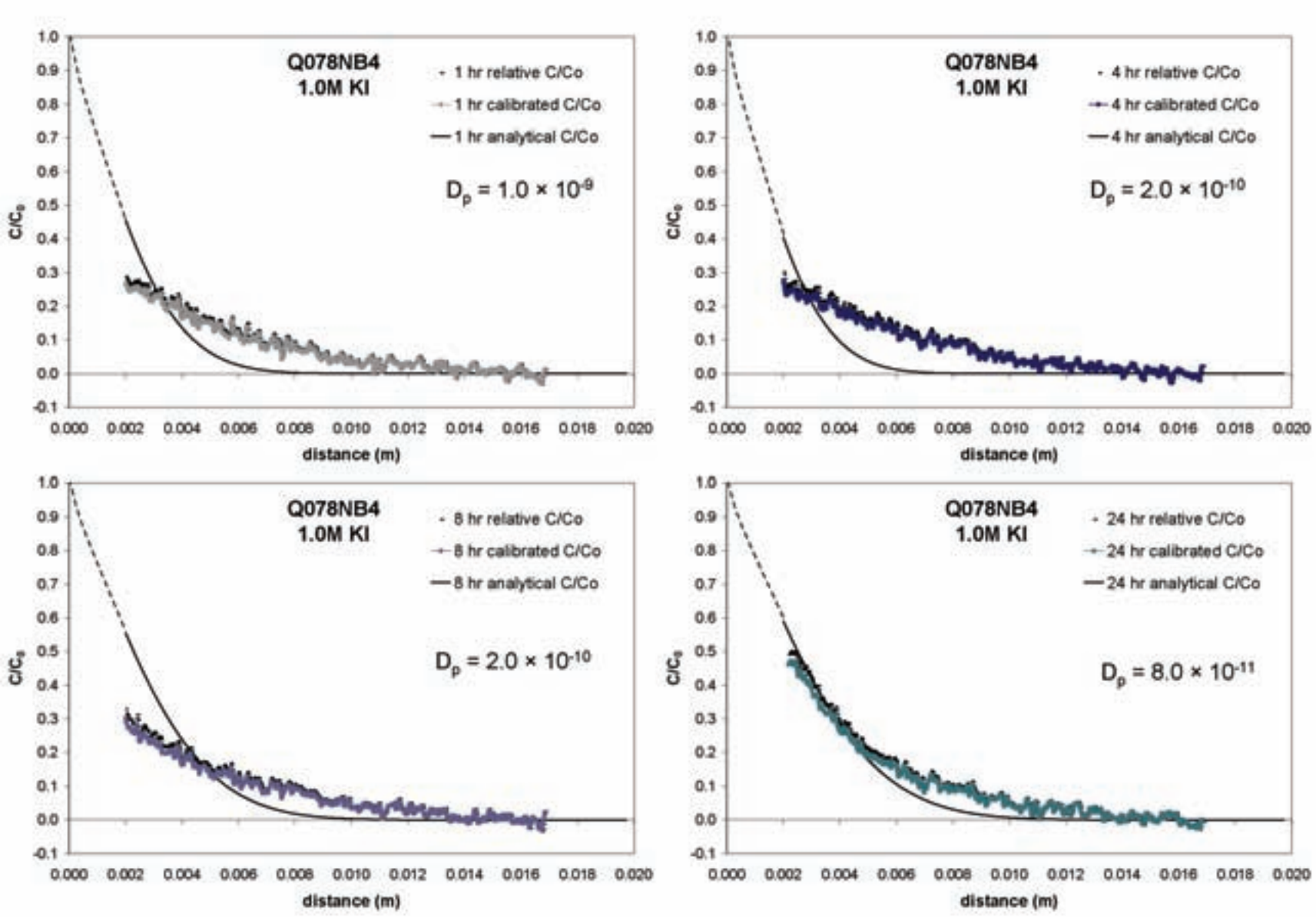

Figure D.4: Iodide concentration profiles and analytical diffusion profiles for Q078NB4.

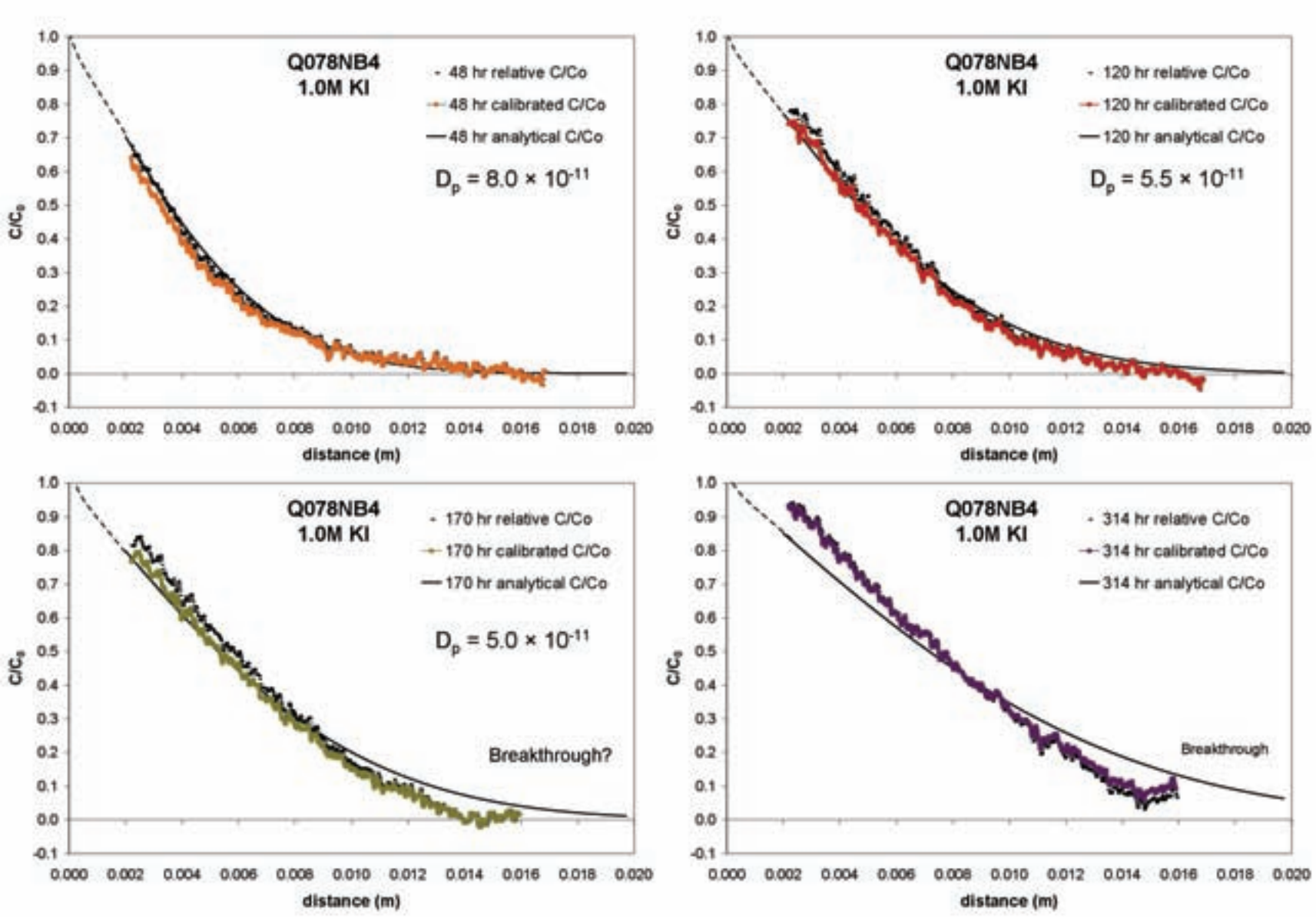

Figure D.4 (continued): Iodide concentration profiles and analytical diffusion profiles for Q078NB4.

D.1.5 Q105NB

Table D.5: Iodide diffusion coefficients for Queenston shale sample Q105NB

Sample: Q105NB	**ϕ_w: 0.0588**	**$\phi_{I,\,av}$: 0.057**	
Time step (hours)	**D_p (m^2/s)**	**D_e (m^2/s)**	**Curve fit**
1	1.0×10^{-9}	5.7×10^{-11}	poor
4	3.0×10^{-10}	1.7×10^{-11}	poor
8	1.5×10^{-10}	8.6×10^{-12}	poor
24	**6.0×10^{-11}**	**3.4×10^{-12}**	**good**
48	**4.5×10^{-11}**	**2.6×10^{-12}**	**good**
120	1.5×10^{-11}	8.6×10^{-13}	fair
170	**2.0×10^{-11}**	**1.1×10^{-12}**	**good**
314	-	-	breakthrough
384	-	-	breakthrough
528	-	-	breakthrough
840	-	-	breakthrough
Mean (24 - 170 hr)	**4.2×10^{-11}**	**2.4×10^{-12}**	**good**

Experimental conditions:

- Sample axis normal to bedding.
- 0.8 M KI tracer in 3 M brine (NaCl).
- Tracer diffusion for 35 days.
- Tracer saturation for 25 days until sample was fully saturated with iodide.
- 1-D porosity profile determined from difference between iodide saturated and zero iodide.
- All concentration data corrected for ϕ_w.
- D_e calculated from $\phi_{I,\,average}$
- Relative concentration profiles calculated from mean $\Delta\mu$ near influx boundaries after 25 days saturation. Not used to fit analytical solution.
- Small fracture at 5.2 mm may influence results.
- x-axis boundary shift: 2.8 mm.

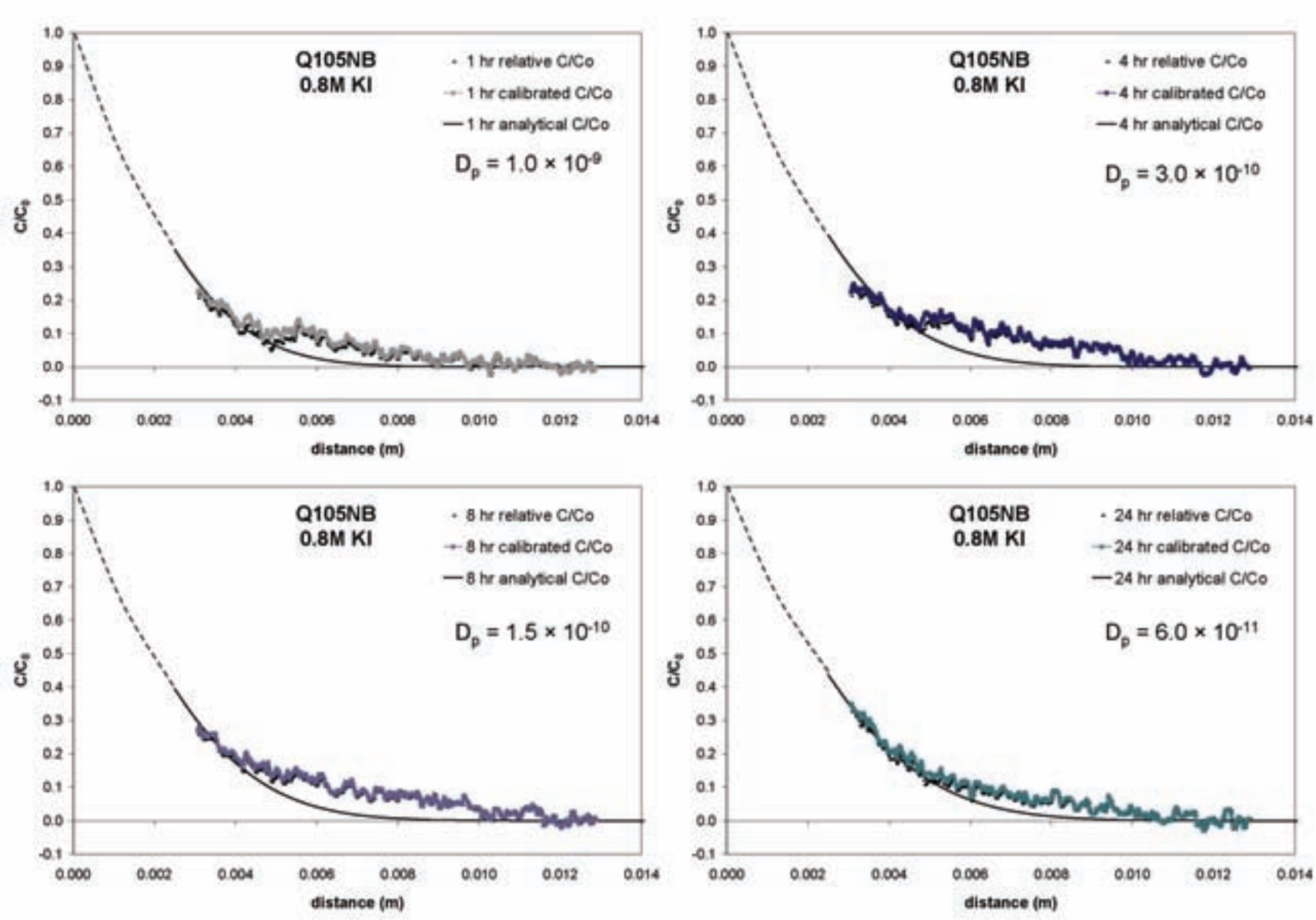

Figure D.5: Iodide concentration profiles and analytical diffusion profiles for Q105NB.

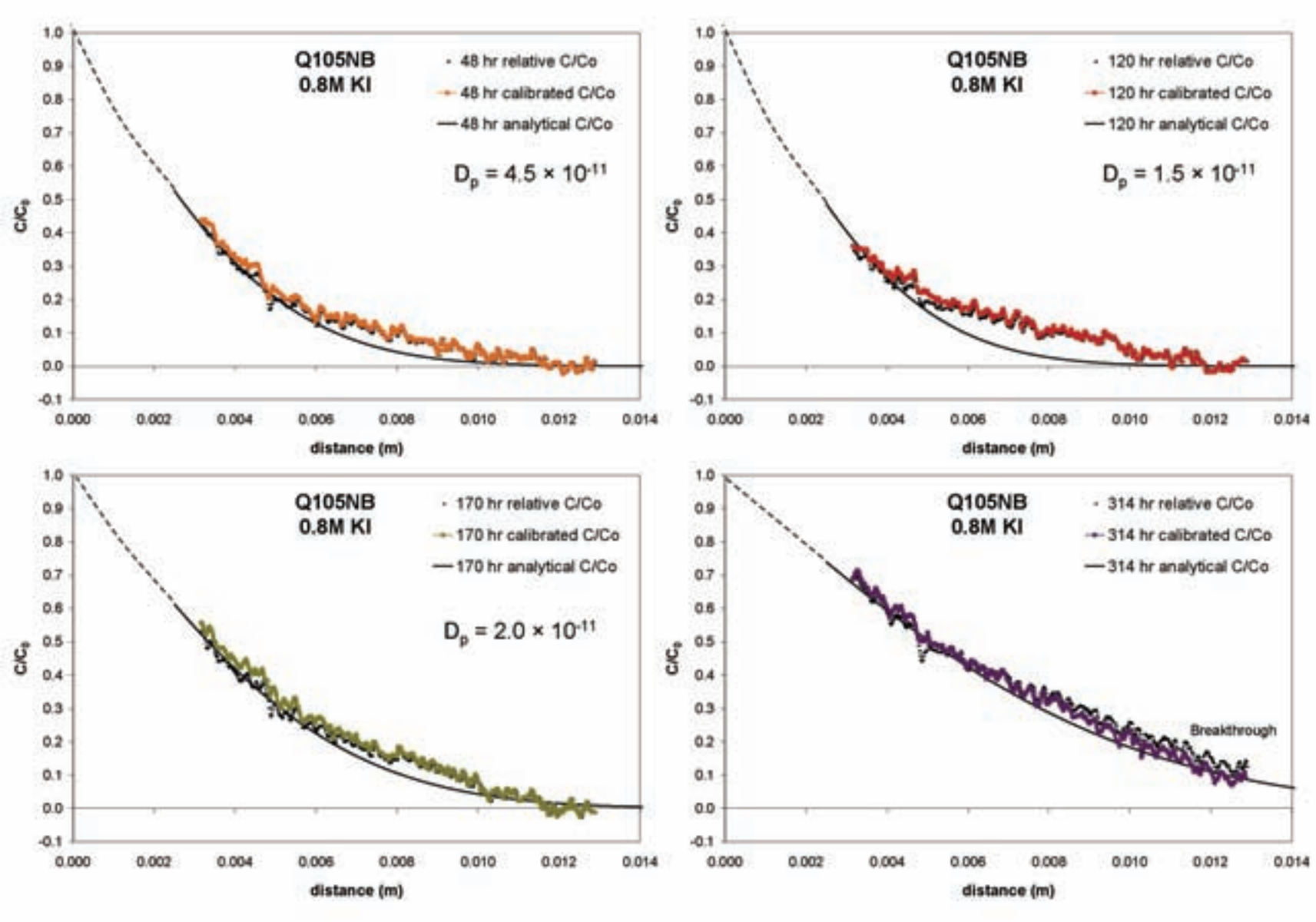

Figure D.5 (continued): Iodide concentration profiles and analytical diffusion profiles for Q105NB.

D.1.6 Q105PB

Table D.6: Iodide diffusion coefficients for Queenston shale sample Q105PB

Sample: Q105PB	**ϕ_w: 0.0588**	**$\phi_{I,\,av}$: 0.062**	
Time step (hours)	**D_p (m^2/s)**	**D_e (m^2/s)**	**Curve fit**
1	1.5×10^{-9}	9.3×10^{-11}	poor
4	4.5×10^{-10}	2.8×10^{-11}	poor
8	2.5×10^{-10}	1.6×10^{-11}	poor
24	**1.2×10^{-10}**	**7.4×10^{-12}**	**good**
48	**8.0×10^{-11}**	**5.0×10^{-12}**	**good**
120	**4.0×10^{-11}**	**2.5×10^{-12}**	**good**
170	**3.0×10^{-11}**	**1.9×10^{-12}**	**fair**
314	-	-	breakthrough
384	-	-	breakthrough
528	-	-	breakthrough
840	-	-	breakthrough
Mean (24 - 170 hr)	**5.8×10^{-11}**	**4.2×10^{-12}**	**good**

Experimental conditions:

- Sample axis parallel to bedding.
- 0.8 M KI tracer in 3 M brine (NaCl).
- Tracer diffusion for 35 days.
- Tracer saturation for 25 days until sample was fully saturated with iodide.
- 1-D porosity profile determined from difference between iodide saturated and zero iodide.
- All concentration data corrected for ϕ_w.
- D_e calculated from $\phi_{I,\,average}$
- Relative concentration profiles calculated from mean $\Delta\mu$ near influx boundaries after 9 to 25 days saturation.
- x-axis boundary shift: 2.5 mm.

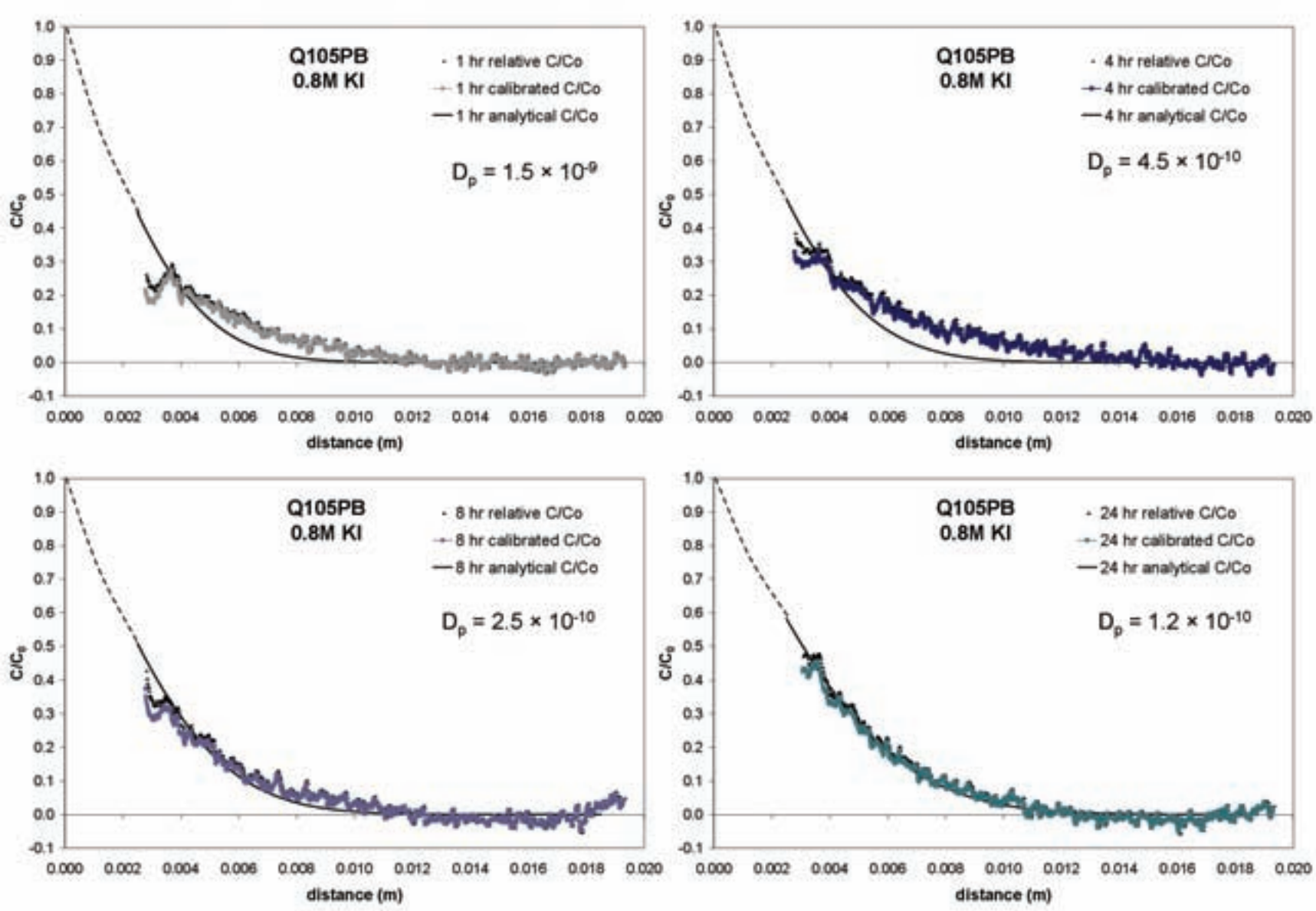

Figure D.6: Iodide concentration profiles and analytical diffusion profiles for Q105PB.

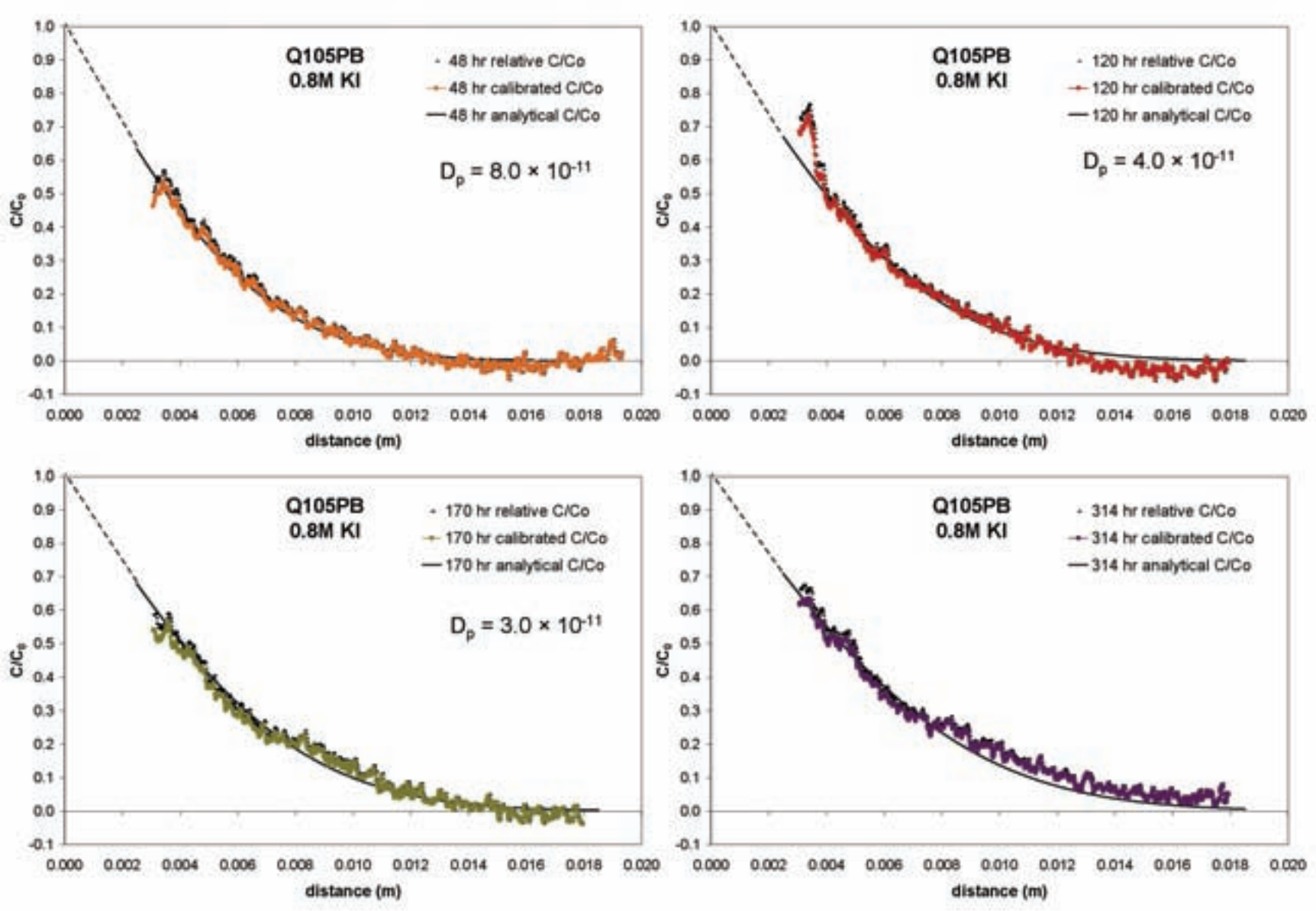

Figure D.6 (continued): Iodide concentration profiles and analytical diffusion profiles for Q105PB.

D.2 COBOURG LIMESTONE SAMPLES

D.2.1 C036NB1

Table D.7: Iodide diffusion coefficients for Cobourg limestone sample C036NB1

Sample: C036NB1	**ϕ_w: 0.0303**	**$\phi_{I,\,av}$: 0.030**	
Time step (hours)	**D_p (m^2/s)**	**D_e (m^2/s)**	**Curve fit**
22	**2.0×10^{-10}**	**6.0×10^{-12}**	**good**
50	**8.0×10^{-11}**	**2.4×10^{-12}**	**fair**
119	**6.0×10^{-11}**	**1.8×10^{-12}**	**good**
215	**4.5×10^{-11}**	**1.4×10^{-12}**	**fair**
383	2.0×10^{-11}	6.0×10^{-13}	breakthrough
Mean (22 - 215 hr)	**9.5×10^{-11}**	**2.9×10^{-12}**	**fair**

Experimental conditions:

- Sample axis normal to bedding.
- 1.0 M KI tracer in 2 M brine (mixed cation-chloride).
- Tracer diffusion for 20 days
- Tracer saturation for 34 days.
- All concentration data corrected for ϕ_w.
- D_e calculated from $\phi_{I,\,average}$
- Relative concentration profiles calculated from mean $\Delta\mu$ near influx boundary at 34 days saturation.
- x-axis boundary shift: 1.8 mm.

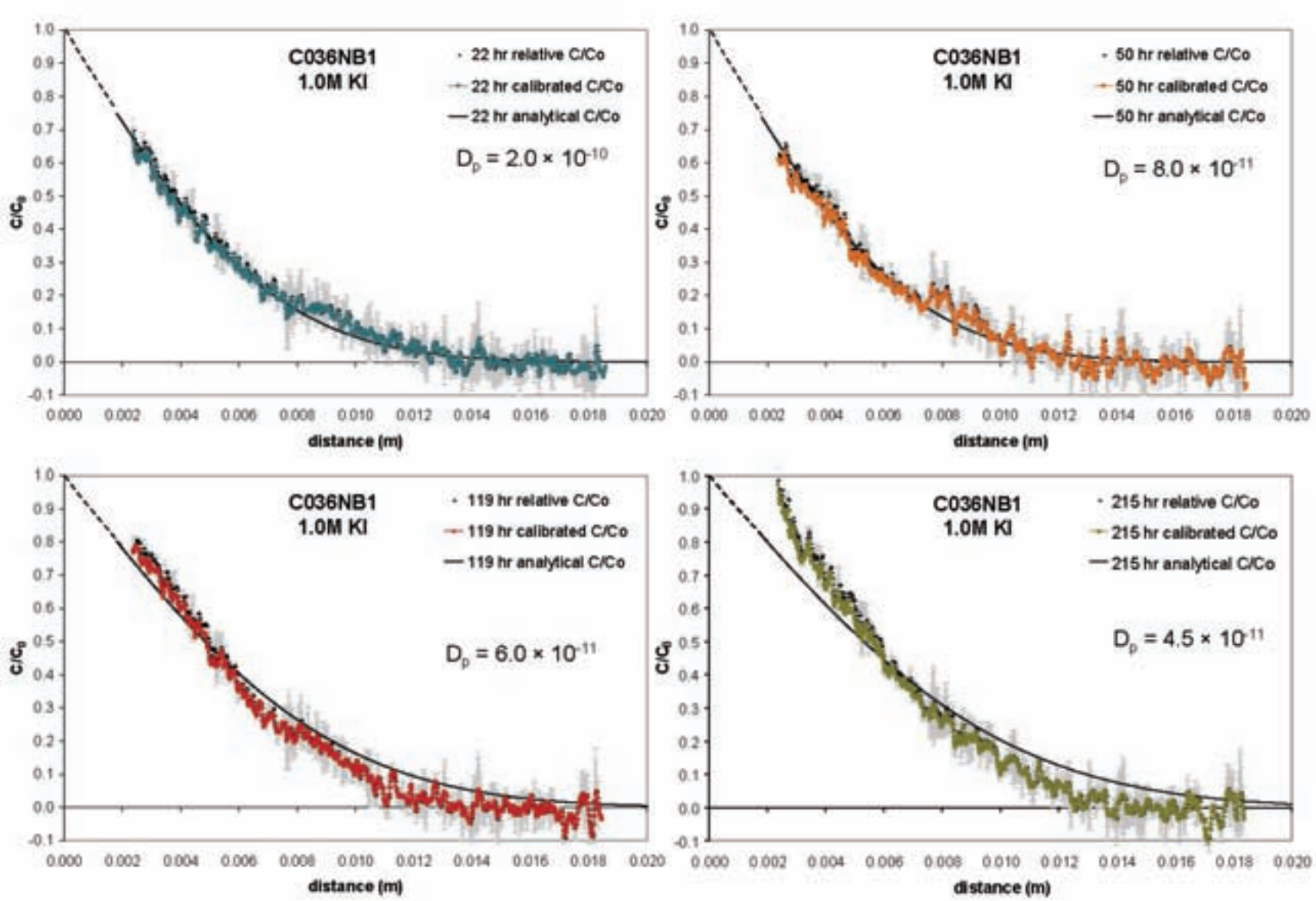

Figure D.7: Iodide concentration profiles and analytical diffusion profiles for C036NB1.

D.2.2 C036PB1

Table D.8: Iodide diffusion coefficients for Cobourg limestone sample C036PB1

Sample: C036PB1	**ϕ_w: 0.0303**	**$\phi_{I,\,av}$: 0.031**	
Time step (hours)	**D_p (m^2/s)**	**D_e (m^2/s)**	**Curve fit**
22	**1.2×10^{-10}**	**3.7×10^{-12}**	**fair**
46	**6.5×10^{-11}**	**2.0×10^{-12}**	**good**
119	**4.0×10^{-11}**	**1.2×10^{-12}**	**fair**
215	**2.0×10^{-11}**	**6.2×10^{-13}**	**fair**
383	2.0×10^{-11}	6.2×10^{-13}	breakthrough
Average (22 - 215 hr)	**6.1×10^{-11}**	**1.9×10^{-12}**	**fair**

Experimental conditions:

- Sample axis parallel to bedding.
- 1.0 M KI tracer in 2 M brine (mixed cation-chloride).
- Tracer diffusion for 20 days
- Tracer saturation for 34 days.
- All concentration data corrected for ϕ_w.
- D_e calculated from $\phi_{I,\,average}$
- Relative concentration profiles calculated from mean Δμ near influx boundaries at 16 days saturation.
- x-axis boundary shift: 1.8 mm.

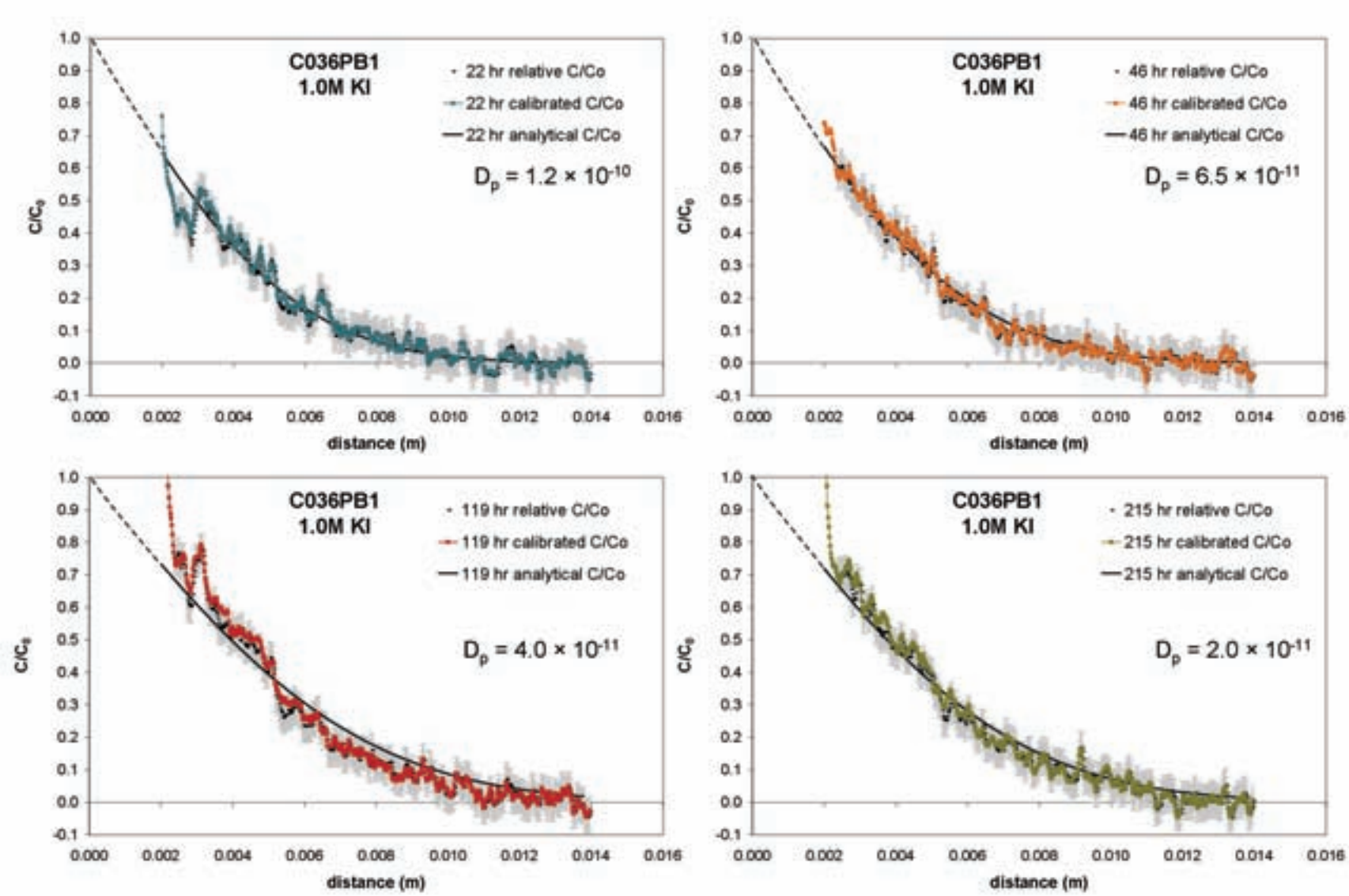

Figure D.8: Iodide concentration profiles and analytical diffusion profiles for C036PB1.

D.2.3 C036NB2

Table D.9: Iodide diffusion coefficients for Cobourg limestone sample C036NB2

Sample: C036NB2	**ϕ_w: 0.0104**	**$\phi_{I,\,av}$: 0.019**	
Time step (hours)	**D_p (m^2/s)**	**D_e (m^2/s)**	**Curve fit**
22	**8.0×10^{-11}**	**1.5×10^{-12}**	**fair**
46	**6.0×10^{-11}**	**1.1×10^{-12}**	**good**
119	**3.5×10^{-11}**	**6.7×10^{-13}**	**good**
215	**2.5×10^{-11}**	**4.8×10^{-13}**	**good**
383	2.5×10^{-11}	4.8×10^{-13}	breakthrough
Average (22 - 215 hr)	**5.0×10^{-11}**	**9.4×10^{-13}**	**fair**

Experimental conditions:

- Sample axis normal to bedding.
- 1.0 M KI tracer in 2 M brine (mixed cation-chloride).
- [1] Measured ϕ_w for C036_2 was 0.0104, but this gave unreasonable results (>1) for calibrated C/C_0 as did the $\phi_{I,}$ average of 0.019. Instead the ϕ_I average of C036PB2 = 0.03 was used.
- Tracer diffusion for 20 days.
- Tracer saturation for 38 days.
- All concentration data corrected for ϕ = 0.03.
- D_e calculated from $\phi_{I,\,average}$
- Relative concentration profiles could not be fitted for this sample.
- X-axis boundary shift: 1.8 mm.

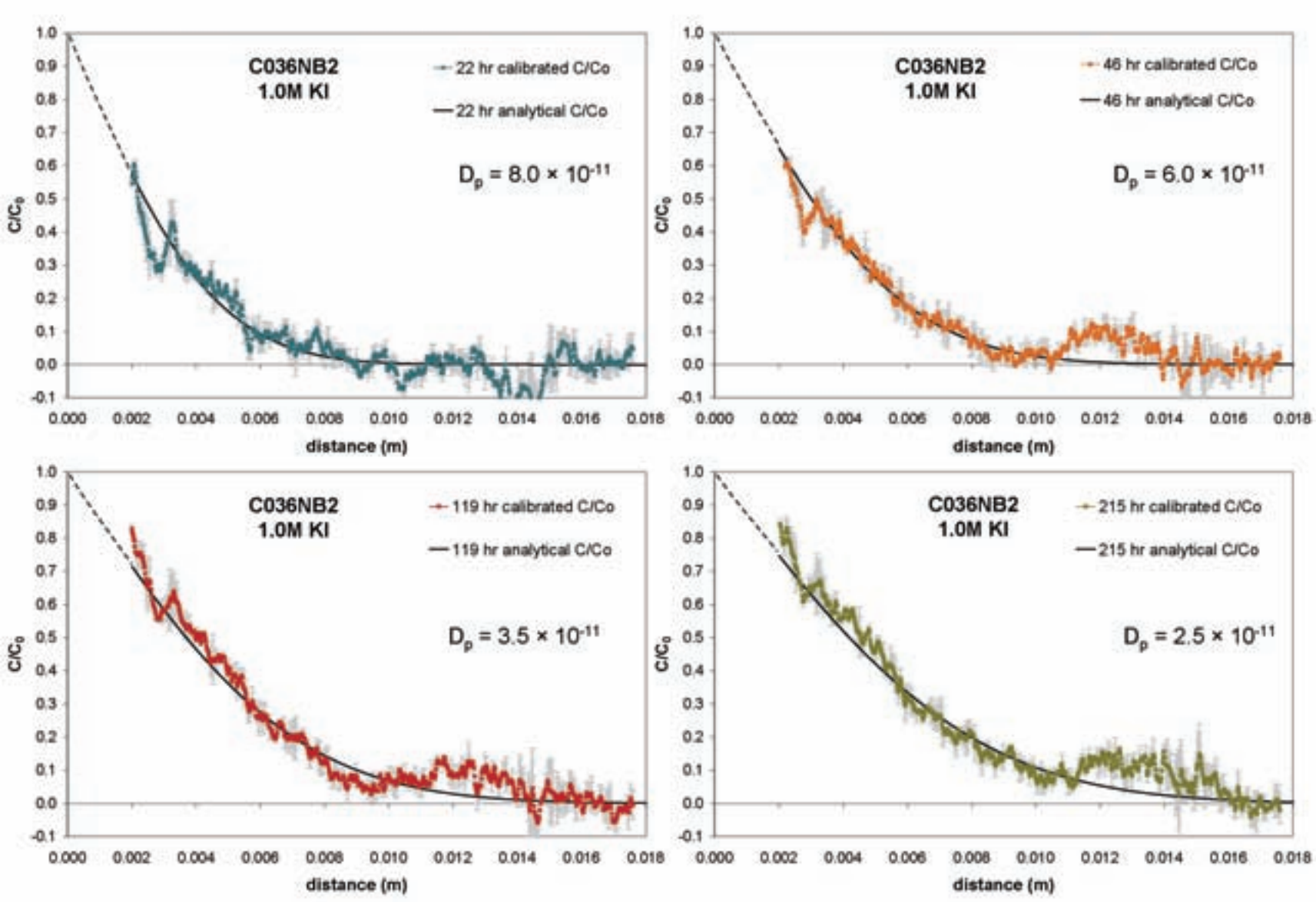

Figure D.9: Iodide concentration profiles and analytical diffusion profiles for C036NB2.

D.2.4 C036PB2

Table D.10: Iodide diffusion coefficients for Cobourg limestone sample L36_2PB

Sample: C036PB2	**ϕ_w: 0.0104[1]**	**$\phi_{I,}$ av: 0.03**	
Time step (hours)	**D_p (m^2/s)**	**D_e (m^2/s)**	**Curve fit**
22	**2.5×10^{-10}**	**7.5×10^{-12}**	**fair**
46	**1.2×10^{-10}**	**3.6×10^{-12}**	**good**
119	**5.0×10^{-11}**	**1.5×10^{-12}**	**fair**
215	**2.5×10^{-11}**	**7.5×10^{-13}**	**fair**
383	1.0×10^{-11}	3.0×10^{-13}	breakthrough
Average (22 - 215 hr)	**1.1×10^{-10}**	**3.3×10^{-12}**	**fair**

Experimental conditions:

- Sample axis parallel to bedding.
- 1.0 M KI tracer in 2 M brine (mixed cation-chloride)
- [1] Measured ϕ_w for C036_2 was 0.0104, but this gave unreasonable results (>1) for calibrated C/C_0. Instead the ϕ_I average of 0.03 was used.
- Tracer diffusion for 20 days.
- Tracer saturation for 38 days.
- All concentration data corrected for $\phi_{I,\ average}$.
- D_e calculated from $\phi_{I,\ average}$
- Relative concentration profiles calculated from average Δμ near influx boundaries at 16 days saturation.
- X-axis boundary shift: 2.0 mm.

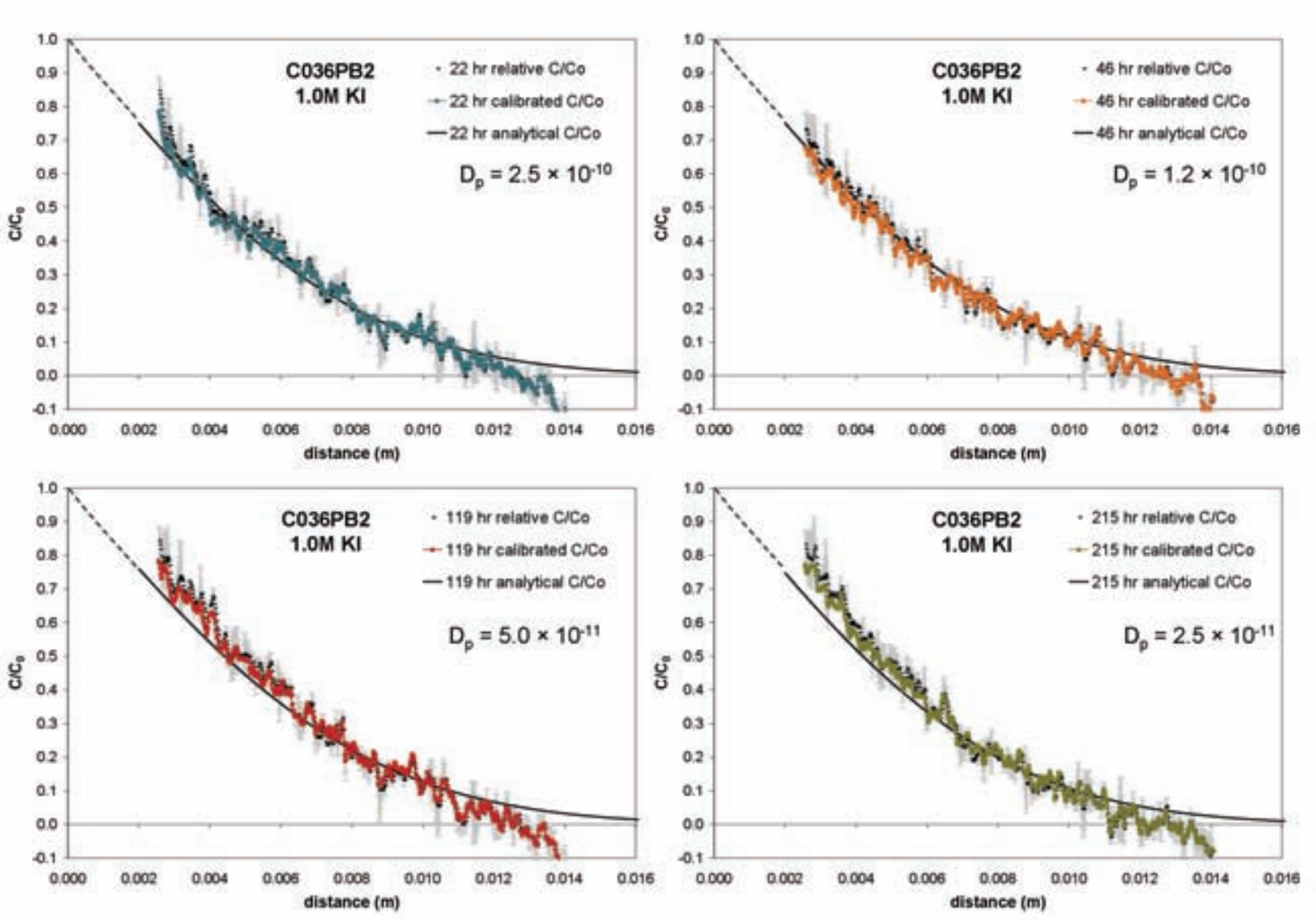

Figure D.10: Iodide concentration profiles and analytical diffusion profiles for C036PB2.

D.2.5 C036NB3

Table D.11: Iodide diffusion coefficients for Cobourg limestone sample C036NB3

Sample: C036NB3	**ϕ_w: 0.0296**	**$\phi_{I,\,av}$: 0.033**	
Time step (hours)	**D_p (m^2/s)**	**D_e (m^2/s)**	**Curve fit**
24	1.3×10^{-10}	4.3×10^{-12}	poor
52	5.0×10^{-11}	1.7×10^{-12}	poor
96	4.0×10^{-11}	1.3×10^{-12}	poor
192	2.5×10^{-11}	8.3×10^{-13}	poor
288	1.0×10^{-11}	3.3×10^{-13}	poor
Average (24 – 192 hr)	**6.1×10^{-11}**	**2.0×10^{-12}**	**poor**

Experimental conditions:

- Sample axis normal to bedding.
- 1.0 M KI tracer in 2 M brine (mixed cation-chloride)
- Radiographs were extracted from CT scan data sets. The image with best separation between the Al wire and the rock was chosen for each time series. These images were collected at slightly longer counting times (10s per frame instead of 8 s per frame) and lower frame averaging (4 instead of 8) than the previous radiographs.
- Two reference scans were collected before introducing the tracer. Both had significantly higher transmitted intensities than the time series images, which could be due to a problem with the source energy. This increases the uncertainty for all the time series profiles, since large normalization factors were used to correct the data.
- Tracer diffusion for 26 days.
- Tracer saturation for 46 days.
- All concentration data corrected for ϕ_w.
- D_e calculated from $\phi_{I,\,average}$
- Relative concentration profiles calculated from average $\Delta\mu$ near influx boundaries at 46 days saturation. Not used to fit analytical solution.
- Uncertain whether sample reached iodide breakthrough.
- X-axis boundary shift: 1.8 mm.
- THIS SAMPLE GAVE POOR FIT FOR ALL TIME SERIES.

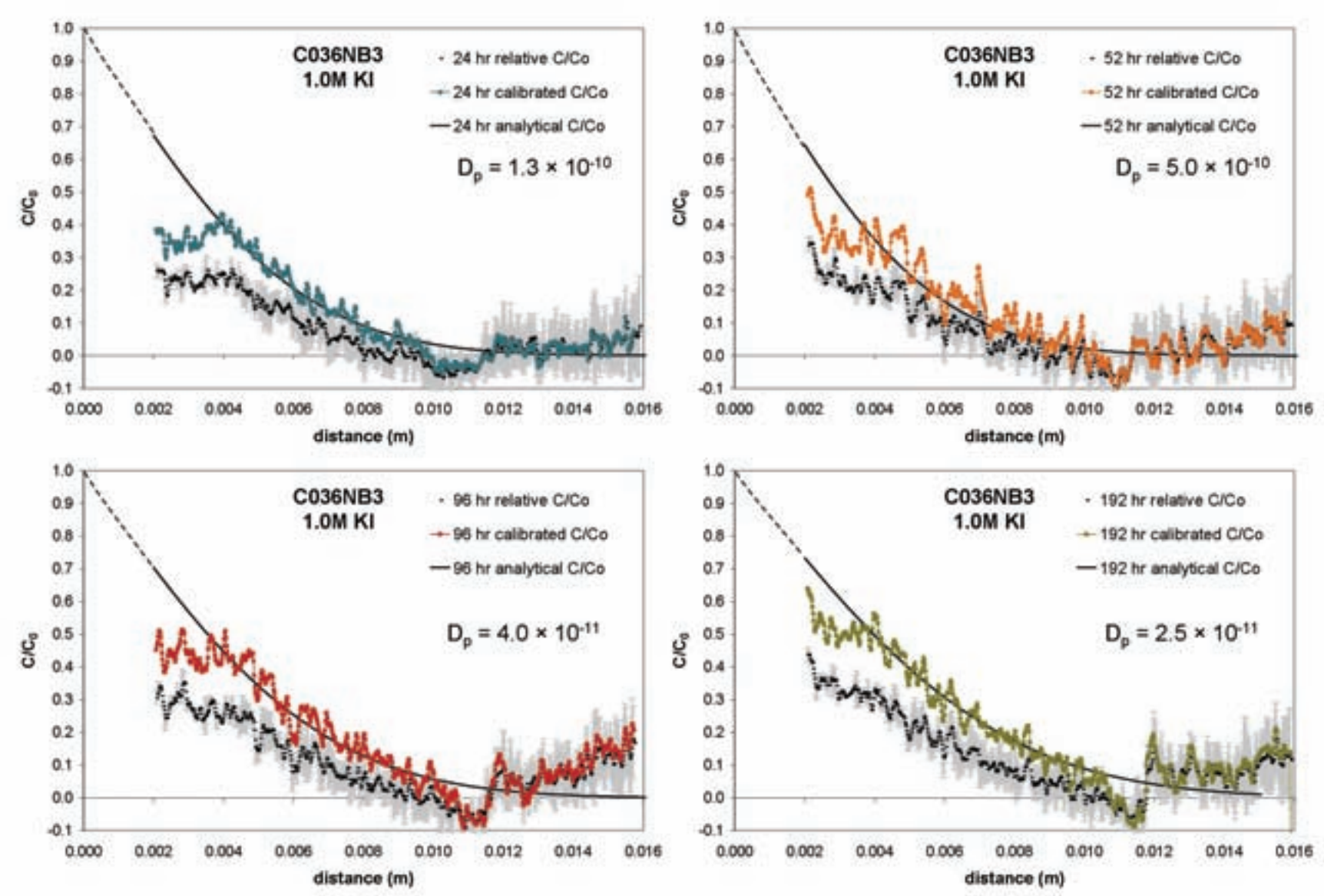

Figure D.11: Iodide concentration profiles and analytical diffusion profiles for C036NB3.

D.2.6. C036PB3

Table D.12: Iodide diffusion coefficients for Cobourg limestone sample C036PB3

Sample: L36_3PB	**ϕ_w: 0.0296**	**$\phi_{I,\,av}$: 0.023**	
Time step (hours)	**D_p (m^2/s)**	**D_e (m^2/s)**	**Curve fit**
24	**7.0×10^{-11}**	**1.6×10^{-12}**	**good**
52	**5.0×10^{-11}**	**1.2×10^{-12}**	**good**
96	**2.5×10^{-11}**	**5.8×10^{-13}**	**good**
192	**1.5×10^{-11}**	**3.5×10^{-13}**	**good**
288	2.5×10^{-11}	5.8×10^{-13}	breakthrough
456	1.0×10^{-12}	2.3×10^{-13}	breakthrough
Average (24 – 192 hr)	**4.0×10^{-11}**	**9.3×10^{-13}**	**good**

Experimental conditions:

- Sample axis parallel to bedding.
- 1.0 M KI tracer in mixed cation-chloride brine.
- Radiographs were extracted from CT scan data sets. The image with best separation between the Al wire and the rock was chosen for each time series. These images were collected at slightly longer counting times (10s per frame instead of 8 s per frame) and lower frame averaging (4 instead of 8) than the previous radiographs.
- Tracer diffusion for 26 days.
- Tracer saturation for 46 days.
- All concentration data corrected for ϕ_w.
- D_e calculated from $\phi_{I,\,average}$
- Relative concentration profiles calculated from average Δμ near influx boundary after 28 and 46 days saturation.
- X-axis boundary shift: 1.8 mm.

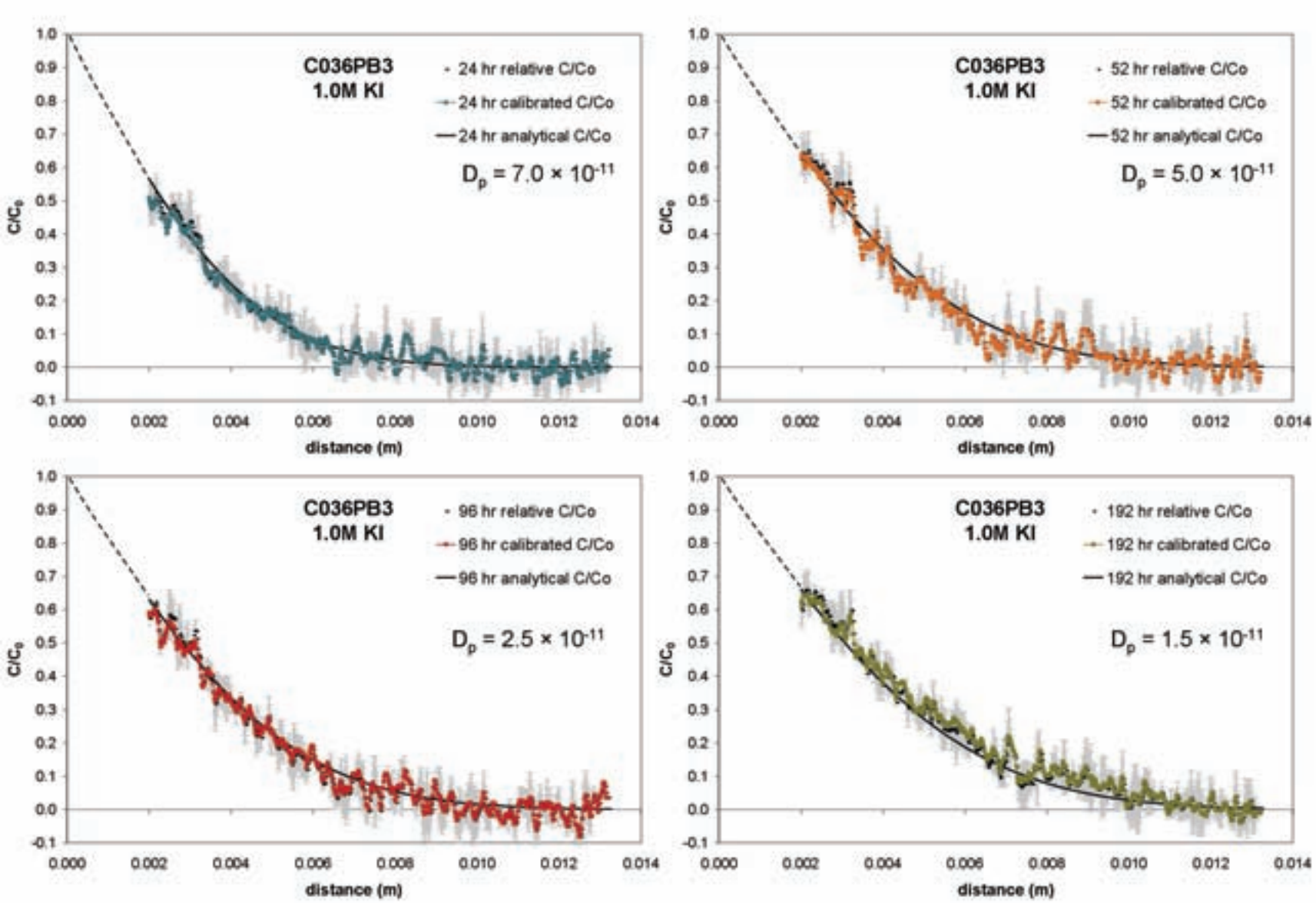

Figure D.12: Iodide concentration profiles and analytical diffusion profiles for C036PB3.